UNIVERSITY OF NAPLES FEDERICO II

Department of Chemical, Materials and Industrial Production Engineering

Ph.D. THESIS IN MATERIALS AND STRUCTURES

ENGINEERING XXVII CYCLE

"Study on Synthesized Azopolymer Brushes as Novel Photoresponsive Biomaterials"

Advisor:

Prof. Paolo Antonio Netti

Tutor:

Dr. Silvia Cavalli

Coordinator:

Prof. Giuseppe Mensitieri

Candidate:

Ravichandran Honnavally Kollarigowda

March 2012 - March 2015

“Do not wait to strike till the iron is hot;

But make it hot by striking”

William Butler Yeats

Table of Contents

Chapter 1

Photoresponsive Polymers and their Emerging Role as Smart Stimuli-Responsive Biomaterials

Abstract. Stimuli-responsive polymers have attracted significant research interest in the past few years as interesting smart types of biomaterials. They offer a wealth of opportunities to design responsive materials triggered by external stimuli and have a number of applications in particular in the fields of biomaterials science and tissue engineering. Among these smart polymeric matters, polymers with azo-chromophores, thus having a photoresponsive nature, act as superior materials that can dynamically alter their properties by the use of light as an external trigger. These types of polymers can be used for nano- to micro-scale surface relief grating (SRG). In this chapter we discuss the current and future challenges of azopolymers, with a special attention on the case of azopolymer brushes (azoPBs), considering their synthesis as well as their photochemistry and showing few SRG formation models. Further, we briefly discuss about the use of photoresponsive PBs for biological applications in the field of dynamic cell instructive materials (dynamic CIMs). The aim and outline of the thesis are also presented in the last part of the Chapter.

1.1 Stimuli-Responsive Polymers

The basic concept underlying the properties of polymer-containing responsive system is a dramatic physico-chemical change caused by external stimuli.[1] At the macromolecular level, polymer chains can be altered in different ways, including changes in hydrophilic-to-hydrophobic balance, conformation, solubility, degradation, and bond cleavage and these characteristics cause detectable behavior changes in the self-assembled structures.[1] Stimuli are commonly classified in three categories: physical, chemical and biological. Physical stimuli (i.e. light,[2] temperature,[3] mechanical force[4] and electric or magnetic field[1]) usually modify chain assembly and dynamics, while chemical stimuli (i.e. solvent, ionic strength, electrochemistry and pH)[4] modulate molecular interactions, either between polymer and solvent molecules, or between polymer chains.[5] Biological stimuli materials undergo macroscopic transition that are triggered by selective enzymes (lipases, proteases, phosphatases, kinases, acyltransferases and redox enzymes).[6,7]

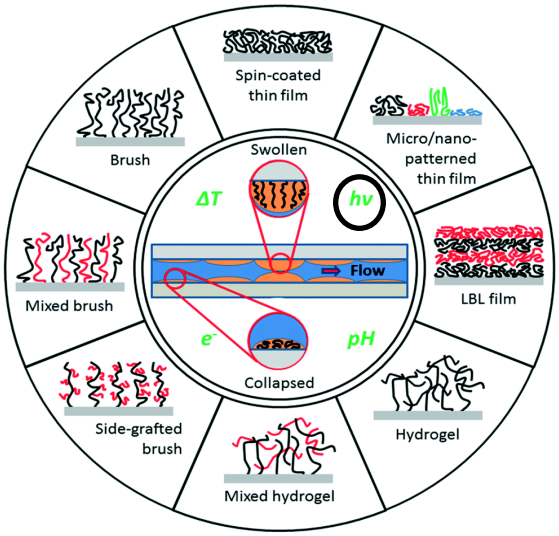

Figure 1.1. Classification of stimuli-responsive polymers.[8]

Another important research area under investigation is the development of substrates that dynamically regulate biological functions in response to applied stimuli, by mimicking the dynamic properties of biological systems.[1,3] Polymer brushes (PBs) those are capable of conformational and chemical changes caused by the external stimuli signal from their environment.[4] These changes are accompanied by variations in the physical properties of the polymers. These surfaces that can modulate biomolecule activity, protein immobilization, cell adhesion and migration at the liquid–solid interface can be tremendously useful in diverse biological and medical applications. For instance, dynamic synthetic substrates that can control the presentation of regulatory signals to a cell provide unprecedented opportunities in the study of cell behaviour.[5] In this respect it is important to understand the mobility and dynamics of stimuli-responsive PBs. So far dynamics of the polymer brushes was studied by Monte Carlo simulation process or by applying thermal stimuli like lower critical solution temperature (LCST) to higher critical solution temperature (HCST). In our research, we discussed dynamics by confocal microscopy exploiting the fluorescence signal coming from our synthesized polymer brushes.

1.1.1 Photoresponsive Polymers

Since light can be applied instantaneously and under specific conditions with high accuracy, it renders light-responsive polymers highly advantageous for several types of applications in particular in the biological field.[2] Lightresponsive materials are usually classified by the chromophore they employ in achieving their photoresponsive properties that fall into two well-defined classes: reversible or irreversible photoswitches. Irreversible photoswitches can involve changes in the

molecular shape by external stimuli, as for example diarylethenes or thiophenefulgides.[9] Whereas, reversible photoswitches can involve dimerization reactions such as those between pairs of cinnamates[10,11] or coumarins.[12] The main drawback when thinking on biological application is the fact that these materials generally tend to be triggered by UV light, which may be damaging biological tissues. Another interesting reversible switcher is azobenzene. The reversibility of the light stimulus is due to the *trans-cis* isomerization triggered by a single photon that can occur in the UV-Visible region depending on the substituents on the phenyl rings.[13]

1.1.2 Azobenzene Photochemistry

Azobenzene, with two phenyl rings separated by an azo (–N=N–) bond, serve as the parent molecule for a broad class of aromatic azocompounds. These chromophores are versatile molecules, and have received much attention in both fundamental and applied research areas.[14] When submitted to irradiation by light, the azobenzene molecule is known to undergo a reversible transition from the *trans* to the *cis* configuration that can be converted back again to the thermodynamically more stable *trans* isomer by light or heat (Figure 1.2).[15,16] Adding substituents to the azobenzene rings may lead to minor or major changes in their spectroscopic character. For example, when the *ortho*- or *para*-position is substituted with an electron donating group (usually an amine, $–NH_2$), a new class of compounds results. In this amino-azobenzene, the $n \rightarrow \pi^*$ and $\pi \rightarrow \pi^*$ UV bands are much closer (Figure 1.3).

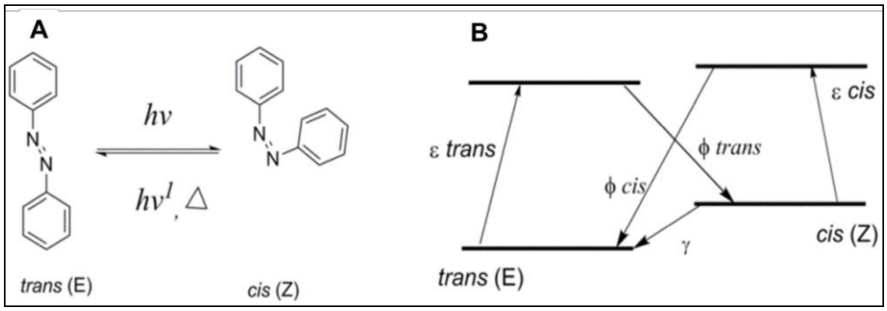

Figure 1.2. (A) Azobenzene can convert between *trans* and *cis* states photo-chemically and relaxes to the more stable *trans* state thermally or applying light. (B) Simplified state model for azobenzene. The *trans* and *cis* extinction coefficients are denoted ε *trans* and ε *cis.* The ϕ refer to quantum yields of photo-isomerization, and γ *is* the thermal relaxation rate constant.[17]

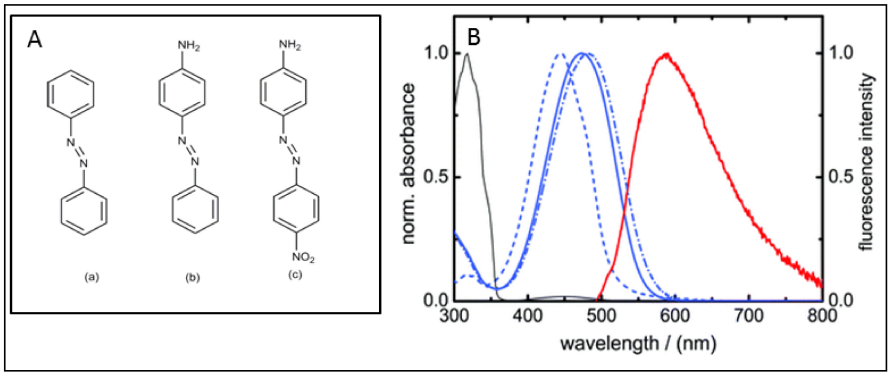

Figure 1.3. (A) Examples of chemical structure of important type of azomolecules, classified as (a) azobenzene, (b) amino-azobenzene, and (c) pseudo-stilbene. (B) Typical absorbance spectra for *trans*-azobenzene. The azobenzene-type molecules (solid black line) have a strong absorption in the UV, and a low-intensity band in the visible (barely visible in the graph). The amino-azobenzene (blue dotted line) and pseudo-stilbenes (blue dashed line) typically have strong overlapped absorptions in the visible region. (Solid blue line) corresponds to pseudo-stilbenes in n-hexane and (solid red line) is the 2FT fluorescence spectrum for disperse red 1 (a commercial available stilbene).[17]

In fact, the $n \rightarrow \pi^*$ may be completely buried beneath the intense $\pi \rightarrow \pi^*$. Whereas, azobenzene is fairly insensitive to solvent polarity, amino-azobenzene absorption bands shift to higher energy in nonpolar solvents

and shift to lower energy in polar solvents. Substituting azobenzene at the two para positions with an electron-donor and an electron-acceptor (such as an amino and a nitro, $-NO_2$, group) leads to a strongly asymmetric electron distribution (often referred to as a "push/pull" substitution pattern). The strong $\pi \rightarrow \pi^*$ absorption with charge-transfer (CT) character is a dominant feature in the visible spectrum, and the $n \rightarrow \pi^*$ transition is hidden by this strong band.

Because of the permanent dipole moment of the ground state and the charge-transfer character of the transition, the absorption band shows a positive solvatochromism (that corresponds to a better stabilization of the molecule in the first excited state with respect to the ground state, with increasing solvent polarity, thus producing a red shift of the absorption band). This ordering of the absorption bands defines the third spectroscopic class, the pseudo-stilbenes (in analogy to stilbene, phenyl C=C phenyl). The pseudo-stilbenes are very sensitive to the local environment of the photoactive molecules on the optical interference pattern.

1.1.3 Azobenzene Orientation

Azobenzene chromophores can be oriented using polarized light, via a statistical selection process, described schematically in Figure 1.4. Azobenzenes preferentially absorb light polarized along their transition dipole axis (long axis of the azomolecules). The probability of absorption varies as $\cos^2 \phi$, where ϕ is the angle between the light polarization and the azo dipole axis. Thus, azomolecules oriented along the polarization of the light will absorb, whereas those oriented against the light polarization will not.

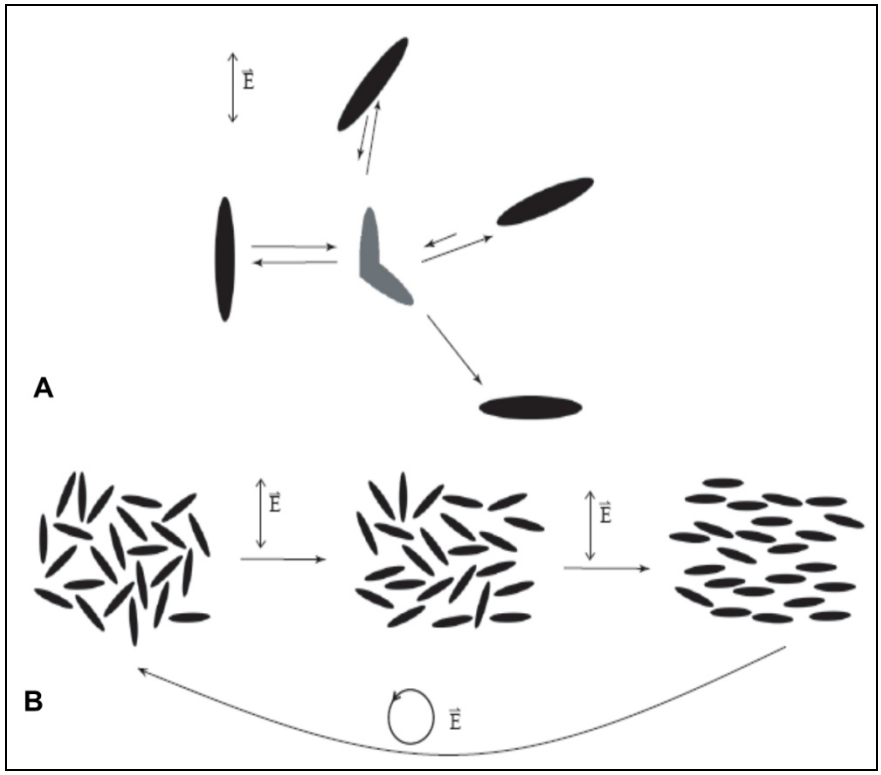

Figure 1.4. Statistical photo-orientation of azo-molecules. (A) The molecules aligned along the polarization direction of the incident light, absorb, isomerize and reorient. Those aligned perpendicular do not absorb and remain fixed. (B) Irradiation of an isotropic samples leads to accumulation of chromophores in the perpendicular direction to the incoming liner polarized light. Circularly polarized light restores isotropy.[17]

For a given initial angular distribution of chromophores, many will absorb, convert into the *cis* form, and then return to the *trans* isomer with a new random direction. Those chromophores that fall perpendicular to the light polarization will no longer isomerize or reorient; hence, there is a net depletion of chromophores aligned with the light polarization, with a concomitant increase in the population of chromophores aligned perpendicular (i.e., orientation hole burning, when the azobenzene chromophore can no longer be electronically

excited and remains in that position, this leads to "angular hole burning"). This statistical reorientation is fast, and gives rise to strong birefringence (anisotropy in refractive index) and dichroism (anisotropy in absorption spectrum) due to the large anisotropy of the azo electronic system. The process is especially efficient owing to the mesogene-like cooperative motion that the azobenzene groups facilitate, even in amorphous samples below *T*g. Since the process requires cycling of the chromophores between *trans* and *cis* states, the pseudo-stilbenes have the fastest response to the light stimuli.[12,20]

The most common azopolymers are acrylates, methacrylates, and isocyanates. Thin films of azopolymers are usually prepared by spin-coating, or spin casting to prepare surface relief grating (SRG) using optical interference setup (i.e. Lloyd's mirror method).

1.1.4 Azopolymer Surface Patterning

Since its discovered in 1995,[18] photo-induced surface-relief pattern has triggered a great amount of interest in both fundamental and applied research (SRG examples are shown in Figure 1.5). Azopolymer possess a unique behavior due to *trans-cis* reversible photo-isomerization, induced by UV-Vis light.[19] If the azobenzene is attached to the polymeric chain, the photo-isomerization of *trans-cis* and *cis-trans* generates conformational changes at the entire chain level, which, in turn, lead to macroscopic variations in the chemical and physical material properties.[8] Although the azobenzene photo-isomerization process has been studied since long time, the mechanism of SRG formation is still not completely elucidated.

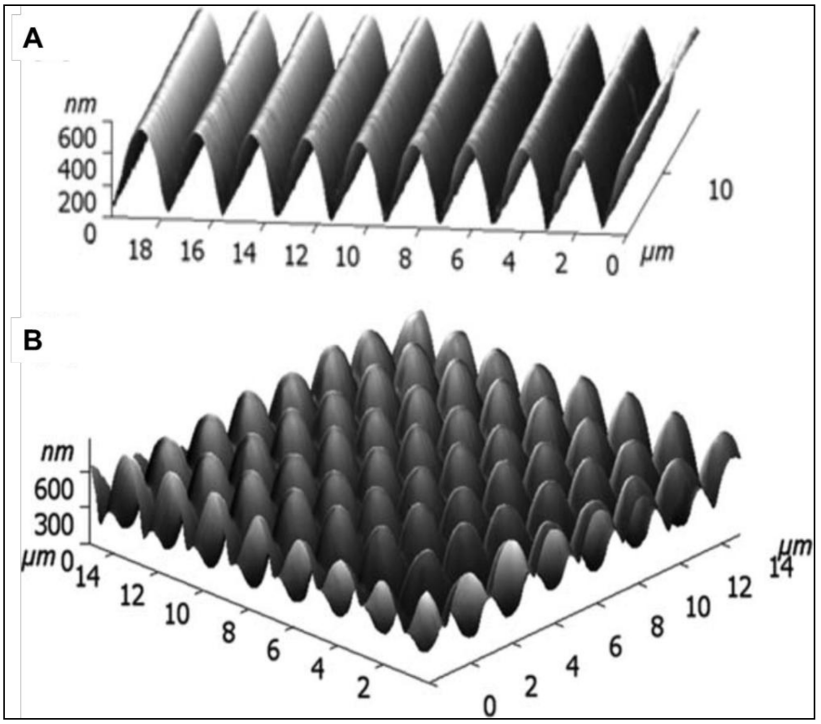

Figure 1.5. Atomic-force microscope (AFM) images of azopolymers illuminated by UV (a) 600 nm pattern height and (b) grid-like structure of azopolymer SRGs.[32]

However, several models have been proposed to explain the photo-induced mass transport, responsible for the creation of SRGs.[20,21] Some, hypothesis such as the isomerization pressure,[20] gradient of the electric force,[22] asymmetric diffusion,[23] mean-field forces[24] and permittivity gradients[25] or conformational instability[26] are assumed to play an important role in the different proposed mechanisms and the most relevant proposed models are listed in detail below.[24-29]

(1) In the free volume model proposed by Barrett and co-workers[30] the driving force responsible for the mass transport was assumed to arise from pressure gradients induced by photo-isomerization of azobenzene groups. Resulting viscoelastic flow of the material from the high-

pressure to the low pressure areas leads to the sinusoidal SRGs and was modeled according to the Navier-Stokes equation. However, this model did not explain the effect of polarization, even though SRG formation is shown to be strictly depended on the polarization of the inscribing light.

(2) The asymmetric diffusion model proposed by Lefin and co-workers[23] relates SRG formation with the creation of concentration gradients. The essential feature of this model is that dye-molecules undergo a 1-D random walk along their photo-excitation direction, thus inducing a net flux of molecules out of illuminated regions toward the darker regions. However this model fails to explain the effect of changing polarization angle and orientation of azobenzene with respect to the linear polarization of light (LPL).

(3) The mean-field theory proposed by Naydenova *et al*[26] assumes that chromophores are subjected to anisotropic intermolecular interactions. The main field of chromophores, which were oriented by light, tends to align other chromophores in the same direction and cause an attractive force between side-by-side chromophores oriented in the same direction causing their order and aggregation. This mechanism properly describes the surface relief formation in side-chain azobenzene liquid crystalline polymers, which show an in-phase SRGs; it means that surface profile maxima are coincident with the maxima of the light intensity pattern. It should be pointed out that such behavior is in contrast to amorphous polymers, where the reverse effect is observed, i.e., the light intensity maxima correspond to surface minima. This mechanism includes the peculiar properties of azobenzene only to explain the photo-induced ordering of chromophores. If this were the dominant mechanism, then it would be expected that any dipolar chromophore in a matrix with

sufficient mobility could generate surface relief gratings, which has not yet been observed.

(4) The field gradient force model proposed by Tripathy's group[31] is based on the forces originating from the optically induced electric field gradient. The movement of polymer chains depends on the spatial variation of the material susceptibility (due to light-induced birefringence and dichroism), the optical field, and the field gradient along the grating wave vector k as shown in Figure 1.6. This model nicely explains the light polarization dependence of the surface relief formation. In fact, the field gradient force mechanism qualitatively explains the magnitude of SRGs obtained for all combinations of polarization states of writing beams. In this mechanism, azobenzene is required for two reasons. Firstly, the light-induced orientation of azobenzene is required to modulate the susceptibility of the material, and second, a photo-induced plasticization is assumed, permitting material mobility well below *Tg*.

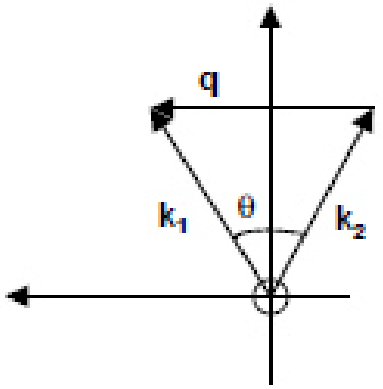

Figure 1.6. Optical arrangement of two-beam. Laser beam is symmetrically oriented around the vertical axis by an angle θ. wave-vectors *k*1, *k*2 and the grating vector *q*.[31]

Thus, despite of several models developed to explain the process of surface relief grating formation on amorphous azopolymer films, none of them could explain the complete process of SRG formation depending upon the parameters like, isomerization of azobenzene during SRG formation, origin of the force and the strength of the force, reversibility of patterned azopolymer at room temperature, direction of the migration of the polymer chains and the final alignment of the polymer chains and so on. At the present time, the gradient force model presented by Tripathy's group appears to be most effective as a rationalization of the diverse set of experimental results, and a promising guide towards further research.

1.1.5 Synthesis of Azopolymer Brushes (azoPBs)

Polymers chemically anchored on a surface, so-called polymer brushes, have received extensive attention for several decades. One synthetic strategy for preparing polymer brushes is the "grafting from" technique, which yields a high grafting density of polymers with controllable coverage on the surface. This "grafting from" approach involves attachment of an initiator on the surface which enables an easy control on the thickness and density of the polymer brush. This "grafting from" approach uses different polymerization techniques such as living ring-opening polymerization (ROMP),[33] anionic polymerization or controlled radical polymerization (CRP) such as nitroxide-mediated polymerization (NMP),[34] atom-transfer radical polymerization (ATRP),[33,35] and reversible addition fragmentation chain transfer polymerization (RAFT).[33,36,37]

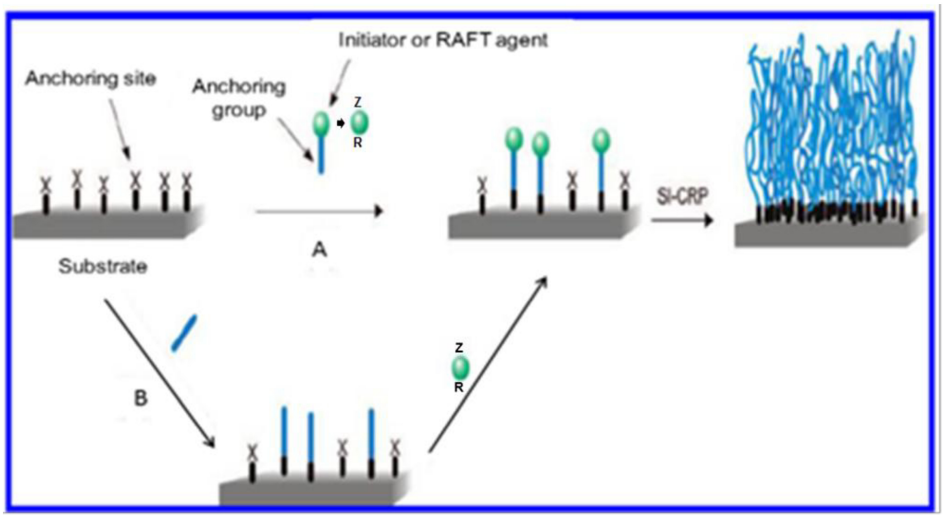

Figure 1.7. Surface modification of substrate with (A) an initiator or an iniferter (a chemical reagent that acts as initiator, chain transfer and terminator) or (B) a RAFT agent.[37]

RAFT polymerization[38] has been successfully applied to grow well-controlled brushes on substrates to alter the surface properties of the materials. RAFT polymerization has also been used to obtain inorganic particles with controlled polymer hair size.[38] The inorganic material investigated using the RAFT process for grafting includes gold, silica/silicon and glass surfaces.[4,39-41] The RAFT agent can be immobilized on the substrate, then initiator and monomer are added together to start the radical polymerization or radicals can be generated on the surface itself by covalent attachment of an initiator and RAFT agent is added in a second stage, while monomer is introduced in the reaction mixture at the very latest stage.[34] Two methods are available for immobilization, the RAFT agent can either be attached via its R- or the Z-group as graphically presented in Figure 1.8.

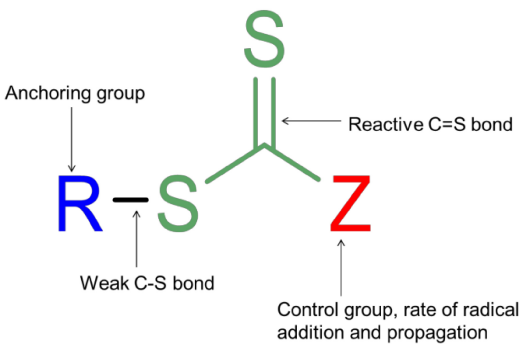

Figure 1.8. Graphical representation of RAFT agent, here, the R-group is the anchoring site and the Z group is the macro initiator that control the rate of radical addition and propagation.

1.1.6 Chromophore Orientation in azoPBs

The orientation of azobenzenes in polymer brushes (azoPBs) is quite different from those in spin-casted films. When spin-casted polymer layers are exposed to light, roughness of azopolymer surfaces increases and the extent of the roughness change is different in the directions parallel and perpendicular to the direction of LPL. In the case of azopolymer brushes, an interesting example was reported by T. Seki,[42] azobenzene molecules adopt a nearly parallel orientation to the substrate surface. This feature leads to the smectic layer orientation directing perpendicular to the substrate. This specific orientation enhances the probability of light absorption, leading to the highly ordered in-plane photo-alignment of chromophores when exposed to LPL.[27,43,44] When the incident beam was set in the azobenzene A direction (the direction of the beam incidence is expressed as X and Y (Figure 1.9A), which are parallel and orthogonal to $\vec{E}$ of the LPL, respectively), in-plane diffraction patterns were observed as shown with two arrows in Figure 1.9A. Thus, the periodic layer structure of the smectic LC phase was

formed perpendicular to the substrate plane with the LC chromophores aligned parallel to the surface. This exhibits a clear contrast with the cases for the ordinary spin-casted films with which the diffractions are observed in the out-of-plane direction.

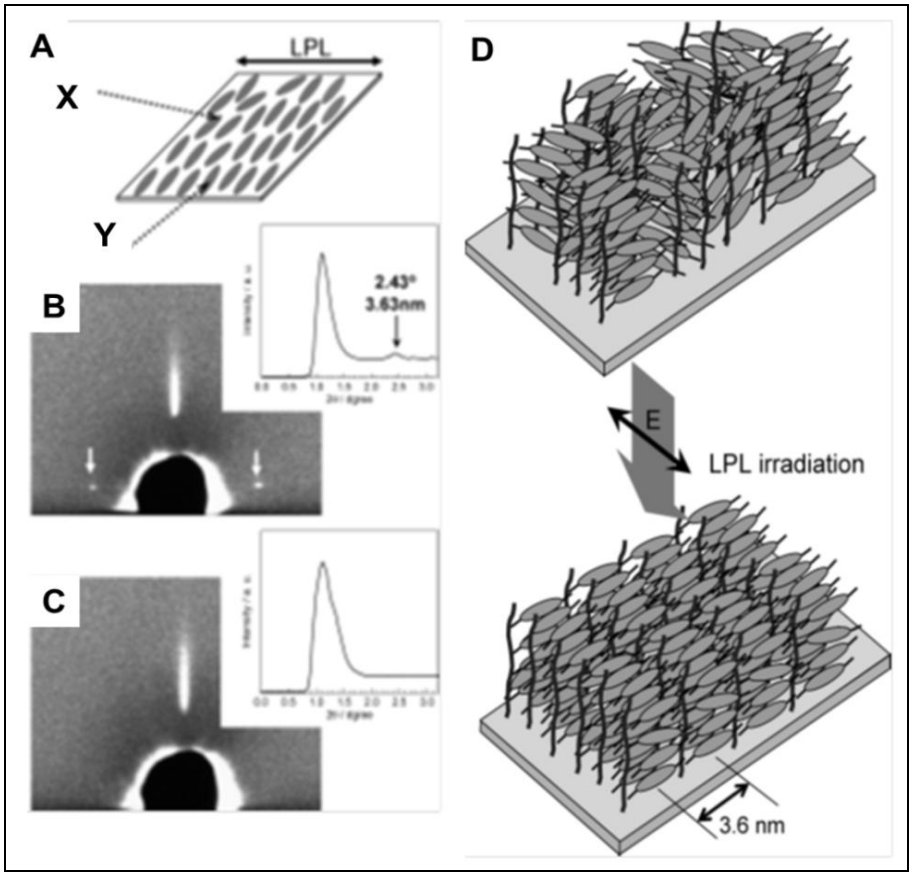

Figure 1.9. (A) Schematic representation of the incident beam direction X and Y for the GI-XRD measurements of the grafted polymer film and 2D GI-XRD patterns of the grafted polymer film recorded on an imaging plate taken with the incident direction X (B) and Y (C). 1D profile in the in-plane direction extracted from the 2D XRD pattern is shown as the inset. (D) Schematic illustration of the photo-induction orientations of azo-mesogens and smectic layers in the grafted film.[45]

The azobenzene orientation is in agreement with the data of the 1D XRD profile monitored in the in-plane direction, a peak was observed at

a 2θ value of 2.43°, which corresponds to the layer spacing of 3.63 nm (inset of Figure 1.9B). The value of the layer spacing suggests the formation of interdigitated structures of azobenzene on the side chains.[45] On the other hand, when the X-ray beam was set in the incident direction of Y no diffraction peak was observed in any direction (Figure 1.9C), indicating that no obvious regular structures derived from the smectic LC layer were observed in this direction. These data show that not only the azobenzene groups are aligned by LPL but the smectic LC layers of the larger assembly hierarchy are also aligned to form a mono domain films over the irradiated area.

1.2 Application of Azopolymers as Lightresponsive Biomaterials

Regenerative medicine is focus on creating therapies for the repairment or replacement of tissues and organs in order to restore impaired function resulting from congenital defects diseases, trauma or aging.[46] Materials science applied to regenerative medicine is focused on designing systems with features that mimic the natural environment of the cells.[47] Smart surfaces, such that can respond to a precise external stimulus in a specific manner, are of increasing interest in research areas as diverse as cell culture.[48-51] When combined with the flexibility provided through molecular synthesis, supramolecular chemistry and surface science, exciting opportunities emerge toward the development of smart molecular materials and devices.[46] Cell–material interaction has been proved to occur through a combination of biochemical and biophysical signals, including interfacial presentation of molecular, topographic and mechanical cues.[52] Indeed, both biochemical and biophysical material features have been reported to affect and somehow influence cell functions by triggering specific molecular events at the

cell-material interface.[53] Cellular activities that are mostly influenced by material properties are adhesion, spreading, migration, proliferation and differentiation.[54]

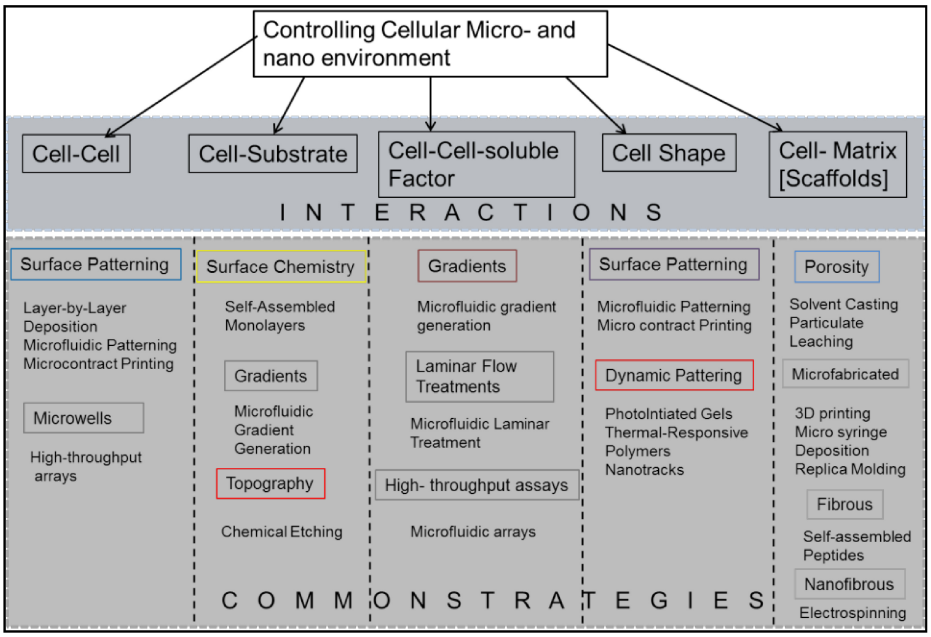

Figure 1.10. An overview of cell-microenvironment interactions and relevant techniques.[53]

Specifically engineered surfaces displaying selected bio-functional groups or micrometre-scale patterns have been used in order to study signal interactions in a systematic way.[55] Owing to technological limitations, however, these kinds of substrates allowed only modest control of signal presentation, in terms of signal dose, spatial arrangement and temporal evolution. Advancements in chemistry, materials science and nanotechnologies greatly improved the possibility of presenting many different signals, according to predefined spatial patterns. In particular, patterns of biochemical signals, topographies on

different length scales and mechanical cues clearly revealed very sophisticated abilities with which cells 'sense' (and react to) external stimuli.[56,57] However, the majority of the studies dealt with single signal types and thus individual senses. This contributed to depicting a scenario in which cells 'taste' chemical moieties, 'see' topographies and 'touch' mechanical properties.[58,59]

In recent times, cell behavior is strongly influenced by material topographic texture. *In vivo* contexts, extracellular environment represents a set of topographic signals, perceived by cells at different length scale. Fibrils and fiber bundles (collagen and fibrin), rough surfaces (crystal deposit in bone) and porous membranes (basement membranes) represent examples of natural topographies. So topographical signals are not to be considered *in vitro* artifacts but they play a relevant role in cell-material interaction through direct alteration in several cellular processes.[55] Recent advancements in micro- and nano-fabrication technologies made it possible to imprint on top of substrate surface topographic feature favouring the study of the role of topography in cell-material interaction. Soft lithography,[60] electron beam lithography[61] and nano-imprint lithography[62] can impress topographic patterns with huge spatial resolution (of a few nanometres).

To describe material topography-cell interactions, it is appropriate to differentiate between length scales that might elicit different responses, consequently topographic features are generally subdivided into macro- micro- and nanoscale topography.[63] Macro topography refers to topographical features exhibiting characteristic dimensions that surpass those of cells (tens of micrometres) providing a geometric confinement of them.[63] Usually micro-topography is related to the use of surface

roughness whose feature varying from few micron to 100 micron. The most extensively studied topographies are grooves and grids, protrusions and pit arrays.[64] The use of micro/nanometric groove patterns is a method to mimic *in vitro* the topographical cues exposed to cell in extracellular environment in *in vivo* contexts.[65] Cells seeded on grooved substrates usually acquire an elongated morphology and alignment to groove direction, reproducing *in vivo* tissue organization, facilitating active self-assembly of ECM (extra cellular matrix) molecules enhancing cell attachment and polarization rate. A wide range of cell types such as fibroblasts,[66] osteoblast[67] and nerve cells[68] respond dramatically to groove substrates.[69,70]

Recently the photoresponsive polymer containing azo-chromophores are emerging as new biomaterials for cell interaction studies.[68,70,71] In general, azopolymers have been used for the fabrication of micron- or nano-scale surface relief grating (SRG),[72,73] due to the photo-reversibility of such SRGs we envision a great potential for guiding the cell orientation and observing cells along the SRGs grooves. Azopolymer SRGs can be used for a reversible control of surface topography by tuning photo-induced erasing or writing processes.[74] In current ongoing research only spin coated/casted azopolymers are used to study the cell to grow over the ridges and results in unidirectional cell orientation. As example primary human astrocytes have been reported to exhibit a preferred direction along the grooves.[75] All together these examples provide valuable experimental research to enrich the body of knowledge on cell–material interaction that represents today a solid foundation for further progress.

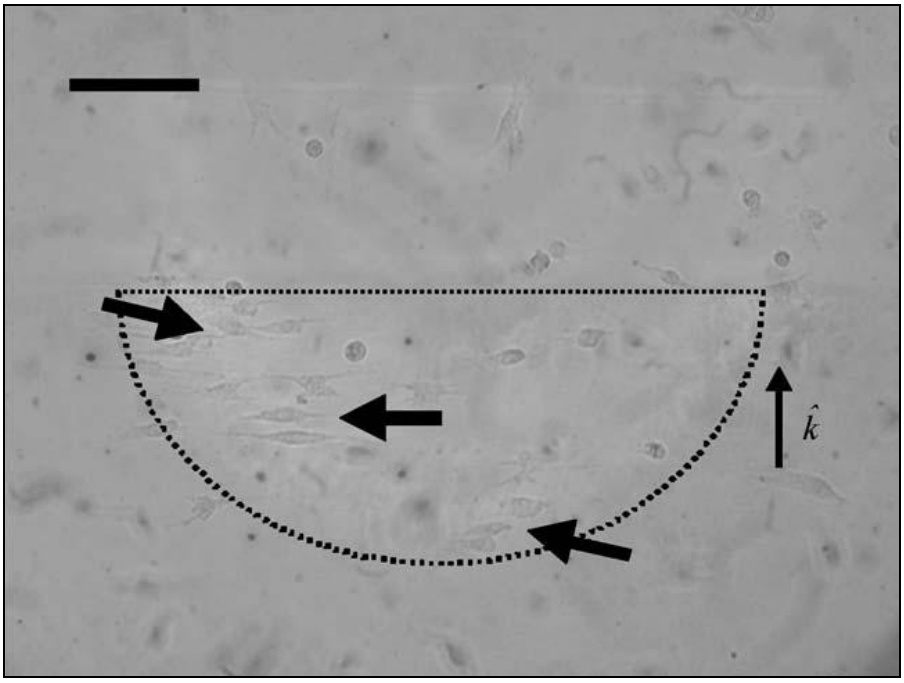

Figure 1.11. The preferred attachment of cells on the SRG a few days after inoculation (scale bar = 100 μm). Cells exist more in the SRG region just inside a dashed half-circle rather than in the outside flat region. The arrows indicate the attached cells forming a monolayer.[75]

To date, no literature supports on patterned azopolymer brushes. We believe that azo-modified polymer brushes would represent new type of cell instructive materials allowing easy reversibility of their topography in biological conditions to control cell behaviour in a dynamic manner. To address this issue we have synthesised azopolymer brushes, studied their dynamics upon excitation by linear polarized light, imprinted topographic patterns on their surface and modified their topography using mild conditions close to physiological environment.

1.3 Aim of the Project and Thesis Outline

The present work describes the design and synthesis of new azopolymer brushes able to generate SRG patterns. Fluorescence correlation

spectroscopy (FCS) technique allowed us to investigate the dynamics of azobenzene-grafted polymer brushes upon photo-induced isomerization process in order to clarify how such a single molecular event can lead to the macroscopic phenomenon of mass-migration and aggregation yielding SRGs. Moreover, Lloyd's mirror method imprinted SRG of 60 nm on these azopolymer brushes. Furthermore, modification of their topography using mild conditions close to physiological environment were tested as well as their biocompatibility in order to confirm them as new light-responsive materials for biological applications in the field of tissue engineering. In **Chapter 2**, we describe the synthesis of all azopolymer brushes via RAFT technique by "grafting from" approach. RAFT polymerization is one of the finest synthetic methodologies to achieve polymers having narrow polydispersity index and high graft density. The thickness of the polymer brushes was controlled by tuning concentration of the RAFT agent immobilized on glass surface as well as polymerization time. Polymer brushes of polymethacrylic acid (pMAb) were firstly prepared and then post modified with a derivative of a well-known azobenzene (Disperse Red 1) on the side chains and a cyanine 5 dye (Cy5) on top of the polymer brush. A comprehensive characterization of each synthesized sample is also presented. In **Chapter 3** the influence of the azobenzene molecules on the polymer brush dynamics was investigated for the first time by Fluorescence Correlation Spectroscopy (FCS). For this purpose three type of azopolymer brushes were used. Two dynamics were observed, a short one coming from the fluctuation of azobenzene and a long one related to the main chain of the polymer brush, where Cy5 was linked. Furthermore, dynamics was reversible. Thanks to FCS data, we could

propose a mechanism of azobenzene dynamics that led to obtain a pattern of micrometric widths, resembling to SRG. In **Chapter 4**, we discuss mainly on the synthesis of a new type of azopolymer brushes, based on acrylamide derivative of Disperse red 1 as monomer, by RAFT approach. Using Lloyd's mirror method SRGs were created and the reversibility of the pattern was obtained by sonication using water at room temperature. Finally, all these azopolymer brushes were tested for their biocompatibility using NIH-3T3 and HUVEC cells and results are discussed at the end of both **Chapter 2** and **4**, envision the possibility to exploit those azopolymer brushes as new biomaterials. Final conclusions and future perspectives, considering features that still need to be optimized are presented and discussed in **Chapter 5**.

References

(1) Liu, F.; Urban, M. W.; Recent advances and challenges in designing stimuli-responsive polymers. *Prog. Polym. Sci.* **2010**, *35,* 2-23.

(2) Schnabel, W.; *Polymers and Light.* Wiley Inter Science: **2007**; 5-400.

(3) Stenzel, M. H.; Zhang, L.; Huck, W. T. S.; Temperature-Responsive Glycopolymer Brushes Synthesized via RAFT Polymerization Using the Z-group Approach. *Macromol. Rapid. Comm.* **2006**, *27,* 1121-1125.

(4) Kumar, S.; Lepage, Y. L. D. M.; Zhao, Y.; Surface-Grafted Stimuli-Responsive Block Copolymer Brushes for the Thermo-, Photo- and pH-Sensitive Release of Dye Molecules. *Macromolecules.* **2011**, *44,* 7385-7393.

(5) Rühe, J.; Knoll, W.; Ciferri, A.; *Supram Polymers.* **2000**; 565.

(6) Ulijn, R. V.; Enzyme-responsive materials: a new class of smart biomaterials. *J. Mater. Chem.* **2006**, *16,* 2217–2225.

(7) Georgiou, M. A. W. a. T. K.; Thermoresponsive Polymers for Biomedical Applications. *Polmers.* **2011**, *3,* 1215-1242.

(8) Kieviet, B. D.; Schon, P. M.; Vancso, G. J.; Stimulus-responsive polymers and other functional polymer surfaces as components in glass microfluidic channels. *Lab. Chip.* **2014**, *14,* 4159–4170.

(9) Szymannski, W.; Beierle, J. M.; Kistemaker, H. A. V.; Velema, W. A.; Feringa, B. L.; Reversible Photocontrol of Biological Systems by the Incorporation of Molecular Photoswitches. *Chem. Rev.* **2012**, *113,* 6114−6178.

(10) Liu, Z.; Tang, Y.; Li, N.; Lu, L.; Deng, J.; Cai, Y.; Modulating Light-Tunable Acid Sensitivity of a Bioinspired Polymer Simply by Adjusting the Position of a Single Methoxy Substituent. *J. Polym. Sci. Pol. Chem.* **2011**, *50,* 495-508.

(11) Shi, D.; Matsusaki, M.; Akashi, M.; Photo-tunable protein release from biodegradable nanoparticles composed of cinnamic acid derivatives. *J. Control. Release.* **2011**, *149,* 182-189.

(12) Trenor, S. R.; Shultz, A. R.; Love, B. J.; Long, T. E.; Coumarins in Polymers: From Light Harvesting to Photo-Cross-Linkable Tissue Scaffolds. *Chem. Rev.* **2004**, *104,* 3059-3077.

(13) Mahimwalla, Z.; Mamiya, K. G. Y. J.-i.; Shishido, A.; Priimagi, A.; Barrett, C. J.; Azobenzene photomechanics: prospects and potential applications. *Polym. Bull.* **2012**, *69,* 967–1006.

(14) Feringa, B. L.; Molecular Swiches. *Wiley-VCH Book, Chapter 13.* **2001**.

(15) Yager, K. G.; Barrett, C. J.; *Light-Induced Nanostructure Formation using Azobenzene Polymers.* **2006**; pp 1-38.

(16) Poprawa-Smoluch, M.; Baggerman, J.; Zhang, H.; Maas, H. P. A.; Cola, L. D.; Brouwer, A. M.; Photoisomerization of Disperse Red 1

Studied with Transient Absorption Spectroscopy and Quantum Chemical Calculations. *J. Phys. Chem. B.* **2006**, *110,* 11926-11937.

(17) Rocha, L.; Paius, C.-M.; Luca-Raicub, A.; Resmeritaa, E.; Rusua, A.; Moleavin, I.-A.; Hamel, M.; Branza-Nichitada, N.; Hurduc, N.; Azobenzene based polymers as photoactive supports and micellarstructures for applications in biology. *J. Photoch. Phtobio. A* **2014**, *291,* 16-25.

(18) Natansohn, A.; Rochon, P.; Photoinduced Motions in Azo-Containing Polymers. *Chem. Rev.* **2002**, *102,* 4139-4175.

(19) Beharry, A. A.; Woolley, G. A.; Small molecules in biology themed issue. *Chem. Soc. Rev.* **2011**, *40*.

(20) Yager, K. G.; Barrett, C. J.; All-optical patterning of azo polymer films. *Curr. Opin. Solid. St. M.* **2001**, *5,* 487-494.

(21) Ubukata, T.; Seki, T.; Ichimura, K.; Surface relief gratings in host-guest supramolecular materials. *Adv. Mater.* **2000**, *12,* 1675-1679

(22) Kumar, J.; Li, L.; Jiang, X. L.; Gradient force: The mechanism for surface relief grating formation in azobenzene functionalized polymers. *Appl. Phys. Lett.* **1998**, *72*.

(23) Lefin, P.; Fiorini, C.; Nunzi, J.-M.; Anisotropy of the photo-induced translation diffusion of azobenzene dyes in polymer matrices. *Pure. Appl. Opt.* **1998**, *7*.

(24) Pedersen, T. G.; Johansen, P. M.; Holme, N. C. R.; Ramanujam, P. S.; Mean-Field Theory of Photoinduced Formation of Surface Reliefs in Side-Chain Azobenzene Polymers. *Phys. Rev. Lett.* **1998**, *80,* 89-92.

(25) Bian, S.; Williams, J. M.; Kim, D. Y.; Li, L.; Balasubramanian, S.; Kumar, J.; Tripathy, S.; Photoinduced surface deformations on azobenzene polymer films. *J. Appl. Phys.* **1999**, *86,* 4498.

(26) Naydenova, I.; Nikolova, L.; Todorov, T.; Diffraction from polarization holographic gratings with surface relief in side-chain azobenzene polyesters. *J. Opt. Soc. Am. B.* **1998**, *15*, 1257-1265

(27) Vishwanathan, N. K.; Balasubramanian, S.; Li, L.; Triphaty, S. K.; Kumar, J.; A Detailed Investigation of the Polarization-Dependent Surface-Relief-Grating Formation Process on Azo Polymer Films. *Jpn. J. Apl. Phys.* **1999**, *38,* 5928–5937.

(28) Ambrosio, A.; Maddalena, P.; Marrucci, L.: Molecular Model for Light-Driven Spiral Mass Transport in Azopolymer Films. *Phys. Rev. Let.* **2013**, 11, 146102-5.

(29) Ambrosio, A.; Marrucci, L.; Borbone, F.; Roviello, A.; Maddalena, P.; Light-induced spiral mass transport in azo-polymer films under vortex-beam illumination. *Nat. Comm.* **2012**, *3,* 1-9.

(30) Barrett, C. J.; Natansohn, A. L.; Mechanism of Optically Inscribed High-Efficiency Diffraction Gratings in Azo Polymer Films. *J.Phys. Chem.* **1996**, *100,* 8836-8842

(31) Kuma, J.; Li, L.; Jiang, X. L.; Gradient force: The mechanism for surface relief grating formation in azobenzene functionalized polymers. *Appl. Phys. Lett.* **1998**, *72*.2096-2098

(32) Arri Priimagi, A. S.; Azopolymer-Based Micro- and Nanopatterning for Photonic Applications. *J. Polym. Sci.Part A: Polym. Chem.* **2013**, *52,* 163–182.

(33) Lee, H.-i.; Pietrasik, J.; Matyjaszewski, K.; Phototunable Temperature-Responsive Molecular Brushes Prepared by ATRP. *Macromolecules.* **2006**, *39,* 3914-3920.

(34) Pyun, J.; Kowalewski, T.; Matyjaszewski, K.; Synthesis of Polymer Brushes Using Atom Transfer Radical Polymerization. *Macromol. Rapid. Comm.* **2003**, *24,* 1043–1059.

(35) Tugulu, S.; Barbey, R.; Harms, M.; Fricke, M.; Volkmer, D.; Rossi, A.; Klok, H.-A.; Synthesis of Poly(methacrylic acid) Brushes via Surface-Initiated Atom Transfer Radical Polymerization of Sodium ethacrylate and Their Use as Substrates for the Mineralization of Calcium Carbonate. *Macromoles.* **2007**, *40,* 168-177.

(36) Mansfeld, U.; Pietsch, C.; Hoogenboom, R.; Becer, R.; Schubert, U. S.; Clickable initiators, monomers and polymers in controlled radical polymerizations – a prospective combination in polymer science. *Roy.Soc.Chem. Poly. Chem.* **2010**, *1,* 1560–1598.

(37) Demirci, S.; Caykara, T.; High Density Cationic Polymer Brushes from Combined ‘‘Click Chemistry’’ and RAFT-Mediated Polymerization. *J. Polym. Sci. Pol. Chem.* **2012**, *50,* 2999-3007.

(38) Keddie, D. J.; A guide to the synthesis of block copolymers using reversible-addition fragmentation chain transfer (RAFT) polymerization. *Chem. Soc. Rev.* **2014**, *43,* 496-505.

(39) Stracke, A.; Wendorff, J. H.; Goldmann, D.; Janietz, D.; Stiller, B.; *Adv. Mater.* **2000**, *12,* 282.

(40) Angiolini, L.; Benelli, T.; Giorgini, L.; Golemme, A.; Salatelli, E.; Termine, R.; Side-Chain Multifunctional Photoresponsive Polymeric Materials. *Intech.* **2000**, *187-212*.

(41) Shi, Y.; Zhu, W.; Chen, Y.; Synthesis of Cylindrical Polymer Brushes with Umbrella-Like Side Chains via a Combination of Grafting-from and grafting-onto Methods. *Macromolecules.* **2013**, *46,* 2391-2398.

(42) Uekusa, T.; Nagano, S.; Seki, T.; Highly Ordered In-Plane Photoalignment Attained by the Brush Architecture of Liquid Crystalline Azobenzene Polymer. *Macromolecules.* **2008**, *42,* 312-318.

(43) Schuh, C.; Lomadze, N.; Rühe, J. r.; Kopyshev, A.; Santer, S.; Photomechanical Degrafting of Azo-Functionalized Poly(methacrylic acid) (PMAA) Brushes. *J. Phys .Chem B.* **2011**, *115,* 10431-10438.

(44) Lomadze, N.; Kopyshev, A.; Rühe, J. r.; Santer, S.; Light-Induced Chain Scission in Photosensitive Polymer Brushes. *Macromolecules.* **2011**, *44,* 7372-7377.
(45) Seki, T.; Photoresponsive self-assembly motions in polymer thin films. *Curr. Opin. Solid. St. M.* **2006**, *10,* 241–248.
(46) Boekhoven, J.; Stupp, S. I.; 25th Anniversary Article: Supramolecular Materials for Regenerative Medicine. *Adv. Mater.* **2014**, *26*, 1642-1659.
(47) Geckil, H.; Xu, F.; Zhang, X.; Moon, S.; Demirci, U.; Engineering hydrogels as extracellular matrix mimics. *PMC. Nanomedicine.* **2010**, *5*, 469–484.
(48) Sun, T.; Feng, L.; Gao, X.; Leijiang; Bioinspired Surfaces with Special Wettability. *Acc. Chem. Res.* **205**, *38,* 644-652.
(49) Palyvoda, O.; Bordenyuk, A. N.; Yatawara, A. K.; McCullen, E.; Chen, C.-C.; Benderski, A. V.; Auner, G. W.; Molecular Organization in SAMs Used for Neuronal Cell Growth. *Langmuir.* **2008**, *24,* 4097-4106.
(50) Mu, L.; Liu, Y.; Cai, S.; Kong, J.; A Smart Surface in a Microfluidic Chip for Controlled Protein Separation *Chem-Eur. J.* **2007**, *13,* 113-120.
(51) Browne, W. R.; Feringa, B. L.; Light Switching of Molecules on Surfaces. *Annu. Rev. Phys. Chem.* **2009**, *60,* 407–428.
(52) Poole, K.; Khairy, K.; Friedrichs, J.; Franz, C.; Cisneros, D. A.; Howard, J.; Mueller, D.; Molecular-scale Topographic Cues Induce the Orientation and Directional Movement of Fibroblasts on Two-dimensional Collagen Surfaces. *J. Mol. Biol.* **2005**, *349,* 380-386.
(53) Ayala, R.; Zhang, C.; Yang, D.; Hwang, Y.; Aung, A.; Shroff, S. S.; Arce, F. T.; Lal, R.; Arya, G.; Varghese, S.; Engineering the cellematerial interface for controlling stem cell adhesion, migration, and differentiation. *Biomaterials.* **2011**, *32,* 3700-3711.
(54) Mitra, J.; Tripathi, G.; Sharma, A.; Basu, B.; Scaffolds for bone tissue engineering: role of surface patterning on osteoblast response. *Roy. Soc. Ch. Advances.* **2013**, *3,* 11073–11094.
(55) Underhill, G. H.; Galie, P.; Chen, C. S.; Bhatia, S. N.; Bioengineering Methods for Analysis of Cells In Vitro. *Annu. Rev. Cell Dev. Bi.* **2012**, *28*. 385-410.
(56) Lehnert, D.; Wehrle-Haller, B.; David, C.; Weiland, U.; Christoph Ballestrem; Imhof, B. A.; Bastmeyer, M.; Cell behaviour on micropatterned substrata: limits of extracellular matrix geometry for spreading and adhesion. *J. Cell. Sci.* **2004**, *117,* 41-52.
(57) Edalat, F.; Sheu, I.; Manoucheri, S.; Khademhosseini, A.; Material strategies for creating artificial cell-instructive niches. *P. Natl. Acad. Sci-biol.* **2012**, *94,* 13661–13665.

(58) Kooten, T. G. v.; Spijker, H. T.; Busscher, H. J.; Plasma-treated polystyrene surfaces: model surfaces for studying cell–biomaterial interactions. *Biomaterials.* **2003**, *25,* 1735-1747.

(59) Ponsonneta, L.; Reybiera, K.; Jaffrezica, N.; Comteb, V.; Lagneaub, C.; Lissacb, M.; Marteleta, C.; Relationship between surface properties (roughness, wettability) of titanium and titanium alloys and cell behaviour. *Mater. Sci. Eng. C.* **2003**, *23,* 551-560.

(60) Braber, E. T. d.; Ruijter, J. E. d.; Ginsel, L. A.; Recum, A. F. v.; Jansen, J. A.; Orientation of ECM protein deposition, fibroblast cytoskeleton, and attachment complex components on silicone microgrooved surfaces. *J. Biomed. Mater. Res. A.* **1997**, *40,* 291–300.

(61) Dalby, M. J.; Biggs, M. J. P.; Gadegaard, N.; Kalna, G.; Wilkinson, C. D. W.; Curtis, A. S. G.; Nanotopographical Stimulation of Mechanotransduction and Changes in Interphase Centromere Positioning. *J. Cell. Biochem.* **2007**, *100,* 326–338.

(62) Gaubert, H. E.; Frey, W.; Highly parallel fabrication of nanopatterned surfaces with nanoscale orthogonal biofunctionalization imprint lithography. *Nanotechnology.* **2007**, *18,* 101–135.

(63) Hadjipanayi, E., University of College London, 2010.

(64) Nuutinen, T.; Silvennoinen, M.; paivasaari, K.; Vahimaa, P.; Control of cultured human cells with femtosecond laser ablated patterns on steel and plastic surfaces. *Biomed. Microdevices.* **2013**, *15,* 279–288.

(65) Kshitiza; Park, J.; Kima, P.; Helen, W.; Engler, A. J.; Levchenko, A.; Kim, D.-H.; Control of stem cell fate and function by engineering physical microenvironments. *PMC. Integr. Biol.* **2012**, *4,* 1008–1018.

(66) Dalby, M. J.; Riehle, M. O.; Yarwood, S. J.; Wilkinson, C. D. W.; Curtis, A. S. G.; Nucleus alignment and cell signaling in fibroblasts: response to a micro-grooved topography. *Exp. Cell. Res.* **2003**, *284,* 274-282.

(67) S, L.; MB, M.; U, M.; L, C.; HP, W.; Osteoblast alignment, elongation and migration on grooved polystyrene surfaces patterned by Langmuir–Blodgett lithography. *Biomaterials.* **2005**, *26,* 563–570.

(68) Yima, E. K. F.; Pangb, S. W.; Leong, K. W.; Synthetic nanostructures inducing differentiation of human mesenchymal stem cells into neuronal lineage. *Exp. Cell. Res.* **2007**, *313,* 1820-1829.

(69) Hatano, R.; Mercurio, K.; Luna, J. I.; Glaser, D. E.; Leppert, V. J.; McCloskey, K. E.; Endothelial cells derived from embryonic stem cells respond to cues from topographical surface patterns. *J. Biol. Eng.* **2013**, *7:18,* 1-12.

(70) Baaca, H.; Leea, J.-H.; Seoa, J.-M.; Parka, T. H.; Chunga, H.; Leed, S.-D.; Kim, S. J.; Submicron-scale topographical control of cell growth using holographic surface relief grating. *Mater. Sci. Eng.* **2004**, *24,* 209-212.

(71) Jae Kyoo Lee, E. J., Sin-Doo Lee, and Sung June Kim; Spatial Patterning of Fibroblast Cells with Fabricating Holographic Patterning on the Photoresponsive Polymer. *Conf. Proc. IEEE Eng. Med. Biol. Soc.* **2005**;*4*:4107-4117.

(72) Lee, J. K.; Baac, H.; Song, S.-H.; Lee, S.-D.; Park, D.; The Topographical Guidance of Neurons cultured on Holographic Photo-Responsive Polymer. *Conf. Proc. IEEE Eng. Med. Biol. Soc.* **2004**, 4970-4973.

(73) Hurduca, N.; Donoseb, B. C.; Macoveic, A.; Paiusa, C.; Ibanescua, C.; Scutarua, D.; Hameld, M.; Nichitab, N. B.-.; Rochad, L.; Direct Observation of Athermal photofluidisation in Azo-Polymer Films. *Soft. Matter.* **2012**, *00,* 1-3.

(74) Rocha, L.; Paius, C.-M.; Luca-Raicub, A.; Resmeritaa, E.; Rusua, A.; Moleavin, I.-A.; Hamel, M.; Branza-Nichitada, N.; Hurduc, N.; Azobenzene based polymers as photoactive supports and micellarstructures for applications in biology. *J.Photochem. Phtobio. A* **2014**, *291,* 16-25.

(75) Barille, R.; Janik, R.; Kucharski, S.; Eyer, J.; Letournel, F.; Photo-responsive polymer with erasable and reconfigurable micro- and nano-patterns: An in vitro study for neuron guidance. *Colloid. Surface. B.* **2011**, *88,* 63-71.

Chapter 2

Synthesis of Azopolymer Brushes via RAFT by "Grafting From" Method

Abstract. A simple and reliable method was developed for synthesizing high graft density polymethacrlyic acid (pMAb) brushes via RAFT polymerization technique using "grafting from" approach. The thickness and graft density of brushes were controlled by varying the RAFT agent concentration and polymerization time. AFM, ellipsometry and contact angle confirmed that the brushes were uniformly grown on the glass surface. Further, these azopolymer brushes were post modified with a derivative of a well-known azobenzene (Disperse Red 1) on the side chains and a cyanine 5 dye (Cy5) on top of the polymer brush. Finally, these azopolymer brushes were found to be biocompatible when tested with NIH-3T3 cells.

2.1 Introduction

Polymer brushes (PBs) can be defined as long-chain macromolecules that are attached with an anchor site to a surface.[1] An interesting class of smart macromolecular brushes consist of stimuli-responsive polymer brushes because their assemble and properties can be tuned in an accurate and predictable manner by using an external stimulus.[2] Such type of smart PBs have attracted substantial research interest in the latest years since they play an important role in a wide range of applications in several areas of materials science research and technology.[3,4] Physico-chemical properties and shape of polymers usually show rapid and reversible changes in response to small changes in the environment (e.g., solvent, ionic strength, electrochemistry and pH).[5-8] Synthetic strategies for preparing polymer thin films made up of polymer brushes use the "grafting from" and "graft to" techniques.[9] The "grafting from" strategy normally yields a higher graft density of polymers with controllable coverage on the surface than "graft to" approach.[10] In the "grafting from" approach, an initiator bound to the substrate enables an easy control on the thickness and density of the polymer brushes using a wide range of polymeric techniques such as living ring-opening metathesis polymerization (ROMP),[11] anionic polymerization or controlled radical polymerization (CRP) i.e. nitroxide-mediated polymerization (NMP),[12] atom-transfer radical polymerization (ATRP)[13] and reversible addition fragmentation chain transfer polymerization (RAFT).[14,15] RAFT polymerization[14] has been successfully applied to grow well-controlled brushes on substrates to alter the surface properties of the materials. This polymerization technique has also been used to obtain inorganic particles with

controlled polymer hair size including gold, silica/silicon as well as glass surfaces.[10,16-18] The RAFT agent can be immobilized on the substrate, then initiator and monomer are added together to start the radical polymerization or radicals can be generated on the surface itself by covalent attachment of an initiator and RAFT agent is added in a second stage, while monomer is introduced in the reaction mixture at the very latest stage.[13] Two methods are available for immobilization, the RAFT agent can either be attached via its R-group (anchoring side) or Z-group, the macroinitiator site, where reaction propagates (for a better understanding of the RAFT method a graphical representation of this approach can be found in Chapter 1 in Figure 1.8).

In our work we have exploited the RAFT strategy to prepare well-defined biocompatible and light sensitive polymer brushes, with the attachment of the RAFT agent via its R-group to a glass surface. In this case, we expect that no thiocarbonylthio group would have been lost during the course of the polymerization since the RAFT agent always stay covalently attached close to the surface. In solution polymerization, some amount of thiocarbonylthio group may cleave due to side reactions (termination by combination of high propagation of RAFT agent) leads to ‘‘dead’’ polymer.[19] In this chapter, we discuss about the synthesis of different type of polymer brushes with the thickness of 150 to 200 nm. Thickness of the brushes was controlled by varying polymerization time as well as concentration of RAFT agent. Furthermore, azopolymer brushes were tested for biocompatibility with NIH-3T3 cell line.

2.2 Experimental section

General Materials and Methods. In general all chemicals and solvents were purchased from Sigma-Aldrich and used as received, while Cyanine 5 maleimide was purchased from Lumiprobe Corporation.

Atomic Force Microscope (AFM). AFM measurements were performed on polymer brush substrates. A JPK AFM Nanowizard was used and commercial tips (Bruker) were employed to scan in contact mode all over the samples with a resonance frequency of 50 kHz and a spring constant of 0.10 N/m. Measurements were carried out in air at 23 °C.

X-Ray Photoelectron Spectroscopy (XPS). XPS data were recorded on a Quantera SXM system from ULVACPHI or on an Axis Ultra from Kratos Analytical. High-resolution spectra were acquired applying pass energy of 69 eV.

XPS experiments were performed in collaboration with Dr. Micaela Castellino under the supervision Prof. Fabrizio Pirri (IIT, Torino. Italy)

Contact Angle. Water contact angles were measured by sessile drop technique using a KSV-CAM 200 instrument. This technique gives information about solid surface tension from contact angle of a liquid drop on a surface, using Young's equation. This can be easily performed by establishing the tangent of the angle at the base, between the solid surface and the drop. Following the standard procedure, contact angle was measured to analyze the wettability of polymer brushes. 4 µl MilliQ (18 MΩ cm^{-1}) water was dropped on polymer brushes with 5.5 µl/sec dispense rate.

Ellipsometry. Spectroscopic ellipsometry measurements were performed with a Nano film ep3SE instrument (Accurion, Germany)

equipped with a He-Ne laser (λ = 658 nm) and a spectroscopy lamp (Xe arc) for multiple-wavelength spectra. Ellipsometry measures the changes in polarization that occurs upon reflection of a light beam from a sample, typically a thin film deposited on a reflective substrate. The changes in polarization depend upon the thickness and refractive index of the composite layers. These features are not measured directly, but calculated from model fitting of the optical parameters, Δ and Ψ, which are related to the changes in polarization of the surface structure of the sample. Ellipsometry measurements were conducted in air configuration at fixed temperature of 25 °C. Measurement was carried out using a xenon lamp and a 5× objective by measuring at 631 nm with a variable angle of incidence (AOI) between 50° and 60° (step of 0.5°). The refractive index of 1.474 for transparent glass was used for data fitting.

UV Spectrophotometer. UV absorption was measured on polymer brushes with a UV CARY 100 scan spectra photometer (VARIAN, Australia). A polymer brush sample was mounted in the center of a 3×1.5 cm cardboard used as holder. Data interval of 1 nm and a scan of 600 nm/min were used. The base line was corrected by using a bare glass with zero transmittance. Spectra were recorded from 350 to 800 nm (glass absorption was till 350 nm).

Gel Permeation Chromatography (GPC). GPC analysis was done on polymer samples in aqueous column (Yarra 3µm SEC 200, 300×7.8 mm), equipped with an ELS detector. The flow rate was 1 ml/minute and pressure was 80 PSI. Four poly(MA) standards (Sigma-Aldrich) were used to calibrate GPC.

Mass Spectrometry (MS). Spectra were acquired with an Agilent Technologies 6530 Accurate Mass instrument, equipped with an ESI

source, operating at 4 kV needle voltage and 320 ºC, with a complete HPLC system, equipped with MS pump, an auto-sampler, a Q-TOF detector which can be coupled with a photo diode array detector (DAD). An extend-C18 column (2.1×50 mm) was used for the analyses. Buffer solutions employed were: known MS reference buffer in acetonitrile; water and acetonitrile with 0.1% of formic acid as eluent solutions and isopropanol with 30% of acetonitrile for column washing. Each sample was prepared at the concentration of 0.5 mg/ml, injecting 5-20 µl each run.

Nuclear Magnetic Resonance Spectroscopy (NMR). ^{1}H and ^{13}C spectra were acquired with an Agilent Premium Compact+ instrument (600 MHz). Chemical shifts are reported in ppm, calibration was done on the deuterated solvent used in the experiments by the related software function. The abbreviations used are: s = singlet, d = doublet, dd = doublet of doublets, t = triplet, m = multiplet and br = broad. 2D homonuclear. All measurements were performed at room temperature solubilizing 2-3 mg of each compound in deuterated solvents.

DOSY NMR. Typically, 1 mg of sample was dissolved in 700 µl of D_2O. ^{1}H and ^{1}H detected DOSY experiments were performed at room temperature on an Agilent DD2 NMR spectrometer operating at 600 MHz and equipped with an Agilent multinuclear *z*-gradient inverse one probe head capable of producing gradients in the *z* direction with a strength of 55 G cm^{-1}.

Synthesis of Sample 1. A cleaned glass coverslip (22x22 mm) was activated by oxygen plasma irradiation (intensity 400 W, oxygen pressure 0.1 mmHg) for 3 minutes in a plasma dry cleaner. Immediately after plasma oxidation, 3-aminopropyltriethoxysilane (APTES) solution

(2.13 mmol of APTES in 100 ml of absolute ethanol and 3 ml of acetic acid) was added on the glass coverslip for 5 minutes at room temperature. Glass substrate was washed with ethyl alcohol and dried in a vacuum oven for 2 hours at room temperature.

Synthesis of Sample 2. 50 ml corning flask was washed and dried. All the chemicals, syringes and corning flask were placed inside the glove box for 30 minutes with nitrogen flow. 0.32 mmol (21.55 mg) of 4-cyano-4-((dodecyl sulfonyl thiocarbonyl) sulfonyl pentanoicacid (RAFT agent), 0.97 mmol 15µl) of 1,3-diisopropylcarbodiimide (DIC) and 0.085 mmol (13 mg) of 1-hydroxybenzotriazole hydrate (HOBt) were added to the corning flask and stirred for 1 hour at room temperature. Glass substrate (Sample 1) was set in the corning flask containing the reagent solution and reaction was conducted at room temperature on an oscillating plate. After 24 hours the reaction was stopped and the unimmobilized RAFT agent and other reagents were washed with *N,N*-dimethylformamide (DMF). The washing process was repeated three times with DMF and then a fourth wash was given with acetone and the sample was dried for two hours at room temperature. The entire process was performed inside the glove box.

Synthesis of poly(MA) brushes (pMAb). 25 ml round bottom flask and 5 ml vial were washed and dried. All chemicals and dried glass apparatus were placed inside the glove box under nitrogen flow for 30 minutes. 8 mmol (689 mg) of methacrylic acid (MA) was weighed and transferred into the 25 ml round bottom flask, followed by 10 ml of dry methanol. 2.4 µmol of 1,1-azobis (cyclohexane carbonitrile) was weighed and transferred into the 5 ml vial and 2 ml of dry methanol was added to dissolve the initiator and made a homogenous solution. Both

monomer and initiator solutions were taken out from the glove box. The monomer in the 25 ml round bottom flask was degassed by a freeze-thaw cycle, repeated three times, to remove dissolved oxygen. Nitrogen was bubbled for 30 minutes to degas the initiator solution. After that, monomer and initiator solutions were transferred into a 50 ml corning flask, which contained RAFT immobilized glass coverslip Sample **2**, under nitrogen atmosphere. The corning flask was sealed by teflon tape and heated at 70 °C for 6 hours. The reaction was stopped by exposure to air. The glass substrate was washed with methanol by sonicating for 20 minutes at room temperature. The washing process was repeated three times to remove unimmobilized polymer on the glass substrate. Washed glass substrate was dried in a vacuum oven at 30 °C for 24 hours with 1 mm Hg of vacuum.

Synthesis of pMA (solution RAFT polymerization). 25 ml round bottom flask and 5 ml vial were washed and dried. All chemicals and dried glass apparatus were placed inside the glove box under nitrogen flow for 30 minutes. 8 mmol (689 mg) of MA and 0.027 mmol (11.5 mg) of RAFT agent were weighed and transferred into the 25 ml round bottom flask, followed by addition of 10 ml of dry methanol. 2.4 µmol of 1,1-azobis(cyclohexane carbonitrile) was weighed and transferred into the 5 ml vial and 2 ml of dry methanol was added to dissolve the initiator and made a homogenous solution. Monomer (MA), RAFT agent and initiator solutions were taken out from the glove box. The monomer solution in the 25 ml round bottom flask was degassed by freeze-thaw cycle, repeated three times, to remove dissolved oxygen, while nitrogen was bubbled for 30 minutes to degas the initiator solution. After that, initiator solution was added into the 25 ml round

bottom flask, which contained RAFT agent and MA monomer, under nitrogen atmosphere. The round bottom flask was sealed by teflon tape and heated at 70 °C for 6 hours. The reaction was stopped by exposure to air. Polymer solution was precipitated in diethyl ether and filtered. Precipitated polymer was again washed with diethyl ether several times to remove unreacted RAFT agent and monomer. Finally polymer (pMA) was dried in a vacuum oven at 50 °C for 24 hours. pMA appeared as white powder.

Synthesis of compound a. 0.32 mmol (100 mg) of Disperse Red 1 (DR) ((*N*-ethyl-*N*-(2-hydroxyethyl)-4-(4-nitrophenylazo) aniline) was dissolved in 10 ml of dichloromethane (DCM). 0.77 mmol (2.4 equiv., 88.19 mg) of methanesulfonyl chloride and 0.96 mmol (3 equiv., 1.33 ml) of triethyl amine (TEA) were added drop wise at 0 °C and the reaction was stirred for 30 minutes at room temperature. The product was confirmed by thin layer chromatography (TLC). The mixture was washed with a saturated solution of bicarbonate, and then the product was extracted with DCM and washed again with a saturated sodium chloride solution. Finally, the DCM layer was dried over sodium sulphate and filtered. The DCM was evaporated to get a fluffy red powder. Crude product was used directly for the next step without further purification. The obtained intermediate product was reacted for 2 hours with 0.64 mmol (2 equiv., 41.60 mg,) of sodium azide in 1.5 ml of DMF at 85 °C. The product was purified by column chromatography by using toluene as an eluent. MS for $C_{15}H_{17}N_7O_2$: calculated for $[M+H]^+$ = 339.14 m/z, found (ESI) $[M+H]^+$ = 339.14 m/z. 0.27 mmol (90 mg) of the desired product was reacted with 0.40 mmol (1.5 equiv., 104 mg) of triphenylphosphine in a mixture of water/tetrahydrofuran (THF) 35/65

(v/v) at room temperature for 24 hours. The reaction was followed by TLC. The THF was evaporated and the product was extracted with DCM. The DCM layer was washed with a saturated bicarbonate solution and a saturated solution of sodium chloride. Finally, the combined DCM layers were dried over sodium sulphate and filtered. The DCM was evaporated to get a fluffy red powder. Further, purification of the product was done by column chromatography with a mixture of methanol/dichloromethane 8/92 (v/v). MS for $C_{15}H_{19}N_5O_2$: calculated for $[M+H]^+$ = 313.15 m/z, found (ESI) $[M+H]^+$ =313.15 m/z. ^{1}H-NMR (600 MHz, DMSO-d6, δ): 8.35 (d, 2H, aa^1), 8.19 (s, 2H, bb^1), 7.91-7.80 (dd, 2H, cc^1), 6.91 (t, 2H, dd^1), 3.45–3.57 (m, 2H, ee^1), 2.75 (t, 2H, f), 1.23 (t, 3H, g). ^{1}H-NMR spectrum and assigned chemical shifts are shown in Figure 2.9.

Synthesis of azo-pMAb 1. Glass substrate of pMAb was transferred into a corning flask and 10 ml of tetrahydrofuran was added and kept shaking for activation of the carbonyl groups. 50 mole % of thionyl chloride with respect to carbonyl groups (0.012 mmol, 1 µl) was added drop wise and the reaction was continued for 12 hours at room temperature. Glass substrate was washed with tetrahydrofuran and dried under nitrogen flow, then the substrate was placed in the 25 ml corning flak and a solution of 50 mole % of compound **a** (DR) (0.012 mmol) in 5 ml of DMF was added. After 12 hours the reaction was stopped and the substrate was washed with water. Washing was repeated for 3 times with DMF and finally with acetone (each washing step was done under sonication for 30 minutes). The quantification of DR on polymer brushes was obtained by UV measurements by applying standard Beers Lamberts law, A= εlc, for molar absorptivity determination. Where, A

is the absorbance of DR at 483 nm, ε is the molar absorptivity ($Lmol^{-1}cm^{-1}$), l is the length of the optical path (1cm) and c is the concentration of the compound. The molar absorptivity of DR in ethanol was calculated as $\varepsilon = 24299\ Lmol^{-1}cm^{-1}$. The 7% DR was grafted on polymer brushes according to above calculation, in short is called as azo-pMAb 2a). Dried glass sample (azo-pMAb 2a) was transferred into a 50 ml corning flask. A solution of 1.5 mmol (125 µl) of propyl amine in 20 ml of DMF was added and the reaction was left shaking on an oscillating plate for 3 hours. 15 mmol (2 mg) of cyanine 5 maleimide (maleimide-Cy5) was added and the reaction was continued for 24 hours at room temperature. After 24 hours the glass substrate was washed with DMF for 30 minutes shaking on an oscillating plate. Washing procedure was repeated for 5 times to remove unreacted maleimide-Cy5 until no fluorescence was left in the washed water. Finally, glass substrate was immersed in DMF for 24 hours, and then washed with acetone and dried in a vacuum oven for 2 hours at 30 °C.

Synthesis of azo-pMAb 2a and 2b. Glass substrate of pMAb was transferred into a corning flask and 10 ml of tetrahydrofuran was added and kept shaking for activation of the carbonyl groups. 50 mole % of thionyl chloride with respect to carbonyl groups (0.012 mmol, 1 µl) was added drop wise and the reaction was continued for 12 hours at room temperature. Glass substrate was washed with tetrahydrofuran and dried under nitrogen flow, then the substrate was placed in the 25 ml corning flak and a solution of 50 mole % of compound **a** (0.012 mmol) in 5 ml of DMF was added. After 12 hours the reaction was stopped and the substrate was washed with water. Washing was repeated for 3 times with DMF and finally with acetone (each washing step was done under

sonication for 30 minutes). To increase DR substitution, reaction time was increased to 12 hours, so that it was possible to obtain a DR grafting up to 20%. Further, increases the reaction time to 24 hours, DR % did not change. The quantification of DR on polymer brushes was obtained by UV measurements by applying standard Beers Lamberts law, A= εlc, for molar absorptivity determination. Where, A is the absorbance of DR at 483 nm, ε ($Lmol^{-1}cm^{-1}$) is the molar absorptivity, l (1 cm) is the length of the optical path and c is the concentration of the compound. The molar absorptivity of DR in ethanol was calculated as ε = 24299 $Lmol^{-1}cm^{-1}$.

Synthesis of Cy5-pMAb. Glass substrate with pMAb was transferred into a 50 ml corning flask. A solution of 1.5 mmol (125 µl) of propyl amine in 20 ml of DMF was added and the reaction was left shaking on an oscillating plate for 3 hours. 15 mmol (2 mg) of maleimide-Cy5 was added and the reaction was continued for 24 hours at room temperature. After 24 hours the glass substrate was washed with DMF for 30 minutes with shaking, and the washing process was repeated for 5 times to remove unreacted maleimide-Cy5. Finally, glass substrate was immersed in DMF for 24 hours, and then washed with acetone and dried in a vacuum oven for 2 hours at 30 °C.

Cell Culture. NIH-3T3 fibroblasts were cultured in low glucose DMEM and incubated at 37 °C in a humidified atmosphere of 95% air and 5% CO_2. Prior to cell seeding, azopolymer brush substrates were sterilized under UV light for 30 minutes. After 24 hours cells were fixed with 4% paraformaldehyde for 20 minutes and then permeabilized with 0.1% Triton X-100 in PBS for 3 minutes. Actin filaments were stained with TRITC-phalloidin. Samples were incubated for 30 minutes at room

temperature in the phalloidin solution (dilution 1:200). Focal adhesions (FAs) were stained with vinculin. Briefly, cells were incubated in an anti-vinculin monoclonal antibody solution (dilution 1:200) for 2 hours and then marked with Alexa Fluor 488 conjugated goat anti-mouse antibody (dilution 1:1000) for 30 minutes at 20 °C. Finally, cells were incubated for 15 minutes at 37 °C in Hoechst solution to stain the cell nuclei. A TCS SP5 confocal microscope (Leica Microsystems) was used to collect fluorescent images of cells on azopolymer films. The laser lines used were 488 nm (vinculin), 543 nm (actin) and 700 nm (nuclei). Emissions were collected in the 500-530 nm, 560-610 nm and 400-450 nm ranges, respectively.

2.3 Results and Discussions

2.3.1 RAFT synthesis of pMAb.

Photosensitive polymer brushes were synthesized via RAFT polymerization technique by "grafting from" approach. RAFT polymerization is one of the finest synthetic methodologies to achieve polymers having narrow polydispersity index and high graft density. Moreover, by using this technique, besides controlling the molecular weight of the polymer, it is possible to obtain functional groups at both ends of the chain (head and tail), thus, following for further modification on these sites. In this work the polymer has grown from one end (the head) from glass surfaces. Glass surface was activated via plasma oxygen treatment and silanized with 3-aminopropyltriethoxysilane (APTES, Sample 1). 4-cyano-4-(dodecylsulfanylthiocarbonyl) sulfonyl pentanoicacid (RAFT agent, also known as Chain Transfer Agent) was reacted with Sample 1 by acid/amine coupling reaction. The AFM and XPS results were in good

agreement with RAFT agent immobilization on silanized glass surface as presented below in Figure 2.1 and 2.2.

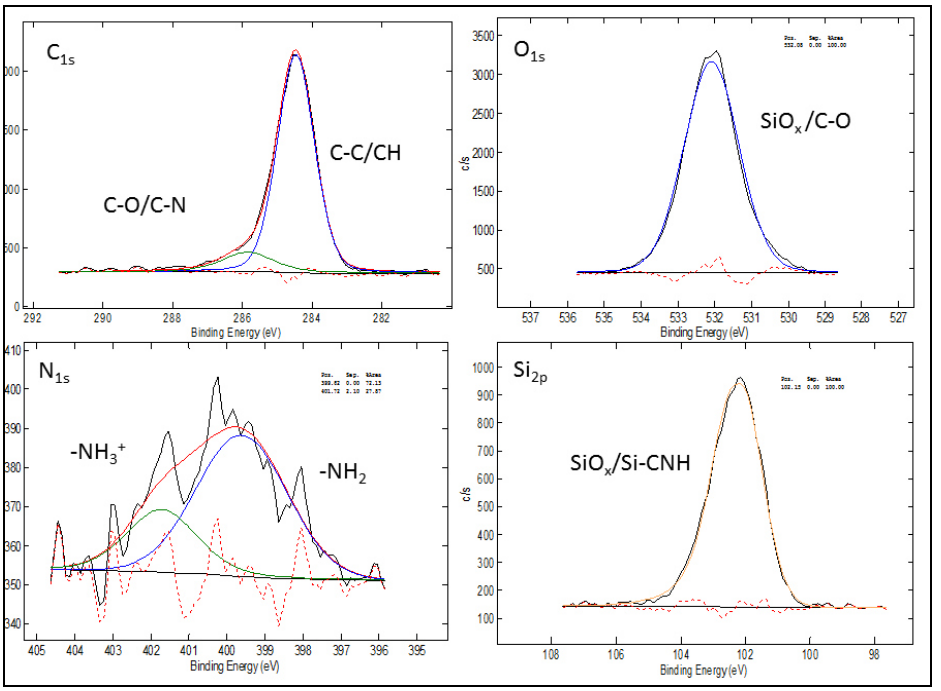

Figure 2.1. Binding energy of silanized glass sample 1 (C_{1s}, O_{1s}, N_{1s} and Si_{2p}) by XPS.

The N_{1s} peak showed a main component at 400.0 eV attributed to amine (NH_2). An additional component appeared clearly near 401.6 eV in silanized samples, indicating the presence of protonated amines. The binding energy of SiO_x was confirmed at 532 eV.

AFM image showed that silanized glass (Sample 1) was 2 nm thick and silanization occurred uniformly on the glass surface as shown in Figure 2.2A. Further treatement with RAFT agent (Sample 2) thickness increased to 6-8 nm (Figure 2.2B). Hence, AFM images revealed that also RAFT agent was uniformly immobilized on the glass surface.

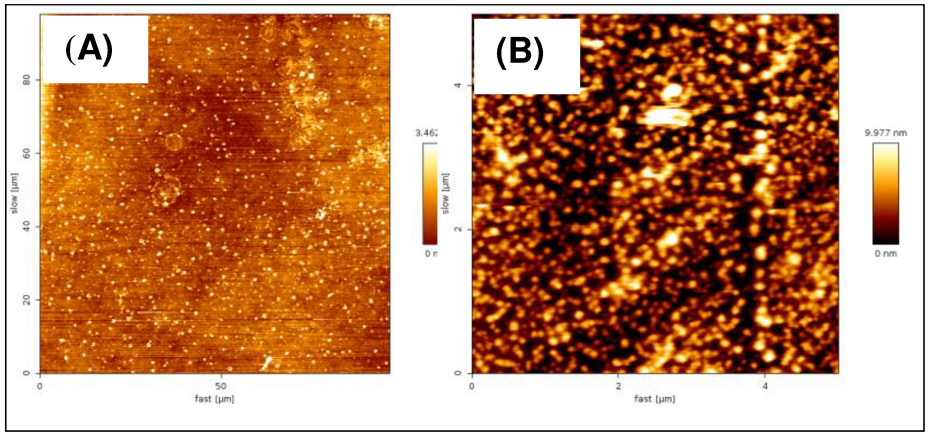

Figure 2.2. AFM images of (A) silanized glass (Sample 1) and (B) RAFT immobilized on silanized glass (Sample 2).

Different polymer brushes were synthesized by reacting with the RAFT immobilized glass (Sample 2) with methacrylic acid (MA) and 1,1′-azobis-(cyanocyclohexane) initiator (I) as shown in Scheme 2.1.

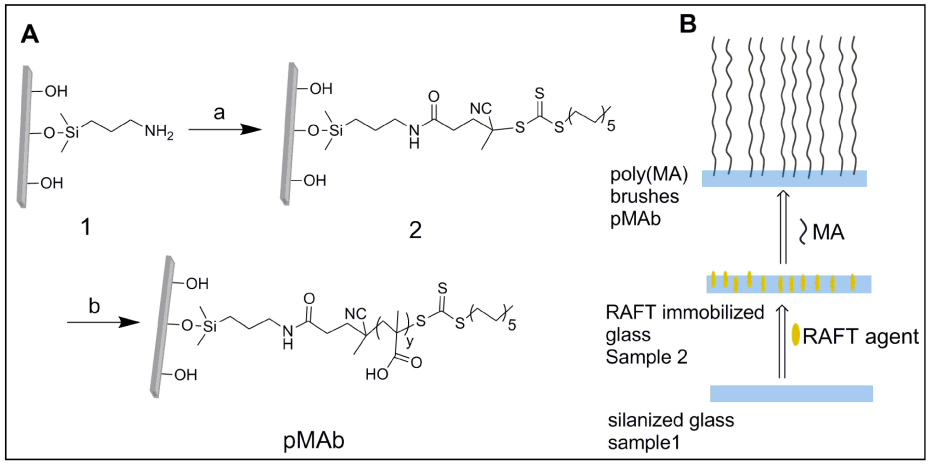

Scheme 2.1. (A) Synthesis of pMAb via RAFT "grafting from" method. Reagents and conditions. a) 1.2 equiv., RAFT agent, DIC, HOBT in DMF at RT for 24 h. b) 689 mg of MA monomer and 1 mg initiator in MeOH at 70 °C for 6h. The DP of MA was around 287 units (n), as calculated by using, thickness (ellipsometry), molecular weight and graft density. (B) Graphical representation of pMAb synthesis.

Polymer brushes having different thickness were obtained by tuning the molar concentration of RAFT agent with respect to monomer (1:1, 0.8:1, 0.7:1, and 0.5:1), as well as the polymerization time (from 6 to 24 hours). All reaction conditions and related thickness of the brushes are summarized in Table 2.1.

Sample	Condition				Thickness
	Time (h)	Temp (^{o}C)	Molar Concentration (M: CTA: I)	CTA (%)	(nm)
A	6	70	7.5:1:0.25	100	150
B	11	70	7.5:1:0.25	100	200
C	6	70	7.5:0.5:0.25	50	150
D	6	70	7.5:0.7:0.25	70	170

Table 2.1. Synthesis of different pMAb prepared at different conditions. CTA stands for Chain Transfer Agent. I means initiator. (* Thickness was measured by ellipsometry).

As presented in Figure 2.3, AFM analysis revealed that pMAb at condition C (0.5:1 RAFT agent, 0.25 mol % of I with respect to MA and 6 hours) was uniformly grown on the glass surface as compared to other conditions (B and D). Furthermore, even though sample A was also quite uniform, AFM images showed that the brushes were denser than in the other three cases and no free volume for further post modification on side chain of the polymer brushes was available. Thus, as we were interested to modify the side chains of the pMAb with disperse red (DR), conditions used for the preparation of sample C (0.5:1 RAFT agent, 0.25 mol% of I with respect to MA and 6 hours of polymerization

time) were selected as the best conditions to prepare polymer brushes of at least 150 nm thickness.

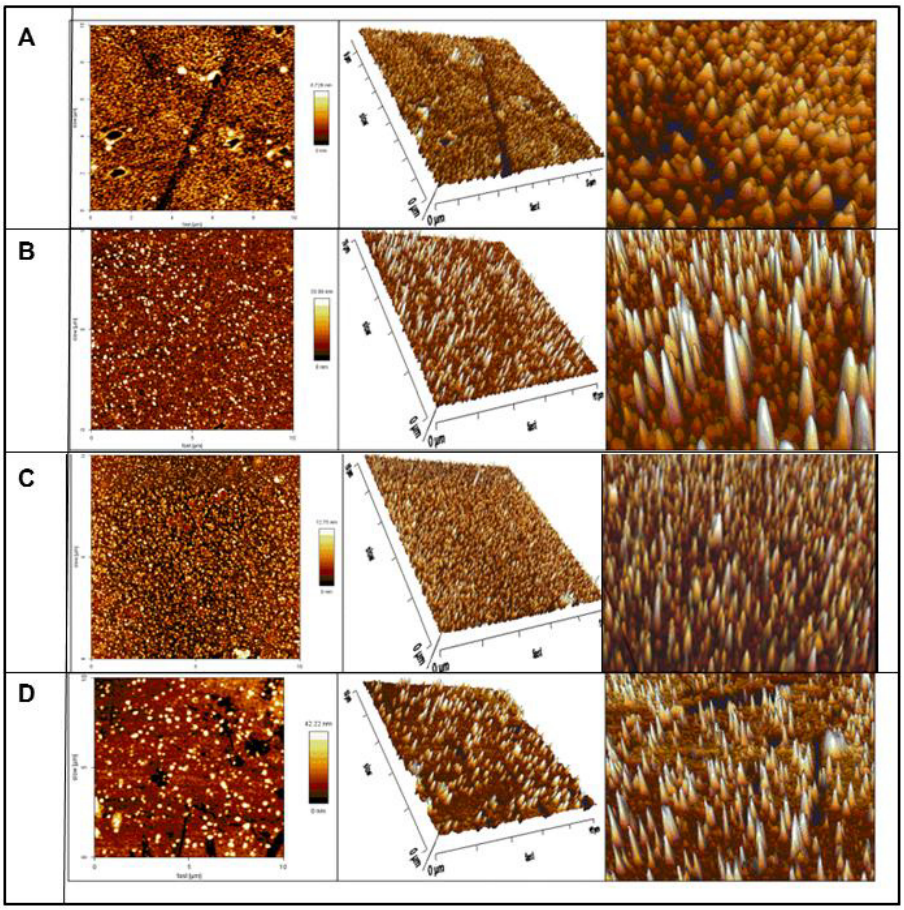

Figure 2.3. AFM images of pMAb synthesized using different conditions. (A) 6 h at 70 °C [M:CTA:I] = [7.5:1:0.25]; (B) 11 h at 70 °C [M:CTA:I] = [7.5:1:0.25], (C) 6 h at 70 °C [M:CTA:I] = [7.5:0.5:0.25] and (D) 6 h at 70 °C [M:CTA:I] = [7.5:0.7:0.25].

To gain information about the molecular weight of polymer brushes, we synthesized the same polymer but this time in solution (solution RAFT polymerization) applying our best conditions as shown in Scheme 2.2. The molecular weight of polymethacrlyic acid (pMA) was characterized

by GPC and found to be almost in the range of the targeted molecular weight planned before synthesis.

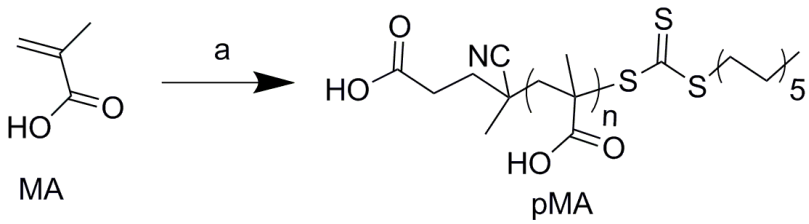

Scheme 2.2. Synthesis of pMA via RAFT method. Reagents and conditions. 689 mg of MA monomer, 0.027 mmol of RAFT agent and 1 mg initiator in MeOH at 70 °C for 6h. The DP of MA was around 287 units (n), as calculated by using, molecular weight (GPC) and DOSY-NMR.

The pMA was eluted by gel permeation chromatography (GPC) in water (Figure 2.4) and Mw was approximately 25000 g/mol.

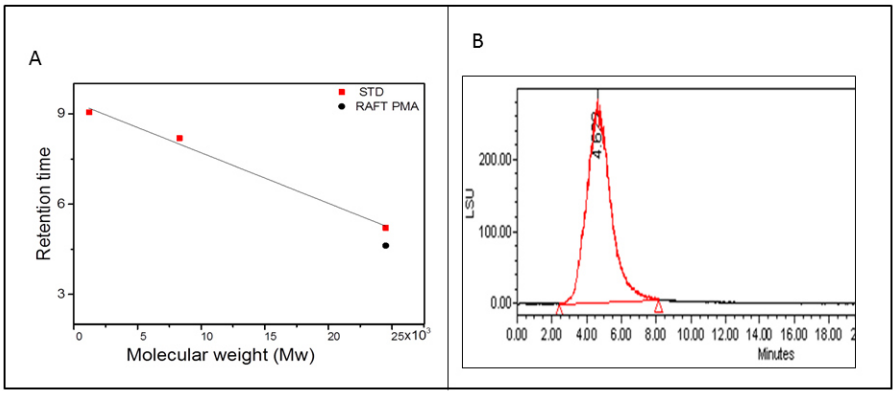

Figure 2.4. (A) Graph of retention time versus estimated molecular weight (red STD and black pMA synthesized by RAFT in solution) and (B) GPC chromatogram of pMA with condition RAFT 0.5 moles for 6 h.

To further check the molecular weight of the synthesized polymer, diffusion-ordered nuclear magnetic resonance spectroscopy (DOSY-NMR) was used as well. In this experiment, Stokes-Einstein equation was applied for estimating the value of diffusion coefficient (D) for

molecular species in aqueous solutions. $D= KT/6\pi\eta R_{h,}$ where *k* is the Boltzmann constant in J/K, *T* is the absolute temperature in K, η is the viscosity of the solution in N s m^{-2} and R_h is the hydrodynamic radius m.

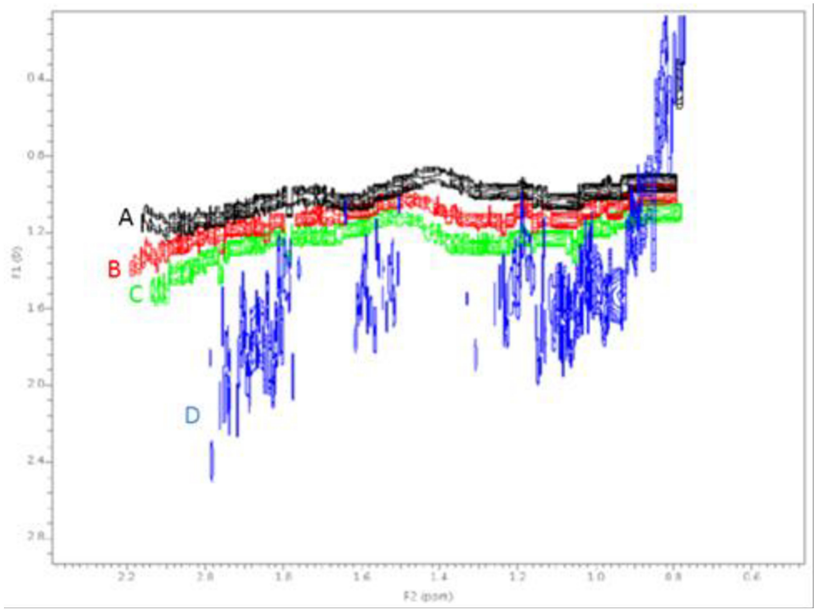

Figure 2.5. 2D DOSY spectra recorded in D_2O at 300 K with different polymerization conditions. (A) 6 h at 70 °C [M:CTA:I] = [7.5:1:0.25]; (B) 11 h at 70 °C [M:CTA:I] = [7.5:1:0.25], (C) 6 h at 70 °C [M:CTA:I] = [7.5:0.5:0.25] and (D) 6 h at 70 °C [M:CTA:I] = [7.5:0.7:0.25].

The linear correlation between the diffusion coefficient determined by DOSY and the molecular weight as originally noted by Johnson via equation $D = k\,[M]^{\alpha}$ was used. Here, D is diffusion coefficient, while k and α are partition coefficients of pMA in water.[20] Known values of partition coefficient k and α were used to obtain a molecular weight (Mw) of 22600 g/mol. Calculated molecular weight was close to the GPC estimated value (25 k to 22 k g/mol). Thus, based on this data

surface graft density of pMAb was estimated as much as 0.03-0.035 chains/nm^2, as calculated from the dry polymer layer height and its molecular weight by the following equation:

$$\mathcal{J}\left(\frac{chains}{nm^2}\right) = Dry\ thickness\ (nm) * \rho\left(\frac{g}{nm^3}\right) * \frac{6.02310^{23}}{Mn\left(\frac{g}{mol}\right)}$$

XPS spectrum of pMAb (Figure 2.6) was done at high-resolution scan of the C_{1s} signal.

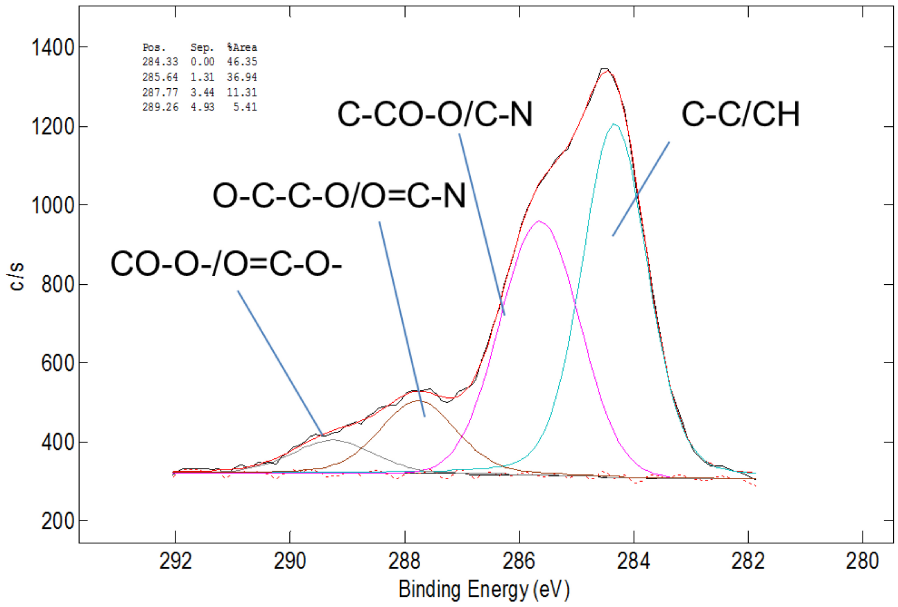

Figure 2.6. XPS results of pMAb.

In agreement with the elemental composition of pMAb, the survey spectrum only showed carbon and oxygen signals.[22] In the C_{1s} high-resolution scan, the carbon atom of the carboxyl group could be clearly distinguished at 288.5 eV relative to the aliphatic carbons. The binding energy of 290 eV showed C=O bond, while 288, 286 and 283 eV confirmed O=C-N, C-CO-O/C-N and C-C/CH bonds, respectively.

Each synthetic step was verified by contact angle measurements. Bare glass surface had a water contact angle of 65°, after immobilization of APTES (Sample 1) it was reduced to 45°, due to the presence of the amine group.

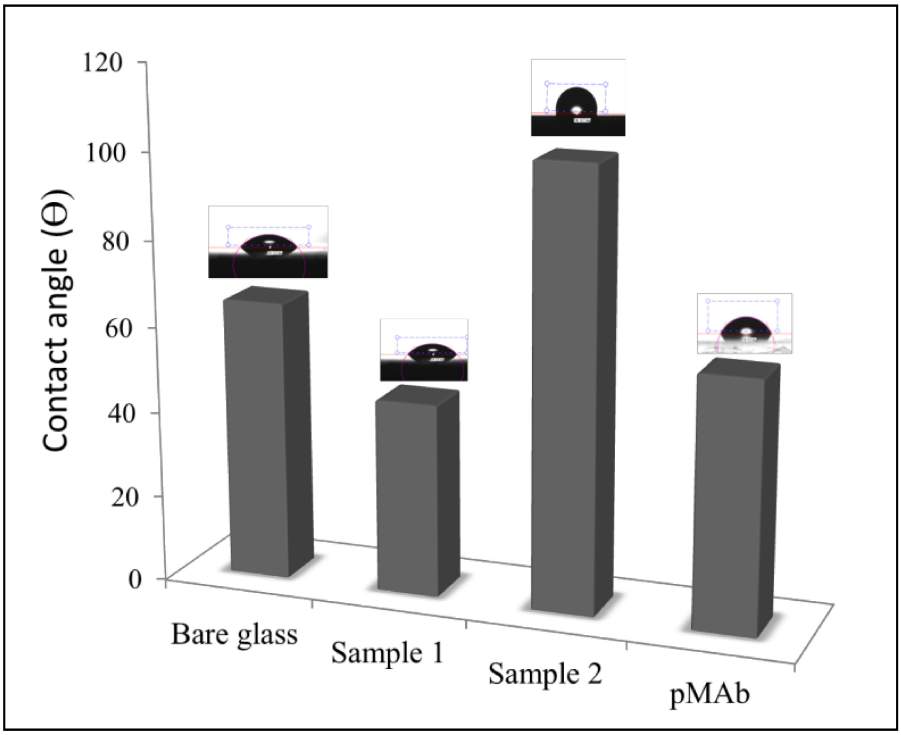

Figure 2.7. Water contact angle of Bare glass, Sample 1, Sample 2 and pMAb.

When RAFT agent was grafted (Sample 2), the contact angle increased to 105°, thus became more hydrophobic, due to the presence of long alkyl chain. Finally, after polymerization, the presence of hydrophilic pMAb (Sample C) was confirmed by a drop in contact angle to 63°.

Although we have analyzed the topology of polymer brushes by AFM, we wanted to know the morphology of pMAb. Hence we decided to characterize the brushes by scanning electron microscopy (SEM).

The morphology of the pMAb brushes was studied by scanning electron microscopy (SEM). However, it was difficult to see the regular morphology because of gold coating on the substrate.

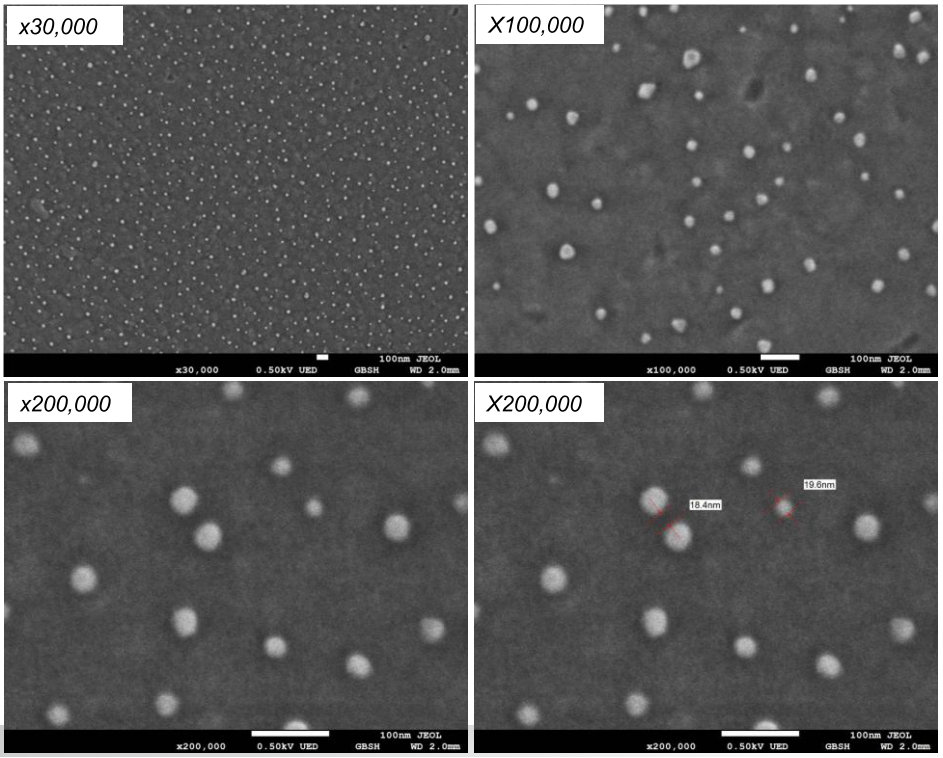

Figure 2.8. SEM images of pMAb 1kV electron gun with GBSH (5kV) and In-lens SE 30× resolution to 200× resolutions. The width of the polymer brushes was almost 19.6 nm and distance between brushes was 18.4 nm. Images were courtesy recorded at Jeol Company (France) that agreed on analyzing our brushes with this special technique.

2.3.2 Post Modification of pMAb

As we are interested in post modification on pMAb, we have further functionalized with azobenzene on the side chain of the pMAb and Cy5 maleimide on top of the polymer chain. An amine derivative of disperse

red 1 (compound **a**) was used,[23] which was synthesized from the commercial well-known disperse red 1 (DR 1) according to Scheme 2.3.

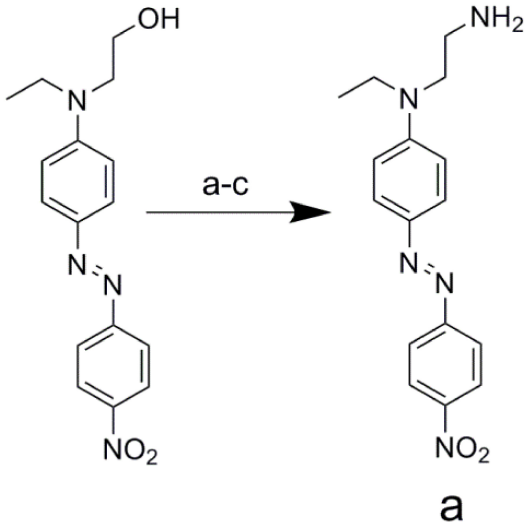

Scheme 2.3. Synthesis of compound **a**. Reagents and conditions. a) 2.4 equiv. of methanesulfonyl chloride, 3 equiv. of triethyl amine in DCM at RT, b) 2 equiv. of sodium azide in DMF at 85 °C for 2 h and c) 1.5 equiv. of triphenyl phosphine at RT for 24 h.

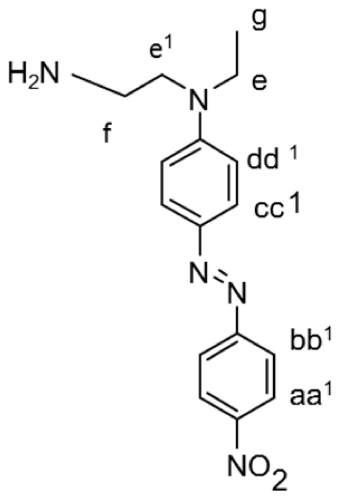

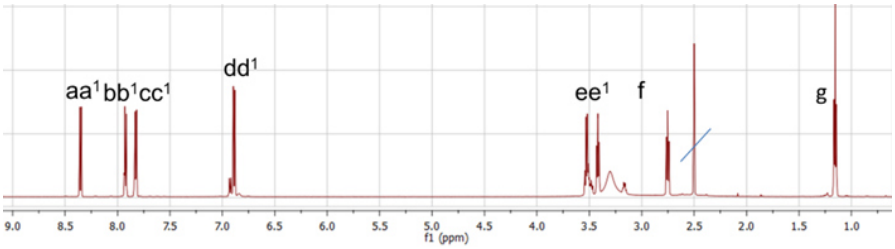

Figure 2.9. ^{1}H-NMR of compound **a** in DMSO-d6 (600 MHz) with assigned chemical shifts.

Azomodified pMAb were prepared by linking azobenzene to the side chain of pMAb by pre-treating the polymer brushes with thionyl chloride and reacting them with compound **a**. Using the above mentioned conditions we were able to achieve 7% of azobenzene functionalization to the side chains of the polymers as quantified by UV spectroscopy (named as azo-pMAb 2a in Scheme 2.4). When we increased reaction time, we could reach up to 20% of azobenzene grafting to the polymer brushes, which we called as azo-pMAb 2b.

Polymer	Condition		Grafted DR (%)
	Time (h)	Temperature (^{O}C)	
azo-pMAb 2a	6	65	7
azo-pMAb 2b	12	65	20
azo-pMAb 2b	24	65	20

Table 2.2. Synthesis of azo-pMAb 2a and 2b. Conditions and grafted DR percentage are reported.

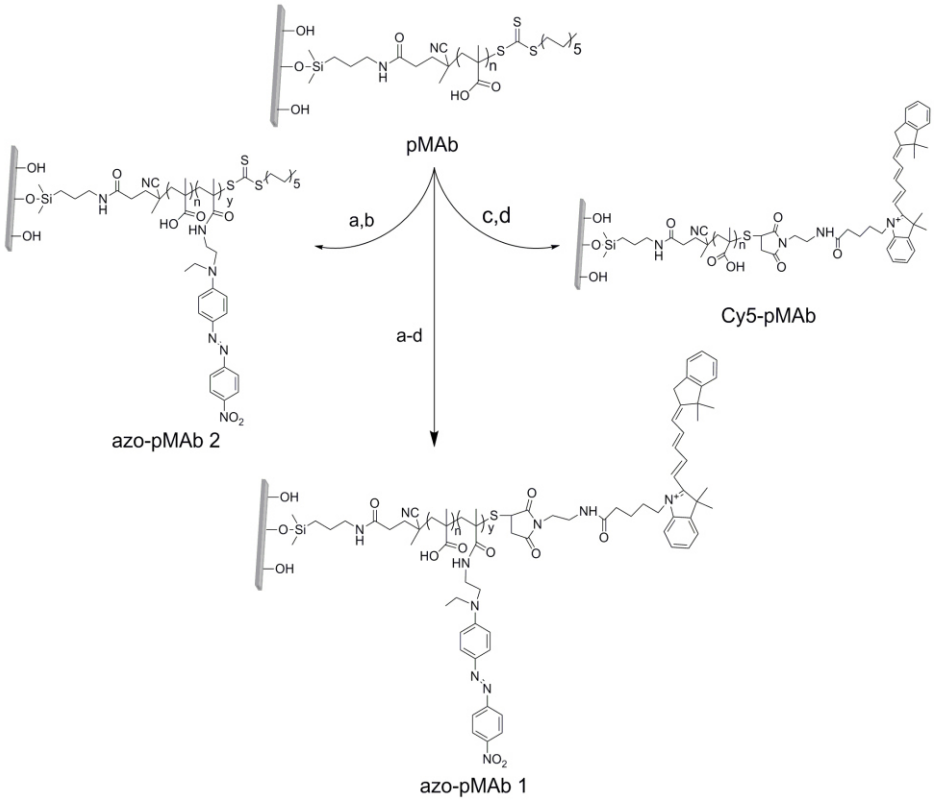

Scheme 2.4. Synthesis of azo-pMAb 1, azo-pMAb 2 and Cy5-pMAb. Reagents and conditions: a) 50 mole % of thionyl chloride in THF at RT for 6 h. b) 50 mole % DR-amine in DMF at RT for 12 h. azo-pMAb 2a (y ~ 7%) and azo-pMAb 2b (y ~ 20%). c) 20 mole % propyl amine in DMF at RT for 3h and d) 20 mole % maleimide-Cy5 in DMF at RT for 24 h. DP of MA was around 287 units (n), as calculated by using ellipsometry, molecular weight and graft density.

Next, 7% azobenzene containing brush was further functionalized with Cy5 dye on "top" of the brush tails by cleaving the alkylchain of the dithiol group with propyl amine through thiol/maleimide chemistry (Cy5-pMAb Scheme 2.4).

2.3.3 Biological Assay on Synthesized Azopolymer Brushes (azo-pMAb 2a).

Photoresponsive materials implemented as thin films provide a well original tools for biological applications.[24] Especially, the specialty of such type of polymers are chemical bond stability and durability in physiological-like conditions, which are important parameters for biological applications[24-28] In this Chapter we have conducted biocompatibility assay using NIH-3T3 cells on the synthesized azopolymer brushes.

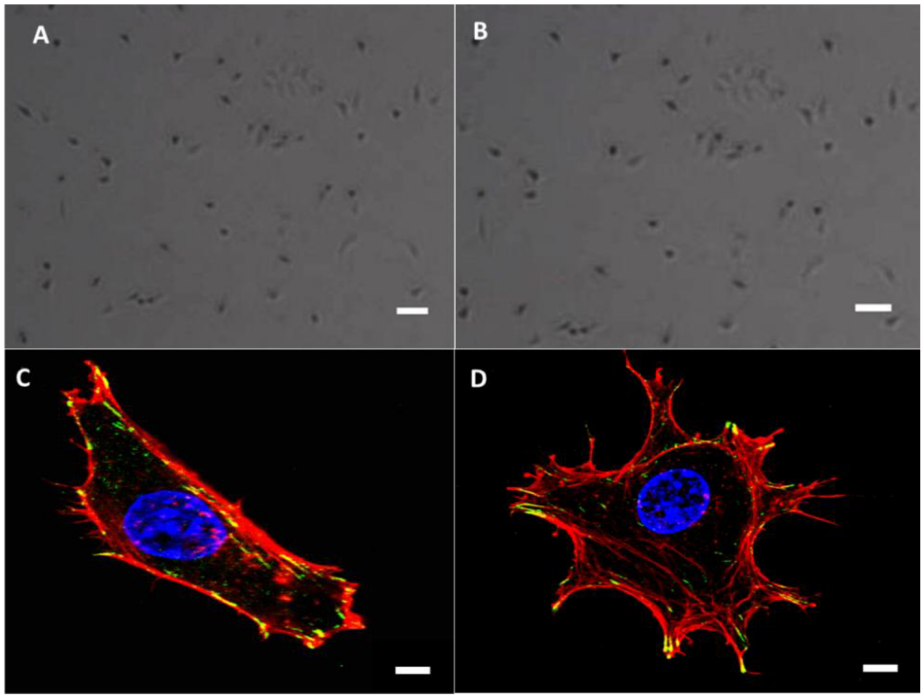

Figure 2.10. Bright field microscopic images, (A) and (B) represents the images of NIH-3T3 cells on azopolymer brushes after 24 h. Confocal images of cells on azopolymer brush. Detail of focal adhesion, stained with Alexa 488 labelled vinculin in green (C and D). Scale bar is 10 μm.

The cells were cultured on azopolymer brushes and observed in the first day after seeding. The cells were alive even after 24 hours (see in Figure 2.10 A and B) and it showed that azopolymer brushes were biocompatible to NIH-3T3. After 24 hours the cells were fixed on azopolymer brush substrate. Confocal microscope was used to collect fluorescent images of cells on azopolymer films (Figure 2.10 C and D).

2.4 Conclusion

A simple and reliable method for synthesizing high graft density polymer brushes via RAFT polymerization technique "grafting from" approach was developed, having thickness of 150 nm and refractive index of 1.50. The thickness and graft density of brushes were controlled by varying RAFT agent concentration and polymerization time. AFM, ellipsometry and contact angle confirmed that the brushes were uniformly grown on the glass surface. Thus, we could say that RAFT polymerization technique using 0.5 mole percentage of 4-cyano-4-((dodecyl sulfonyl thiocarbonyl) sulfonyl pentanoicacid (RAFT agent) and 0.25 mole percentage of initiator 1,1′-azobis-(cyanocyclohexane) with respect to monomer and 6 hours of polymerization time were the best conditions to synthesize high graft density polymer brushes (pMAb). Polymer brushes were further functionalized at their side chains with an azobenzene using an amine derivative of commercial disperse red 1 and a Cy5 dye was linked to the top of their tails. Furthermore, biocompatibility test was performed with these synthesized azopolymer brushes seeding NIH-3T3 cell line.

References

(1) Krieg, A.; Pietsch, C.; Baumgaertel, A.; Hager, M. D.; Becer, C. R.; Schubert, U. S.; Dual hydrophilic polymers based on (meth)acrylic acid and poly(ethylene glycol)-synthesis and water uptake behavior. *Polym. Chem.* **2010**, *1,* 1669-1676.

(2) Brown, A. A.; Azzaroni, O.; Huck, W. T. S.; Photoresponsive Polymer Brushes for Hydrophilic Patterning. *Langmuir.* **2009**, *25,* 1744-1749.

(3) Zhao, Y.; Ikeda, T.; *Smart Light-Responsive Materials: Azobenzene-Containing Polymers and Liquid Crystals.* Zhao, Y.;Ikeda, T., Eds. **2009**.

(4) Goulet-Hanssens, A.; Sun, K. L. W.; Kennedy, T. E.; Barrett, C. J.; Photoreversible Surfaces to Regulate Cell Adhesion. *Biomacromolecules.* **2012**, *13,* 2958-2963.

(5) Demirci, S.; Caykara, T.; High Density Cationic Polymer Brushes from Combined ‘‘Click Chemistry’’ and RAFT-Mediated Polymerization. *J. Polym. Sci. Pol. Chem.* **2012**, *50,* 2999-3007.

(6) Advincula, R. C.; Brittain, W.; Caster, K. C.; Rühe, J.; *Polymer Brushes.* **2004**; 1-250.

(7) Lee, H.-i.; Pietrasik, J.; Matyjaszewski, K.; Phototunable Temperature-Responsive Molecular Brushes Prepared by ATRP. *Macromolecules.* **2006**, *39,* 3914-3920.

(8) Idota, N.; Kikuchi, A.; Kobayashi, J.; Akiyama, Y.; Sakai, K.; Okano, T.; Thermal Modulated Interaction of Aqueous Steroids Using Polymer-Grafted Capillaries. *Langmuir.* **2006**, *22,* 425-430.

(9) Penga, S.; Bhushan, B.; Smart polymer brushes and their emerging applications. *Roy. Soc. Ch. Advances.* **2012**, *2,* 8557–8578.

(10) Kumar, S.; Lepage, Y. L. D. M.; Zhao, Y.; Surface-Grafted Stimuli-Responsive Block Copolymer Brushes for the Thermo-, Photo- and pH-Sensitive Release of Dye Molecules. *Macromolecules.* **2011**, *44,* 7385-7393.

(11) Edmondson, S.; Osborne, V. L.; Huck, W. T. S.; Polymer brushes via surface-initiated polymerizations. *Chem. Soc. Rev.* **2004**, *33,* 14-22.

(12) Mansfeld, U.; Pietsch, C.; Hoogenboom, R.; Becer, R.; Schubert, U. S.; Clickable initiators, monomers and polymers in controlled radical polymerizations – a prospective combination in polymer science. *Polym. Chem.* **2010**, *1,* 1560–1598.

(13) Pyun, J.; Kowalewski, T.; Matyjaszewski, K.; Synthesis of Polymer Brushes Using Atom Transfer Radical Polymerization. *Macromol. Rapid. Comm.* **2003**, *24,* 1043–1059.

(14) Keddie, D. J.; A guide to the synthesis of block copolymers using reversible-addition fragmentation chain transfer (RAFT) polymerization. *Chem. Soc. Rev.* **2014**, *43,* 496-505.

(15) Stenzel, M. H.; Zhang, L.; Huck, W. T. S.; Temperature-Responsive Glycopolymer Brushes Synthesized via RAFT Polymerization Using

the Z-group Approach. *Macromol. Rapid. Comm.* **2006**, *27,* 1121-1126.

(16) Stracke, A.; Wendorff, J. H.; Goldmann, D.; Janietz, D.; Stiller, B.; *Adv. Mater.* **2000**, *12,* 282.

(17) Angiolini, L.; Benelli, T.; Giorgini, L.; Golemme, A.; Salatelli, E.; Termine, R.; Side-Chain Multifunctional Photoresponsive Polymeric Materials. *Intech.* **200**, *187-212*.

(18) Shi, Y.; Zhu, W.; Chen, Y.; Synthesis of Cylindrical Polymer Brushes with Umbrella-Like Side Chains via a Combination of Grafting-from and grafting-onto Methods. *Macromolecules.* **2013**, *46,* 2391-2398.

(19) Stenzel, M. H.; Hairy Core–Shell Nanoparticles via RAFT:Where are the Opportunities and Where are the Problems and Challenges. *Macromol. Rapid Commun.* **2009**, *30,* 1603–1624.

(20) Liu, Y.; Bo, S.; Zhu, Y.; Zhang, W.; Determination of molecular weight and molecular sizes of polymers by high temperature gel permeation chromatography with a static and dynamic laser light scattering detector. *Polymer.* **2003**, *44,* 7209–7220.

(21) Sharma, K.; Kumar, V.; Kaith, B. S.; Som, S.; Kumar, V.; Pandey, A.; Kalia, S.; Swart, H. C.; Synthesis of Biodegradable Gum ghatti Based Poly(methacrylic acid-aniline) Conducting IPN Hydrogel for Controlled Release of Amoxicillin Trihydrate. *Ind. Eng. Chem. Res.* **2014**, *45-55,* 232–234.

(22) Tugulu, S.; Barbey, R.; Harms, M.; Fricke, M.; Volkmer, D.; Rossi, A.; Klok, H.-A.; Synthesis of Poly(methacrylic acid) Brushes via Surface-Initiated Atom Transfer Radical Polymerization of Sodium ethacrylate and Their Use as Substrates for the Mineralization of Calcium Carbonate. *Macromolecules.* **2007**, *40,* 168-177.

(23) Schuh, C.; Lomadze, N.; Rühe, J. r.; Kopyshev, A.; Santer, S.; Photomechanical Degrafting of Azo-Functionalized Poly(methacrylic acid) (PMAA) Brushes. *J. Phys .Chem B.* **2011**, *115,* 10431-10438.

(24) Baaca, H.; Leea, J.-H.; Seoa, J.-M.; Parka, T. H.; Chunga, H.; Leed, S.-D.; Kim, S. J.; Submicron-scale topographical control of cell growth using holographic surface relief grating. *Mater. Sci. Eng.* **2004**, *24,* 209-212.

(25) Barille, R.; Janik, R.; Kucharski, S.; Eyer, J.; Letournel, F.; Photo-responsive polymer with erasable and reconfigurable micro- and nano-patterns: An in vitro study for neuron guidance. *Colloid. Surface. B.* **2011**, *88,* 63-71.

(26) Ahmadi-Kandjani, S.; Self-organized surface relief gratings in azo-polymerthin-lms. *Ph.D. thesis.* **2007**, 1-193.

(27) Lee, J. K.; Baac, H.; Song, S.-H.; Lee, S.-D.; Park, D.; The Topographical Guidance of Neurons cultured on Holographic Photo-Responsive Polymer. *Conf. Proc. IEEE Eng. Med. Biol. Soc.* **2004**, 4970-4973.

(28) Georgiou, M. A. W. a. T. K.; Thermoresponsive Polymers for Biomedical Applications. *Polymers.* **2011**, *3,* 1215-1242.

Chapter 3

Studies on Azopolymer Brush Mobility by Fluorescence Correlation Spectroscopy

Abstract. The influence of the azobenzene molecules on azopolymer brush dynamics was investigated for the first time by fluorescence correlation spectroscopy (FCS). For this purpose we studied three types of polymer brushes: one containing a Disperse Red 1 derivative (DR) on the side chains and a cyanine 5 dye (Cy5) on top of the polymer brush (here named as azo-pMAb 1) and two other polymer brushes, one having only DR on the side chains, named azo-pMAb 2, and the last one with just Cy5 on top of the chains (Cy5-pMAb). In the case of azo-pMAb 1, two dynamics were observed, a short one coming from the fluctuations of azobenzene (DR) and a long one related to the main chain of the polymer brush, where Cy5 was linked. The reversibility of azo-pMAb 1 dynamics was investigated upon excitation at 488 nm in wet condition with 15 minutes of interval time. Furthermore, by using the 488 nm channel, we were able to study the *trans-cis-trans* isomerization process of azobenzene itself. Finally, when we increased the DR concentration on the polymer brushes (20% of DR functionalization, azo-pMAb 2b), a micrometric width pattern, resembling to SRG was observed.

The work described in this Chapter is part of a manuscript in preparation. R. H. Kollarigowda, I. De Santo, C. Rianna, A. C. Manikas, S. Cavalli and P. A. Netti. Shedding Light on Azopolymer Brush Mobility by Fluorescence Correlation Spectroscopy.

3.1 Introduction

Azopolymers have become versatile materials for the design and fabrication of smart light-responsive functional devices such as optical storage components, sensors, and biomaterials.[1-3] For this reason azomodified photosensitive materials received increasing attention over the last decades.[4] Specifically, irradiation of azobenzene with light causes a fast and efficient change of its molecular configuration.[1,4] In fact, upon irradiation with light,[5] the azobenzene molecule is known to undergo a reversible transition from the *trans* to the *cis* configuration that can be converted back again to the thermodynamically more stable *trans* isomer by light or heat.[6,7] When the azobenzene is linked to a polymer, the photo-isomerization reaction affects the properties of the entire polymeric material over several length scales.[8] The double bond of azobenzene (-N=N-) has different bonding angles in the *trans* and *cis* form, both length and shape of the photosensitive molecule change considerably, so that for the *cis* configuration changes in the volume occur that translate in a different topography of the whole materials.[7] Azopolymers have the distinctive physical phenomena to form surface relief gratings (SRGs) upon irradiation with interference patterns (e.g. Lloyd's mirror setup), that induces motion of the polymer chains and their accumulation on the surface with a profile that follow the light intensity pattern.[9] One of the earlier attempts made to explain this photoinduced mass-migration of the azobenzene containing polymer chains was considering pressure gradient using volume changes caused by the isomerization of the azobenzene.[10] However, this model could not explain the strong polarization dependence of the writing process. Among several theories developed to explain the mechanism of SRGs

formation,[11] Thripathy's group could clearly clarify about the light polarization dependence of the SRG formation investigating on azopolymer spin-coated materials.[12] The motion of the azo-chromophore depends on the driving forces, which are optically induced by electric field gradients.[13] The *trans-cis-trans* isomerization cycle is considered the trigger that assists in local plasticization of the film during exposure. Thus, in general, the formation of SRG on azopolymer thin films and diffraction efficiency depend on intensity modulation and total electric field vector pattern produced by the two polarized interfering beams and azobenzene chromophores are responsible for the strong polarization dependence of the grating formation.

In the case of azopolymer brushes, on the contrary, only a few recent examples of investigation on SRG formation are known. In particular, Santer and co-workers[14] showed the formation of an 100 nm pattern exploiting the classical Lloyd's mirror setup irradiating synthesized azopolymer brushes with linear polarized light.[14,15] However, little information is available on in-depth explanation about SRG formation within azopolymer brushes. Here we present an important argument on this issue. In fact, we report on the isomerization process of a specific azobenzene (Disperse Red 1, here in short DR) using fluorescence correlation spectroscopy (FCS),[16-19] that was recently demonstrated a useful technique for polymer dynamic studies[20,21] also in non-conventional situations.[22] Indeed, this technique, based on excitation through linear polarized light, prove to be a novel and powerful tool to study the dynamic of polymer brushes. In detail, we prepared a set of polymer brushes on glass surfaces by reversible fragmentation chain transfer radical polymerization (RAFT) technology using the "grafting

from" strategy. Then, a derivative of a well-known azobenzene, DR, was covalently linked to the side chains of the polymer brushes, while a cyanine dye (Cy5) was bound on "top" of the brush tails. FCS monitored the DR *trans* and *cis* state through variation in fluorescence intensities and fluctuations of both dyes. Furthermore, it allowed measuring the dynamics of azomolecules upon irradiation through the autocorrelation analysis of fluorescence intensity fluctuations of brushes in the wet state. This methodology allowed obtaining global information about azopolymer brushes mobility and aggregation process recording the polymer lateral mobility through their diffusion time (τ_{diff}). Finally, excitation through linear polarized light, commonly available in an optical microscopy setup, proved to be an innovative approach that permitted to generate SRG-like structures in a straightforward and easily observable manner.

3.2 Experimental Section

General Materials and Methods. Rhodamine 6G (Rh6g) and solvents were purchased from Sigma-Aldrich and used as received, while Cyanine 5 maleimide was purchased from Lumiprobe Corporation.

Fluorescence Correlation Spectroscopy (FCS). A commercial confocal fluorescence correlation spectroscope, Confocor III, (Carl Zeiss, Jena, Germany) was used to carry out FCS experiments. The polymer brushes were excited by Argon laser light at 488 nm (S polarizer, 25 mW), while Cy5 was excited by He-Ne at 633 nm (P polarizer, 5 mW). The laser beam was focused by an Apochromat 40× water immersion objective (numerical aperture 1.2). The emitted fluorescent light was collected by the same objective and separated from the excitation light by a dichroic mirror. The emission beam was

mapped onto a pinhole in the image plane of the objective (pinhole 35 μm). Fluorescent emission was sent to a 530-610 nm BP filter or to a 655 LP filter in correspondence of the two beam lengths, respectively and then acquired on the avalanche photodiodes (APDs). Fluorescence was detected by an APD in single-photon-counting mode. All ACFs were calculated directly from signal trajectories. The maximum lag time was set to 20 s for calibration measurements and to 100 s for measurements in polymer brush samples. Averaging was performed over an acquisition period up to 30 minutes for polymer brush measurements via a post ACF calculation.

Nanomolar solutions of Cy5 and Rhodamine 6G in water were freshly prepared for FCS calibration. Before performing FCS experiments, polymer brush glasses were washed with methanol and dried in a vacuum oven at 30 °C for 3 hours. The focus was positioned in correspondence of the maximum molecular brightness. Each experiment was carried out at least 5 times to have statistical information.

FCS analysis. Focal volume dimensions were calculated from $w_{xy}^2 = 4D\,\tau_{diff.}$. Here, the diffusion time, τ_{diff} was fit from ACFs of Rhodamine 6G (Rh6g) and Cy5 dye diffusing in water to a 3D diffusion model

$$G(\tau) = \frac{1}{\langle N \rangle}(1+\Theta)\left(\frac{1}{1+(\tau/\tau_{diff})}\right)\sqrt{\frac{1}{1+s^2(\tau/\tau_{diff})}} \qquad (1)$$

Where $\langle N \rangle$ is the mean number of particles, Θ is expressed as $\theta/(1-\theta)$ exp $(-\tau/\tau_\tau)$ where θ is the triplet kinetics fraction, τ_τ the triplet time and s the structure parameter, $s = w_z/w_{xy}$. The diffusion coefficients considered for each reference dye were D_{Rh6g} (25 °C) = 4.0×10^{-6} cm^2s^{-1} and D_{Cy5} (25 °C) = 3.6×10^{-6} cm^2s^{-1} Θ parameters were kept fixed to the values found in bulk measurements for both dyes ($\theta = 0.43 \pm 0.04$ and

τ_τ = 85 and Rh6g, respectively). For the measurement of Cy5 solutions, the lateral radius of w_{xy} was 260 ± 14 nm and the effective volume (V_{eff}) was 1 fl. Since DR 1 is not soluble in water and no information about its diffusion coefficient is available in the literature, we calibrated the optical path with Argon laser 488 nm excitation by using Rhodamine 6G (Rh6g). The lateral radius of w_{xy} was 220 ± 10 nm and effective volume V_{eff} was 1.3 ± 0.05 μm.

The diffusion times were normalized in order to compare measurements on different optical paths by the following equation $D=w_{xy}^2/4\tau_{diff}$. It comes, $\tau^R_{diff} / \tau^C_{diff} = w^R_{xy}{}^2 / w^C_{xy}{}^2 = 0.7$, where R and C represent Rh6g and Cy5 channels, respectively.

Since polymer brushes were grown on glass surface, all FCS data were analyzed with standard expression for 2D diffusion in a Gaussian excitation volume,[23] a single component 2D model was used.

$$G(\tau) = \frac{1}{\langle N \rangle}(1+\Theta)\left(\frac{1}{1+(\tau/\tau_{diff})}\right) \qquad (2)$$

Raman Spectroscopy. Spectra were acquired at room temperature with a DXR Raman spectrometer (Thermo Fischer Scientific) with 20 mW laser power. The Raman spectra were obtained using a diode laser at 532 nm with different intensity for each investigated sample (1÷5 mW). For 2D measurements on solid substrates a 50×/0.75 NA objective was utilized to focus the laser beam on the surface. The investigated area was chosen as a map of 950×600 μm size, with a step of 75 μm between each point (13×8 points map).

3.3 Results and Discussions

This work addresses the lack of information about the events that take part to the formation of SRG. Although many theories and models have

been used to explain the formation of SRG by using linear polarized light,[12,24,25] there are important issues, such as isomerization or aggregation process, that occurred at molecular level, which still need to be addressed. In our work, FCS technique allowed us to investigate the dynamics of photoinduced isomerization process in order to clarify how such a single molecular event can lead to the macroscopic phenomenon of mass- migration and aggregation yielding SRGs.

Synthesis of photoresponsive polymer brush was shown in detail in Chapter 2. In brief, polymer brushes were synthesized by RAFT technique using the "grafting from" strategy. An amine derivative of disperse red 1 (DR-amine, compound **a**)[14] as described in Scheme 2.3 (Chapter 2) was covalently bond to the side chain of pMAb by pre-treating the polymer brushes with thionyl chloride. Using these conditions we were able to achieve 7 to 20% of azobenzene functionalization to the side chains of the polymers as quantified by UV spectroscopy. Next, a Cy5 dye was linked on "top" of the brush tails by cleaving the akylchain in the dithiol group by propyl amine allowing thiol/maleimide coupling to occur (Scheme 2.4 in Chapter 2). Different polymer brushes were prepared and the corresponding short names and sketched structures are summarized in Chart 1.

These photoresponsive polymer brushes contain photosensitive groups in the side chains of the polymer backbone. According to T. Seki[26] the azobenzene groups orient preferentially parallel to the substrate, while polymer tail is growing perpendicular to that. In our FCS set up, linear polarized light is coming from the bottom perpendicular to the substrate itself with an S type of polarization (for Argon laser), thus in-plane with the chromophores, as illustrated in Figure 3.1A.

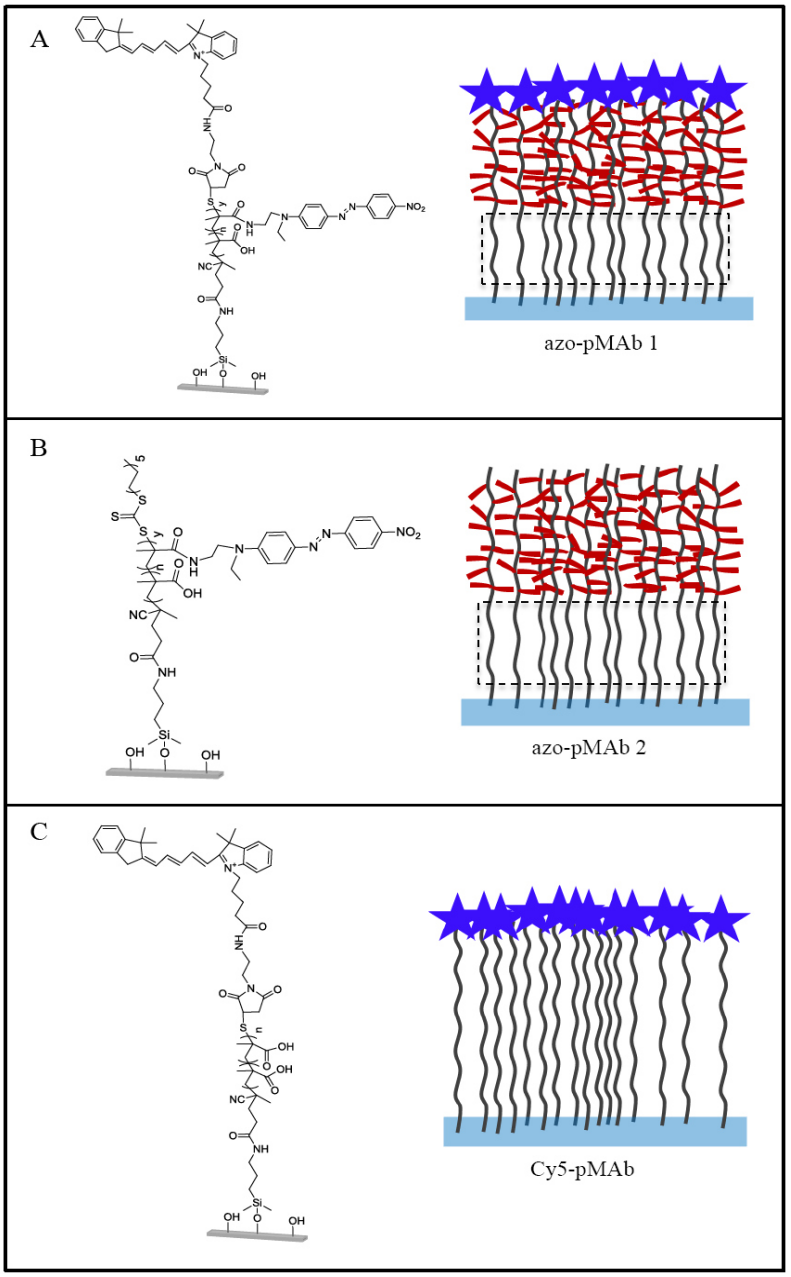

Chart 3.1. Polymer brush structures and schematic representations of (A) azo-pMAb 1 (y ~ 7%), (B) azo-pMAb 2a (y ~ 7%) and azo-pMAb 2b (y ~ 20%) and (C) Cy5-pMAb. The DP of MA was around 287 units (n).

We believe that these are optima conditions to excite azobenzene moieties present in our polymer brushes.[14] In order to address this issue, we designed the polymer brush azo-pMAb 1, having a DR at the side of the polymer backbone and Cy5 on "top" of the chains (as represented schematically in Chart 1A) and two other molecules, having only DR on the side chain (azo-pMAb 2 in Chart 1B) or only Cy5 on "top" (Cy5-pMAb in Chart 1C).

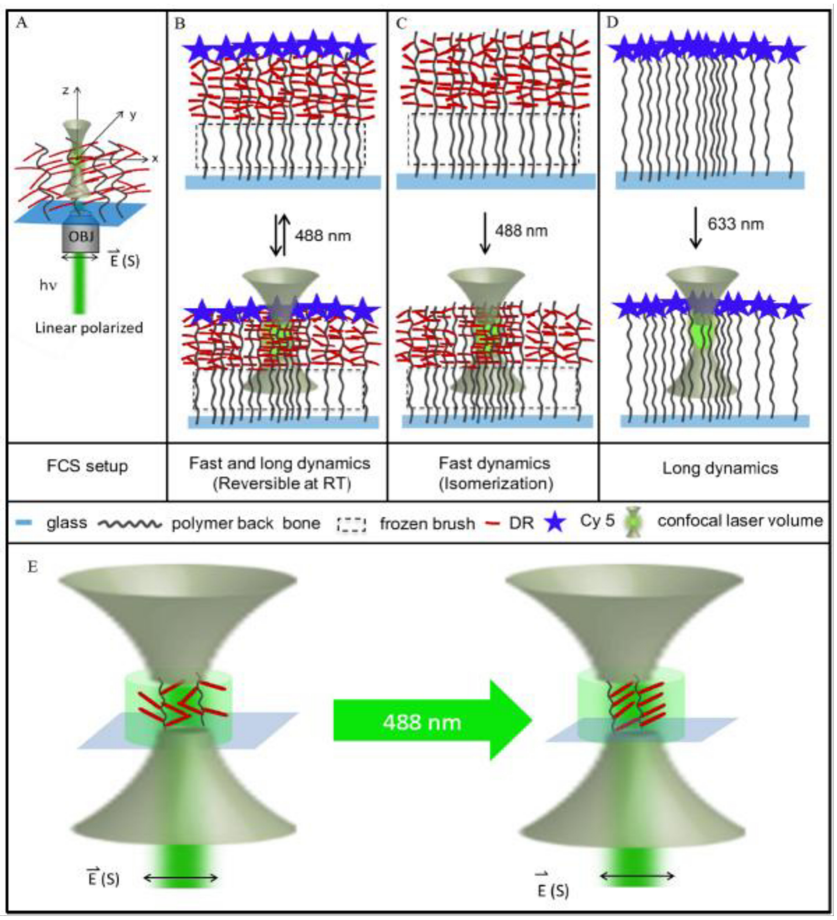

Figure 3.1. Polymer brush structures and schematic representations of (A) azo-pMAb 1 (y ~ 7%), (B) azo-pMAb 2a (y ~ 7%) and azo-pMAb 2b (y ~ 20%) and (C) Cy5-pMAb. The DP of MA was around 287 units (n). (E) Graphical sketch of azobenzene alignment perpendicular to $\vec{E}$ (S) of the incoming linear polarized laser light.

3.3.1 Dynamics of azo-pMAb 1

azo-pMAb 1 could be imaged through confocal microscopy at both 488 and 633 nm wavelengths. Interestingly, the fluorescent intensity of both dyes was strong enough to get uniform signal all over the imaged area even in the 488 nm channel, that is where we could observe DR signal (Figure 3.2A-C).

FCS was used to measure the dynamics of azopolymer brushes in the areas where both signals were homogeneously distributed. Since polymer brushes are considered as 2D systems, diffusion is perceived as confined within a plane whose dimensions correspond to the lateral dimension of the confocal volume, w_{xy}, as estimated from calibration procedures. For this purpose, FCS was calibrated at room temperature (23 °C) on two different optical paths, by measuring the mobility of reference dyes in water, in particular Cy5 for the excitation at 633 nm and Rhodamine 6G (Rh6g) for the excitation with the Argon laser at 488 nm. Since the diffusion coefficient of DR was not available, Rhodamine 6G was used instead for calibration using the same setting (notice that it is also excited at 488 nm).

We first explored the effect of different wavelengths on azopolymer brush dynamics and the mechanism of reversibility upon irradiation, as schematically represented in Figure 3.2B. The fluorescence intensity fluctuations (count rates, CRs) and the autocorrelation function (ACF) curves at different excitation wavelengths (458, 488, 514 and 633 nm, respectively) are presented in Figure 3.2D-I. In particular, in Figure 3.2D and 3.2G the recorded intensity traces at 458 and 633 nm are reported and no changes in fluctuations were observed, thus, as expected no excitation of DR molecules occurred. In fact, DR molecules

are supposed not to be excited at such wavelengths (the UV spectrum of the azopolymer is shown in Figure 3.6).

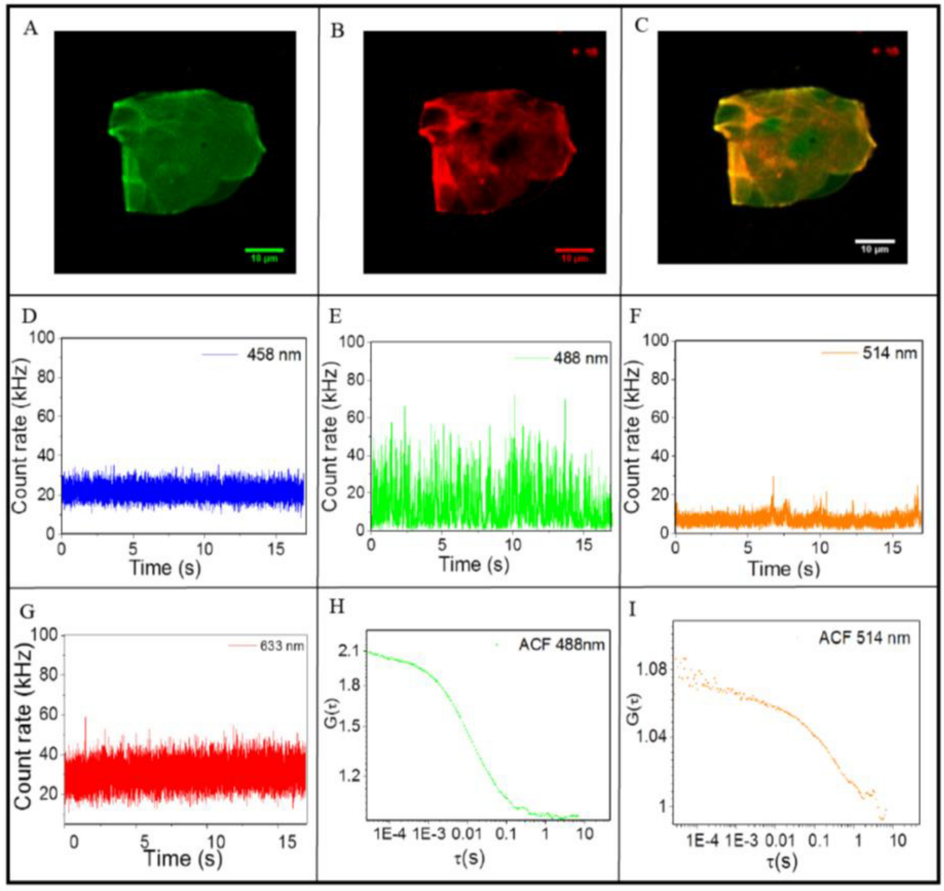

Figure 3.2. Confocal images of azo-pMAb 1 (A) 488 nm channel, (B) 633 nm channel, (C) merged fluorescent signals at both 488 and 633 nm. (D-G) represents count rate measured for azo-pMAb 1 at different excitation wavelengths by using 100% laser power and measuring in the 633 nm channel (1% laser power). Count rates obtained by exciting at (D) 458 nm, (E) 488 nm, (F) 514 nm and (G) 633 nm. Figures (H to I) represent the ACF plots with different excitation wavelengths. (H) 488 nm and (I) 514 nm.

In any case, it should also be taken into account that at 633 nm a He-Ne laser was used that, in our FCS instrument, had an inverted type of polarization (p-polarized light), which is not favourable for DR excitation present in our samples. While observing the intensity trace recorded when exciting at 488 nm (Figure 3.2E) instead an increased occurrence of fluctuations arose. Furthermore, it appeared that at this wavelength most of the DR molecules got excited. Indeed, the increased intensity reported in Figure 3.2E is in good agreement with UV spectra of azo-pMAb 2 that showed a maximum absorption at 482 nm due to the DR (Figure 3.6). As a further confirmation of this effect, only partial excitation was observed at 514 nm as small fluctuations could be recorded (Figure 3.2F). Another important information came from the ACFs measured at 488 nm that shifted to small decorellation times, thus revealing a faster dynamics, while at 514 nm the ACFs were only partially shifting to smaller decorellation times, indicating that dynamics was still slower compared to what measured when exciting at 488 nm. To sum up, the dynamics showed to be strongly related to DR excitation and that 488 nm wavelength was indeed highly affecting the perceived mobility.

3.3.2 Reversibility Cycle of azo-pMAb 1

Next, we analyzed the effect on Cy5 mobility before and after excitation at 488 nm. For this purpose, 100 s excitation time and full laser intensity (25 mW) were selected as the best conditions for illuminating our DR-containing polymer brush, while He-Ne at 633 nm wavelength (0.1 mW laser power) was used to measure the diffusion time of the brushes by illuminating the linked Cy5 on top of the chains. The normalized ACF measured before exciting DR molecules in a selected point of the

brushes (black ACF, t) and after excitation at 488 nm (green triangles, Ex_1), are presented in Figure 3.3. The diffusion time before excitation (t) was around 101±11, as recorded in the far red channel at 633 nm. The single component 2D diffusion model was used to fit data (equation 2 in Experimental Section). In this model, the triplet fraction and time were fixed to Cy5 parameters found in solution, thus, τ_{diff} was the only fitted parameter. After excitation, the corresponding τ_{diff} was as small as 6±1 ms (Ex_1).

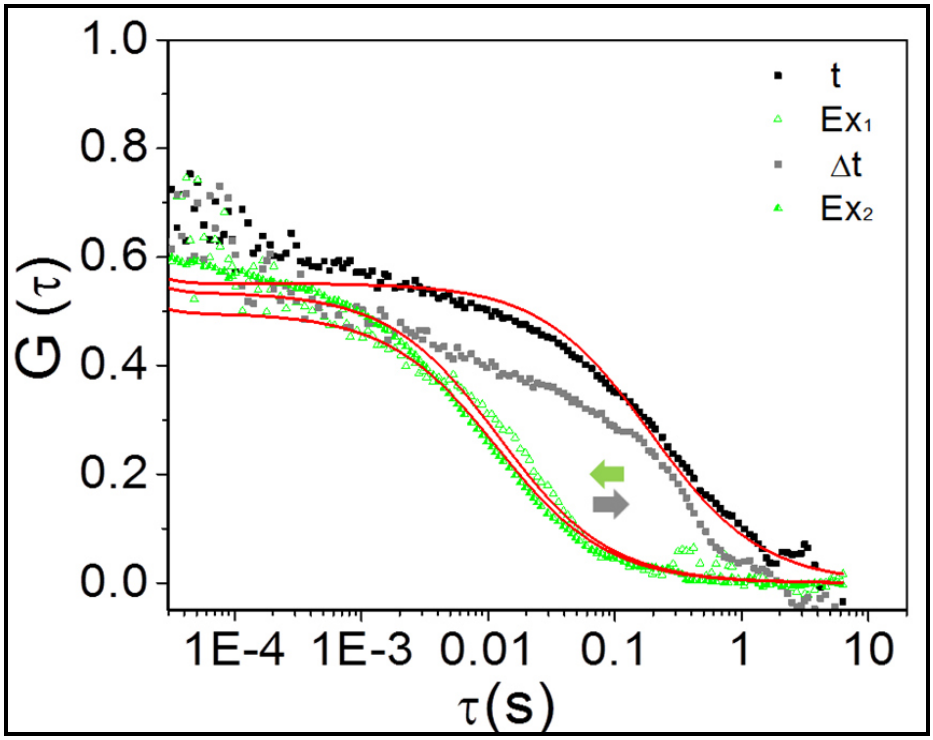

Figure 3.3. ACFs of the reversible cycle of azo-pMAb 1 by exciting at 488 nm and recording at 633 nm channel.

The dynamics was much faster upon excitation of azobenzene moieties and the diffusion time decreased from 101 to 6 ms. After waiting 10 minutes (Δt), the measured τ_{diff} increased to 39±7 ms (gray dots). The

mobility was recovered to the original situation in a total time of 15 minutes. The ACF of 10 minutes waiting time did not fit to the single classic component diffusion model (equation 2 in Experimental Section), while an "anomalous" diffusion model[20] was better interpreting the data (data not shown). This could be due to the fact that during the waiting time, relaxation to another configuration of the polymer brushes was ongoing and an additional process with a different characteristic time was affecting the dynamics. Again, we excited (Ex_2) in the same position and we recorded a comparable increment in mobility of the brushes (empty triangles) with respect to Ex_1. We also measured the mobility of the chains at 1-2 μm from the excitation spot and we found a comparable behaviour as when measuring in the excitation site itself. This suggested that the mechanism was not only localized and the excitation was also affecting the chains few microns away from the illuminated area (data not shown). This reversible cycle was repeated twice with 15 minutes of interval time in wet conditions at room temperature, and the results were consistent, as graphically represented in Figure 3.1B, while so far azopolymer aggregations obtained illuminating by linear polarized light are shown to be reversed thermally or using circular polarized light.[15,10,27] In general, it is known that the movement of polymer chains depends on several parameters including the spatial variation of the material susceptibility due to light-induced birefringence and dichroism, the optical field and the field gradient along the grating wave vector k.[25,12,28] From these FCS experiments, we understood that, in the case of long diffusion time (in particular 100 s of ms) could be recorded, which might be coming from the main chain of the polymer brush linked to Cy5, since only upon

excitation with 488 nm, the diffusion time was decreasing. This phenomenon is reasonably addressed to DR excitation. Finally, we assume that the higher mobility occurred as a consequence of the excitation of azobenzene molecules, which underwent a fast isomerization process (from *trans* to *cis* isomer and back).

3.3.3 Dynamics of azo-pMAb 2

To confirm our hypothesis, we analyzed a polymer brush sample that contained only DR in the side chain (azo-pMAb 2a). Sample was analyzed by both exciting at different laser intensities and collecting on the same 488 nm channel that was previously calibrated, as discussed above, exploiting the fluorescent signal coming from DR itself (Figure 3.4A).

Figure 3.4B shows the normalized ACFs at four selected laser intensities (10, 20, 50 and 70% of laser intensity that correspond to 2.5, 5, 12.5 and 17.5 mW, respectively). Upon increasing the laser power, the normalized ACFs were shifting to small decorellation times. The obtained fitting parameters from equation 2 of the ACFs are summarized in Figure 3C, where the diffusion times are shown against percentage of laser intensities. During this process, when brushes are excited with 2.5 mW laser power, τ_{diff} values were 1 ± 0.2 ms, while by increasing the laser intensity to 12.5 mW, the diffusion time was decreased to less than 50 μs. Figure 3.4D shows not normalized ACF plots. The values of the ACF at zero lag time, G(0), were progressively lowering down when excitation was increased. This corresponds to an increase of the number of emitting particles moving within the confocal volume.[29]

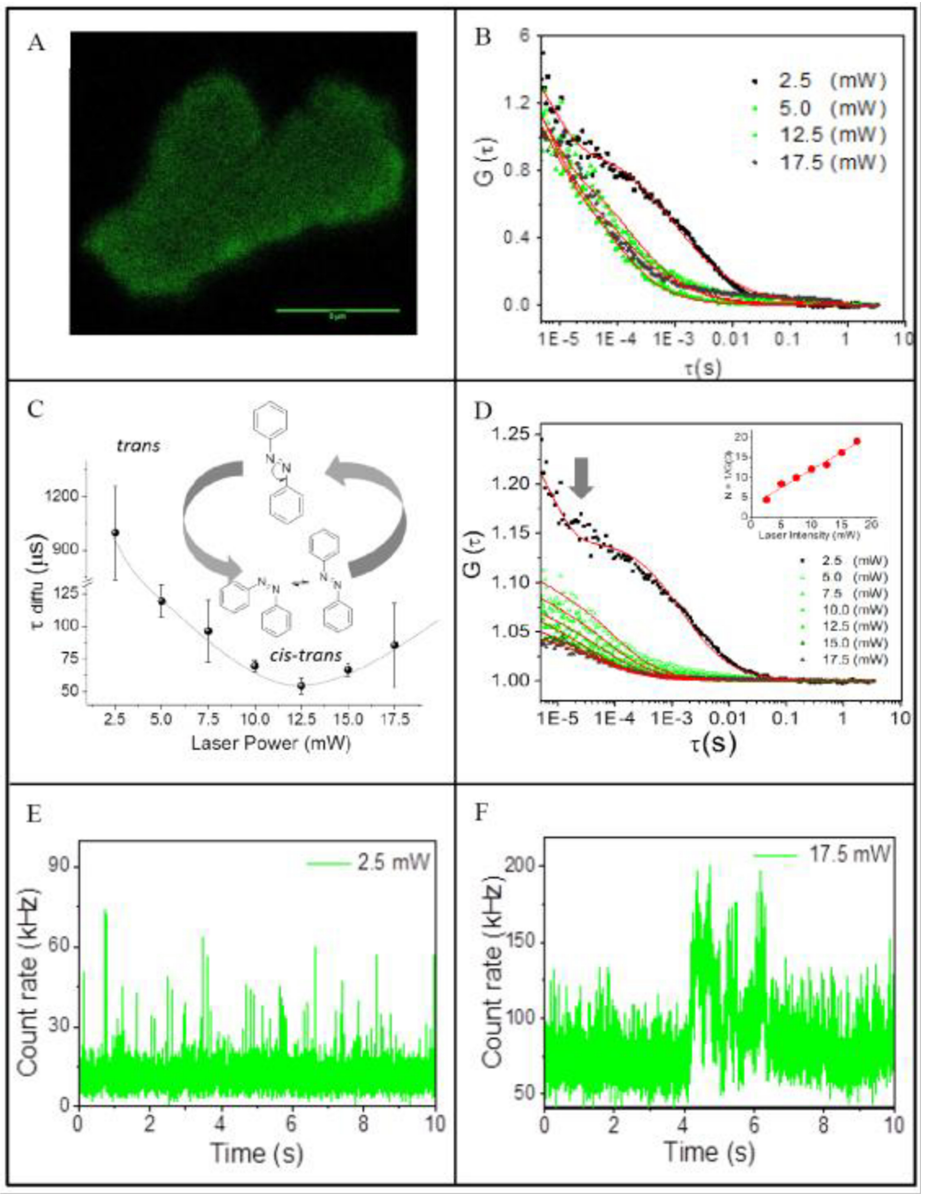

Figure 3.4. (A) Confocal images of azo-pMAb 2a in the 488 nm channel. (B) Normalized ACF plots of the diffusion time (τ) of azo-pMAb 2a. (C) Graph of the diffusion time (τ) versus laser intensity. (D) ACFs of the diffusion time (τ) of azo-pMAb 2a with different laser intensities, inset shows the measured average number of molecules. Count rates of azo-pMAb 2a excited with different laser power and acquired in the 488 nm channel (E) 2.5 mW and (F) 17.5 mW.

This phenomenon might occur because, upon laser excitation, azobenzene molecules isomerized from *trans* to *cis* moving fast inside the volume. In addition, an increased number in molecules, occupying the confocal volume, was measured. As we increase the intensity of laser light the diffusion time got faster till 12.5 mW. That is, all azobenzene moieties got excited until a saturation level was reached; in fact τ_{diff} decreased from 1±0.2 ms to 50±5 μs. This stage is most likely related to the complete *trans*-to-*cis* and *cis*-*trans* back-isomerization process. Therefore, presumably by saturating the system both *trans*-to-*cis* and *cis*-to-*trans* isomerizations occurred almost instantaneously, while exciting at the same wavelength (488 nm). After saturation level, even though the laser intensity still increased, the dynamics slowed down and τ_{diff} increased from 50 μs to 80±33 μs most probably due to the fact that azobenzene molecules underwent *trans*-*cis*-*trans* cycle and moved until they aligned all still parallel to the substrate but perpendicular to the $\vec{E}$ (S) of the incident LPL (situation in which they are no longer excitable), as schematically shown in Figure 3.1E.[30-32] As we further increase the laser power, azobenzene molecules aggregated probably due to a mass-transport and a cooperative self-assembling process[31] (Figure 3.1C), thus, explaining why slower dynamics and increasing number of emitting particles in the confocal volume were observed at 17.5 mW laser power excitation (Figure 3. 4B and 3.4D). In fact, as indicated in Figure 3.4E and 3.4F, the count rate was changing drastically comparing 2.5 mW and 17.5 mW laser power excitations, as a big jump in the trace was observed at higher power that resembles aggregation.[33] When theoretically doubling the molecular mass of the diffusive species, an increase of 0.7 times in diffusion time expected.

Indeed, almost doubled diffusion time was measured corresponding to an increase of 0.62 times that is very close to theoretical predictions).[34] Thus, suggesting a dimer-type of cooperative assemble. A further confirmation of an on-going aggregation was given by Raman mapping carried out by tracking the stretching of 1012 cm^{-1}, which corresponds to the aromatic bond of the phenyl rings in DR. The mapped area before excitation presented in Figure 3.5A shows that DR was uniformly distributed on the surface (homogenous blue colour corresponding to a low scale). After excitation, in Figure 3.5B, yellow and red spots (related to high scale) rose in the excited region indicating local higher DR concentration areas and, thus, aggregation. AFM confirmed the aggregation of azo-pMAb 2a after excitation by FCS as shown in Figure 3.5D. In fact, polymer brush topography before illumination was characterized by a homogenous roughness of about 20 nm (AFM image in Figure 3.5C), while after excitation by FCS, the formation of high clusters in the illuminated region was observed. Confirmation of the aggregation process provided by Raman and AFM measurements contributes in discarding other reasons for an increased number of molecules within the confocal volume (Figure 3.4D), such as photodegradation of the azobenzene molecules, or changes in molecular brightness perceived as diverse diffusing species.[35,36] In addition, the effect of DR concentration was also checked by analysing azobenzene polymer brushes with higher percentage of DR (up to 20%, here named as azo-pMAb 2b). In addition, the effect of DR concentration was also checked by analysing azobenzene brushes with higher percentage of DR (up to 20%, here names as azo-pMAb 2b).

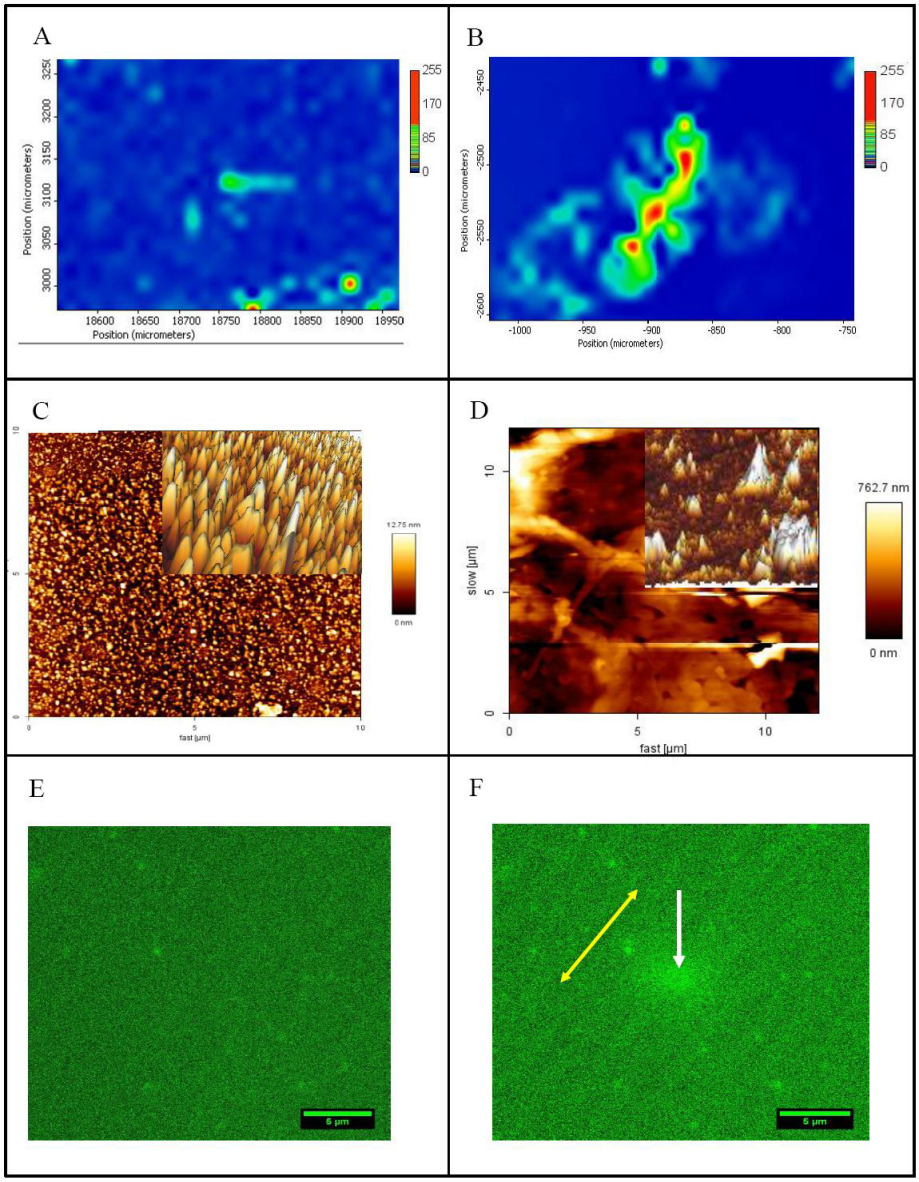

Figure 3.5. Raman mapping of azo-pMAb 2a (A) before excitation and (B) after excitation during the FCS experiments. AFM images of azo-pMAb 2a (C) before excitation (insert 3D view of the brush) and (D) after excitation (insert 3D view of the brush) during the FCS experiments. Confocal images of azo-pMAb 2b (E) before and (F) after excitation during the FCS experiments (white arrow shows aggregation at the center and yellow arrows represent the pattern direction). Scale bar 5µm.

Though the large number of measured particles was above the sensibility of FCS technique, that is normally suited for few molecules observations, thus impairing mobility studies, we were still able to observe the effect of laser excitation by confocal imaging. Interestingly, as it can be seen in the confocal images in Figure 3.5F, when the laser was used to excite at 488 nm for 20 s, a pattern of micrometric widths was created that resemble to SRG structures that one normally obtained by interferometry system (e.g. Lloyd's mirror method).[15,37]

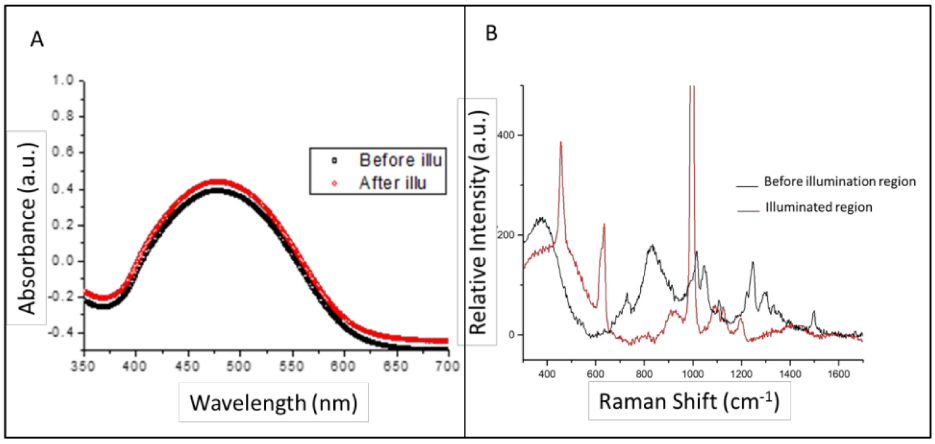

Figure 3.6. (a) UV spectra of azo-pMAb 2a (black line) before and (red line) after illumination. (b) Raman spectra of azo-pMAb 2a before (black line) and after (red line) illumination during FCS experiments.

As already discussed, due to interferometric diffraction of the laser light, azobenzene isomerization induces mass transport that can generate a pattern.[10] Here, we observed the formation of a pattern by simply illuminating with a confocal microscope type of set up (FCS). Unfortunately, the pattern created was not deep enough and could not be measured by AFM. However, in the excited region the azopolymer brushes aggregated inside the confocal volume, as shown in Figure 3.5

by the local increase in intensity when imaging before (Figure 3.5E) and after (Figure 3.5F) excitation. As we discussed above and schematically represented in Figure 3.1E, we hypothesized that also in this case excited azobenzene molecules tend to orient perpendicular to the $\vec{E}$ (S) and due to mass movement of polymer material and a cooperative self-assembling, aggregation in the illuminated area occurred (white arrow).

3.3.4 Mobility of Cy5-pMAb

As a further control, we also analyzed brushes that did not contain azobenzene, but only having Cy5 linked on top (Cy5-pMAb in Chart 1C). FCS was used to record the dynamics of the polymer chains when exciting Cy5 with the 633 nm laser light. The diffusion time of Cy5-pMAb was 38±9 ms, as expected long dynamics was observed if comparing to the case of azo-pMAb 2 (Figure 3.1D). However, ACFs were plotted comparing with azo-PMAb 1 before excitation (t), and their dynamics was still slightly different from the long dynamics of azo-pMAb 1 (101±11 ms). We believe that brush without DR can move much more freely compared to azobenzene containing brushes, as in azo-pMAb1, where DR molecules were linked to the side chains and probably hindered their movement.

In short, our FCS experiments confirm that the azobenzene-containing brushes, azo-pMAb 1 and azo-pMAb 2, were characterized by a shorter dynamics (on the 50 μs scale) by 488 nm excitation, while azobenzene-free polymer brushes moved with a characteristic long dynamics on 100 s of ms scale.

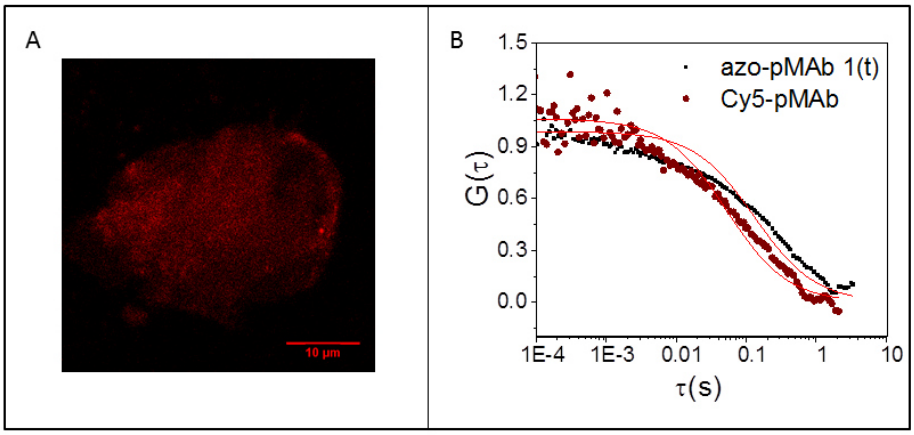

Figure 3.7. (A) Confocal image of Cy5-pMAb in the 633 nm channel. (B) ACFs of diffusion time (τ_{diff}) of Cy5-pMAb.

3.4 Conclusion

In summary, we synthesized a set of azopolymer brushes to study their dynamics by FCS. For this purpose we synthesized three types of polymer brushes: one containing DR on the side chains and Cy5 on top of the polymer brush (azo-pMAb 1) and two other polymer brushes, one having only DR on the side chains, named azo-pMAb 2, and the last one with just Cy5 on top of the chains (Cy5-pMAb). FCS results show a mobility dependence of brushes upon the excitation of azobenzene molecules and a summary of all hypothesized mechanisms for explaining each observed mobility in all three brushes is sketched in Figure 3.1. In particular, short diffusion times were only measured when DR were laterally grafted to the chains and excited with 488 nm light, while, long diffusion time was measured through Cy5 illumination in both brushes were no DR excitation was caused, thus to be addressed to the main chain of the polymer brushes. The azo-pMAb 1 dynamics was reversible from short to long diffusion times within 15 minutes of time interval at room temperature in wet conditions. By using 488 nm as

excitation as well as measuring wavelength, we were able to study the short dynamics of azobenzene isomerization mechanism of *trans-cis-trans* cycle with increasing the laser power. In our proposed mechanism, with 17.5 mW laser power, azopolymer brushes aggregate in the confocal volume (increase number of emitting particles moving within the confocal volume) and this is most likely due to the mass movement of azobenzene polymers excited by in-plane linear polarized light and their concomitant cooperative self-assembling. In addition, when we increase the DR concentration on polymer brushes (20%), we were able to observe pattern of micrometric widths, resembling to SRGs. We believe that this is caused by a spatial reorientation of azobenzenes that, since they are randomly oriented parallel to the substrate and in-plane with the linear polarized light, get favourably excited until they align all in a preferential direction that is perpendicular to $\vec{E}$(S), situation in which they are no longer excitable and aggregate in a cooperative self-assemble manner. However, as we still do not have proper information about DR orientation, studies on this issue will be carried out using similar confocal microscope setup by tilting the laser polarization angle.

References

(1) Arri Priimagi, A. S.; Azopolymer-Based Micro- and Nanopatterning for Photonic Applications. *J. Polym. Sci.Part A: Polym. Chem.* **2013**, *52,* 163–182.

(2) Rocha, L.; Paius, C.-M.; Luca-Raicub, A.; Resmeritaa, E.; Rusua, A.; Moleavin, I.-A.; Hamel, M.; Branza-Nichitada, N.; Hurduc, N.; Azobenzene based polymers as photoactive supports and micellarstructures for applications in biology. *J. Photoch. Phtobio. A* **2014**, *291,* 16-25.

(3) Baaca, H.; Leea, J.-H.; Seoa, J.-M.; Parka, T. H.; Chunga, H.; Leed, S.-D.; Kim, S. J.; Submicron-scale topographical control of cell growth using holographic surface relief grating. *Mater. Sci. Eng.* **2004**, *24,* 209-212.

(4) Yager, K. G.; Barrett, C. J.; Novel photo-switching using azobenzene functional materials. *J. Photoch. Photobio. A.* **2006**, *182,* 250-261.

(5) Feringa, B. L.; Molecular Swiches. *Wiley-VCH Book, Chapter 13.* **2001**.

(6) Yager, K. G.; Barrett, C. J.; *Light-Induced Nanostructure Formation using Azobenzene Polymers.* Boca Raton; Nalwa, H. S.;Miyata, S., Eds. **2006**; 1-38.

(7) Poprawa-Smoluch, M.; Baggerman, J.; Zhang, H.; Maas, H. P. A.; Cola, L. D.; Brouwer, A. M.; Photoisomerization of Disperse Red 1 Studied with Transient Absorption Spectroscopy and Quantum Chemical Calculations. *J. Phys. Chem. B.* **2006**, *110,* 11926-11937.

(8) Schuh, C.; Lomadze, N.; Ruhe, J.; Kopyshev, A.; Santer, S.; Photomechanical degrafting of azo functionalized poly(methacrylic acid) (PMMA) Brushes. *J. Phys. Chem. B.* **2011**, *115,* 10431–10438.

(9) Norman, L. L.; Barrett, C. J.; Solution properties of self-assembled amphiphilic copolymers determined by isomerization spectroscopy. *J. Phys. Chem. B.* **2002**, *106,* 8499-8503.

(10) Barrett, C. J.; Natansohn, A. L.; Mechanism of Optically Inscribed High-Efficiency Diffraction Gratings in Azo Polymer Films. *J. Phys. Chem.* **1996**, *100,* 8836-8842.

(11) Yager, K. G.; Barrett, C. J.; All-optical patterning of azo polymer films. *Curr. Opin. Solid. St. M.* **2001**, *5,* 487-494.

(12) Kuma, J.; Li, L.; Jiang, X. L.; Gradient force: The mechanism for surface relief grating formation in azobenzene functionalized polymers. *Appl. Phys. Lett.* **1998**, *72*,2096-2098

(13) Vishwanathan, N. K.; Balasubramanian, S.; Li, L.; Triphaty, S. K.; Kumar, J.; A Detailed Investigation of the Polarization-Dependent Surface-Relief-Grating Formation Process on Azo Polymer Films. *Jpn. J. Apl. Phys.* **1999**, *38,* 5928–5937.

(14) Schuh, C.; Lomadze, N.; Rühe, J. r.; Kopyshev, A.; Santer, S.; Photomechanical Degrafting of Azo-Functionalized Poly(methacrylic acid) (PMAA) Brushes. *J. Phys .Chem B.* **2011**, *115,* 10431-10438.

(15) Lomadze, N.; Kopyshev, A.; Ruhe, J.; Santer, S.; Light-Induced Chain Scission in Photosensitive Polymer Brushes. *Macromolecules.* **2011**, *44,* 7372–7377.

(16) Weisshart, K.; Fluorescence Correlation Spectroscopy: A Powerful Tool to Study Dynamic Processes on a Single-Molecule Level. *Rev. Las. Eng.* **2002**, *6,* 88-391.

(17) Kaspusta, P.; Gmbh, P.; Absolute Diffusion Coefficients: Compliation of Reference Data for FCS Calibration. *Picco. Quant.* **2010**, 1-2.

(18) Buschmann, V.; Krämer, B.; Koberling, F.; Macdonald, P. G. R.; Rüttinger, S.; Bundesanstalt, P. T.; Quantitative FCS: Determination of the Confocal Volume by FCS and Bead Scanning with the MicroTime 200. *Pico. Quant.* **2009**,*.1,* 1-8.

(19) Weisshart, K.; Flourescence Correlation Spectroscopy: A powerful Tool to Study Dyanmic Processes on a Single-Molecule Level. *Las. Rev.* **2002**, *31*, 388-391.

(20) Santo, I. D.; Causa, F.; Netti, P. A.; Subdiffusive Molecular Motion in Nanochannels Observed by Fluorescence Correlation Spectroscopy. *Anal. Chem.* **2010**, *82,* 997–1005.

(21) Santo, I. D.; Causa, F.; Netti, P. A.; Temperature Driven Macromolecule Separation by Nanoconfinement. *Macromolecules.* **2014**, *47,* 8754-8760.

(22) Sanguigno, L.; Santo, I. D.; Causa, F.; Netti, P.; A Closed Form for Fluorescence Correlation Spectroscopy Experiments in Submicrometer Structures. *Anal. Chem.* **2010**, *82,* 9663-9670.

(23) Doose, S. r.; Tsay, J. M.; Pinaud, F.; Weiss, S.; Comparison of Photophysical and Colloidal Properties of Biocompatible Semiconductor Nanocrystals Using Fluorescence Correlation Spectroscopy. *Anal. Chem.* **2005**, *77,* 2235-2242.

(24) Ambrosio, A.; Maddalena, P.; Marrucci, L.; Molecular Model for Light-Driven Spiral Mass Transport in Azopolymer Films. *Phys. Rev. Lett.* **2013**, *110,* 146102-146105.

(25) Bian, S.; Liu, W.; Williams, J.; Samuelson, L.; Kumar, J.; Tripathy, S.; Photoinduced Surface Relief Grating on Amorphous Poly(4-phenylazophenol) Films. *Chem. Mater.* **2000**, *12,* 1585-1590.

(26) Uekusa, T.; Nagano, S.; Seki, T.; Highly Ordered In-Plane Photoalignment Attained by the Brush Architecture of Liquid Crystalline Azobenzene Polymer. *Macromolecules.* **2008**, *42,* 312-318.

(27) Yager, K. G.; Barrett, C.; All-optical patterning of azo polymer films. *Curr. Opin. Solid. St. M.* **2001**, *5,* 487–494.

(28) Barille, R.; Tajalli, P.; Kucharski, S.; Ortyl, E.; Nunzi, J. M.; Photoinduced deformation of azopolymer nanometric spheres. *Appl. Phys. Lett.* **2010**, *96*. 450-457
(29) Magde, E. L. E. a. D.; Fluorescence correlation spectroscopy. I. Conceptual basis and theory. *Bio. Poly.* **1974**, *13,* 1-27.
(30) Schnabel, W.; *Polymers and Light.* Wiley Inter Science; **2007**; 5-400.
(31) Seki, T.; Photoresponsive self-assembly motions in polymer thin films. *Curr. Opin. Solid. St. M.* **2006**, *10,* 241–248.
(32) Fukuhara, K.; Fujii, Y.; Nagashima, Y.; Hara, M.; Nagano, S.; Seki, T.; Liquid-Crystalline Polymer and Block Copolymer Domain Alignment Controlled by Free-Surface Segregation. *Angew. Chem. Int. Edit.* **2013**, *52,* 5988–5991.
(33) Yang, J.; Wu, D.; Xie, D.; Feng, F.; Schanze, K. S.; Ion-Induced Aggregation of Conjugated Polyelectrolytes Studied by Fluorescence Correlation Spectroscopy. *J. Phys. Chem. B.* **2013**, *117,* 16314-17324.
(34) Wachsmuth, M.; Caudron-Herger, M.; Rippe, K.; Genome organization: Balancing stability and plasticity. *Biochim. Biophys. ACTA.* **2008**, *1783,* 2061-2079.
(35) Eggeling, C.; Widengren, J.; Rigler, R.; Seidel, C. A. M.; Photobleaching of Fluorescent Dyes under Conditions Used for Single-Molecule Detection: Evidence of Two-Step Photolysis. *Anal. Chem.* **1998**, *70,* 2651-2659.
(36) Heuff, R. F.; Swift, J. L.; Cramb, D. T.; Fluorescence correlation spectroscopy using quantum dots: advances,challenges and opportunities. *Phys. Chem. Chem. Phys.* **2007**, *9,* 1870–1880.
(37) Kulikovska, O.; Gharagozloo-Hubmann, K.; Stumpe, J.; Huey, B. D.; Bliznyuk, V. N.; Formation of surface relief grating in polymers with pendant azobenzene chromophores as studied by AFM/UFM. *J. Nano. Tech.* **2012**, *23,* 1-14.

Chapter 4

Surface Relief Grating Formation in Synthesized Azopolymer Brush for Biological Applications

Abstract. New type of azopolymer brushes, based on an acrylamide derivative of a well-known azobenzene (Disperse red 1) used as monomer, have been synthesized by reversible addition fragmentation chain transfer radical polymerization (RAFT) approach on glass surfaces. Surface relief grating (SRG) was created by using Lloyd's mirror method and reversibility of the pattern was obtained by sonication using water at room temperature. Further, fluorescence correlation spectroscopy (FCS) was used to illuminate again the SRG structures and study the movement of material from the crest (bright area in the confocal image) to the trough (darker regions) of the grooves upon excitation at 488 nm. Further, these azopolymer brushes were shown to be biocompatible using NIH-3T3 and HUVEC cells. In addition to that HUVECs were aligned along the direction of the grooves on the patterned azopolymer brushes. These results envision the possibility to use the new synthesized azopolymer brushes as novel light-responsive cells instructive biomaterials.

The work described in this Chapter is part of a manuscript in preparation. R. H. Kollarigowda, C. Fedele, I. De Santo, S. Cavalli and P. A. Netti. New Azopolymer Brushes as Smart Light-Responsive Biomaterials.

4.1 Introduction

Photoresponsive materials implemented as thick or thin films provide a well original tools for biological applications.[1] Especially, the photoresponsive polymers containing azo-chromophores can be used for micro-scale surface relief grating (SRG) formation.[1-4] Furthermore, the photo-reversibility of the SRG holds a great potential for achieving reversible control of surface topography by tuning photo-induced erasing or writing processes. In fact, the topological cue on a biomaterial surface is important for playing a role in guiding the cell orientation and its dynamic on the materials.[5] Another specialty of such type of polymers is chemical bond stability and durability in physiological-like conditions, which are important parameters for biological applications.[1,3,4,6,7] In particular polymer having amide linkage are more stable than standard ester derivatives and, thus, more appropriate for biological use.[7] Azobenzene possess a unique behaviour due to *trans-cis* reversible photo-isomerization, induced by the UV/Vis light.[8] If the azobenzene is attached to the polymeric chain, the photo-isomerization of *trans-cis-trans* generates conformational changes at the entire chain level, which, in turn, lead to macroscopic variations in the chemical and physical properties of the material.[8] Although the azobenzene photo-isomerization process has been studied since long time, the mechanism of surface relief grating (SRG) is still not completely elucidated. However, several models have been proposed to explain the photo-induced mass transport, responsible for the SRGs.[9,10] Some, models have been proposed in which the isomerization pressure,[9] gradient of the electric force,[11] asymmetric diffusion,[12] mean-field forces[13] and permittivity gradients[14] or conformational instability[15] are

assumed to play an important role in the different proposed mechanisms.[13-18] A very exhaustive method with detailed explanation of SRG phenomena was given by Kumar and Tripathy group, using a two beam interference technique.[11,16] They showed that SRG formation was strongly dependent on the polarization directions of the writing beams. In this model, molecular migration of the polymer is based on the forces originating from the optically induced electric field gradient. The azopolymer material moved spatially due to the optical field component in the direction of field gradient along the grating wave vector k.[11,19,20]

When it comes to azopolymer brushes, the Seki[21] and Santer[22] groups have been independently studied on the orientation of azomolecules and SRG formation in polymer brushes by Lloyd's mirror method.[22-25] In particular, Seki and co-workers explained the alignment of azobenzene in polymeric materials.[21] Azopolymer brushes orient differently than spin coated azopolymers. In the former case, azobenzenes that are grafted to the side chain of polymer brushes preferentially parallel to the substrate, thus when S-type linear polarized light (S-LPL) is used they are oriented in-plain with the incident laser light and get favorable to get excited.[26] While in the latter case chromophores orient completely random parallel to the plane of the sample.

Another important feature of SRG patterns is that they can be reversed either thermally or using circular polarized/incoherent light.[23] The challenge of this work is erasing the pattern in ambient condition which is feasible in biological environment.

In our work, we synthesized new azopolymer brushes by reversible addition fragmentation chain transfer polymerization (RAFT) technique. The azopolymer brush was illuminated by the Lloyd's mirror method

and we obtained 60 nm of pattern height. Further, we described a protocol to erase the pattern applying sonication in mild conditions. Fluorescence correlation spectroscopy (FCS)[27,28] was used to illuminate again the SRG structures and study the movement of material from the crest (bright area in the confocal image) to the trough (darker regions) of the grooves upon excitation at 488 nm. Furthermore, we have conducted biocompatibility assay using NIH-3T3 and HUVEC cells. These azopolymer brushes were found to be biocompatible and we envision the possibility to use them for further biological application to study cell behaviour by modifying the topography of the brushes.

4.2 Experimental Section

General Materials and Methods. All chemicals and solvents were purchased from Sigma-Aldrich and used without further purification. All instrumental methods were reported in Chapter 2.

Surface Relief Grating Inscription. A 442 nm He-Cd laser (power of about 60 mW) was used in a Lloyd's mirror configuration in order to project an interference pattern of light on the azopolymer films, thus inducing mass migration and SRG formation. In more details, the azopolymer sample was glued to one of the mirror edge and horizontally, vertically as well as 45° oriented polarized laser beam was reflected on it, thus realizing an interference pattern of light. The pattern pitch was given by $2d=\lambda \cdot \sin(\vartheta)$, where λ is the laser wavelength and ϑ is the angle between the incident beam and the mirror. Additionally, a beam from a He-Ne laser emitting at 632 nm was used for a real-time control of the inscription process by monitoring the diffraction efficiency of the inscribed grating. SRG experiments were performed in

collaboration with CNR-Istituto di Cibernetica "E. Caianiello" in Pozzuoli (Naples, Italy), under the supervision of Prof. Pietro Ferraro.

Synthesis of monomer A. 0.34 mmol (1.2 equiv., 29.7 mg) methacrylic acid (MA), 0.48 mmol (1.5 equiv., 92 mg of *N*-(3-dimethylaminopropyl)-*N'*-ethylcarbodiimide hydrochloride (EDC·HCl), 0.48 mmol (1.5 equiv., 97.02 mg) 1-hydroxy benzotriazole (HOBt) and 0.96 mmol and (3 equiv., 133 µl) of triethylamine (TEA) were taken in a 25 ml round bottom flask. 4 ml of DMF was added in to the flask and kept for stirring. 0.28 mmol of compound **a** (synthetic procedure is explained in Chapter 2) was added and the reaction was continued for 24 hours at room temperature. The product was confirmed by thin layer chromatography (TLC) and purified by column chromatography with a mixture of methanol/dichloromethane 8/92 (v/v). MS for $C_{20}H_{23}N_5O_3$: calculated for $[M+H]^+$ = 382.18 m/z; found (ESI) $[M+H]^+$ = 382.18 m/z. ^{1}H-NMR (600 MHz, DMSO-d6, δ): 8.39 (d, 2H, aa[1]); 7.91-7.80 (dd, 2H, bb[1]); 6.91 (t, 2H, c); 5.4, 5.5 (s, 2H, gg[1]); 3.45-3.57 (m, 2H, ee[1]); 1.9 (s, 3H, h); 1.23 (t, 3H, f). ^{1}H-NMR spectrum and assigned chemical shifts are shown in Figure 4.1.

Synthesis of poly(MA-DR)b. A 25 ml round bottom flask and a 5 ml vial were washed and dried. All chemicals and dried glass apparatus were placed inside the glove box under nitrogen flow for 30 minutes. 1.53 mmol (600 mg) of monomer **A** was weighed and transferred into 25 ml round bottom flask with 10 ml of a solution of dry methanol/1,4-dioxane (1/1, v/v). 2.4 µmol of 1,1-azobis(cyclohexanecarbonitrile) was weighed and transferred into the 5 ml vial and 2 ml of a dry methanol/1,4-dioxane (1/1, v/v) solvent mixture was added to dissolve initiator and to make a homogeneous solution. Both monomer and

initiator solutions were taken out from the glove box. The monomer in the 25 ml round bottom flask was degassed by freeze-thaw cycle, which was repeated three times for the complete removal of dissolved oxygen. While, the initiator solution was degassed by bubbling nitrogen for 30 minutes. After that, monomer and initiator solutions were transferred into a 50 ml corning flask, which contained Sample 2 (RAFT immobilized glass coverslip, Synthesis of Sample 2 is reported in Chapter 2), under nitrogen atmosphere. The corning flask was sealed with teflon tape and heated at 70 °C for 48 hours. The reaction was stopped by exposure to air. The glass substrate was washed with methanol by sonication for 20 minutes at room temperature, the washing process was continued for three times to remove unimmobilized polymer on the glass substrate and finally it was dried in a vacuum oven at 30 °C for 24 hours.

Synthesis of poly(MA-DR) (solution RAFT polymerization). 25 ml round bottom flask and 5 ml vial were washed and dried. All chemicals and dried glass apparatus were placed inside the glove box under nitrogen flow for 30 minutes. 1.55 mmol (600 mg) of monomer **A** and 0.0298 mmol (12 mg) of 4-cyano-4-((dodecyl sulfonyl thiocarbonyl) sulfonyl pentanoic acid (RAFT agent), was weighed and transferred into 25 ml round bottom flask, followed by 10 ml of a solution of dry methanol/1,4-dioxane (1/1, v/v). 2.4 µmol of initiator (1,1-azobis(cyclohexane carbonitrile)) was weighed and transferred in the 5 ml vial and 2 ml of a dry methanol/1,4-dioxane (1/1, v/v) solvent mixture was added to dissolve initiator and to make a homogenous solution. Both monomer and initiator solutions were taken out from the glove box. The monomer in the 25 ml round bottom flask was degassed

by freeze-thaw cycle, repeated three times, to remove dissolved oxygen. The initiator solution was degassed by bubbling nitrogen for 30 minutes. After that, initiator solution was added into 25 ml round bottom flask, which contained RAFT agent and monomer **A**, under nitrogen atmosphere. The round bottom flask was sealed by teflon tape and heated at 70 °C for 48 hours. The reaction was stopped by exposure to air. The polymer solution was precipitated in hexane and filtered off. The precipitated red powder was washed with hexane to remove unreacted RAFT agent and monomer. Finally the filtered polymer was dried in a vacuum oven at 50 °C for 24 hours.

Spin Casted Procedure. 1.6 mg of synthesized poly(MA-DR) was dissolved in 1000 μl of DMF and kept for sonication for 3 minutes to make a solution. The hot plate was heated to 100 °C, the glass coverslips (washed with acetone twice using sonication) was placed on the hot plate and 60 μl of a polymer solution in DMF was dropped on the glass and left for 5-10 minutes to evaporate DMF. Finally, drop casted glass coverslips was kept under vacuum for overnight at 30 °C.

Sonication Procedure. Azopolymer brush glass substrate was kept in a beaker with 10 ml of water and sonicated (59 kHz) for 10 minutes at room temperature, the substrate was washed with water and dried in a vacuum oven for 24 hours with 1 mm of Hg. After 24 hours, the sample was characterized by AFM.

Cell Culture. NIH-3T3 fibroblasts were seeded in low glucose DMEM (Dulbecco's Modified Eagle Medium) and incubated at 37 °C in a humidified atmosphere of 95% air and 5% CO_2.

Human umbilical vein endothelial cells (HUVEC) were purchased from LONZA. Cells were cultured in gelatin-coated flasks in an incubator at

37 °C and humidified atmosphere with 5% of CO_2. Cell medium M200 supplemented with LSGS Kit (fetal bovine serum 2% v/v, hydrocortisone 1 µg/ml, human epidermal growth factor 10 ng/ml, basic fibroblast growth factor 3 ng/ml, heparin 10 µg/ml) was used. Cells were detached with trypsin/EDTA (0.25% w/v trypsin/0.02 mM EDTA) and counted with the Neubauer cell counting chamber before seeding on solid substrates.

Substrates were sterilized under UV light for 30 minutes prior to cell culture. After 24 hours cells were observed with an Olympus CKX41 microscope and images were taken by using a Manta GigE Vision camera (Allied Vision Technologies).

In the case of the experiment of ultrasonic cavitation with HUVECs to erase pattern, cells were cultured in a medium supplemented with 4-(2-Hydroxyethyl)piperazine-1-ethanesulfonic acid buffer and sonication bath was set to 37 °C, in order to mimic physiological conditions. Cells were sonicated for 8 minutes at 59 kHz, observed with a bright field optical microscope and incubated for 2 hours at 37 °C in a humidified atmosphere of 95% air and 5% CO_2 before final observation.

4.3 Results and discussions

4.3.1 Synthesis of poly(MA-DR)b

To synthesize photosensitive polymers, firstly, monomer **A** was prepared according to Scheme 4.1.[26] Amino azobenzene derivative of disperse red 1 (compound **a**) was synthesized accordingly to Scheme 2.3 (presented in Chapter 2).

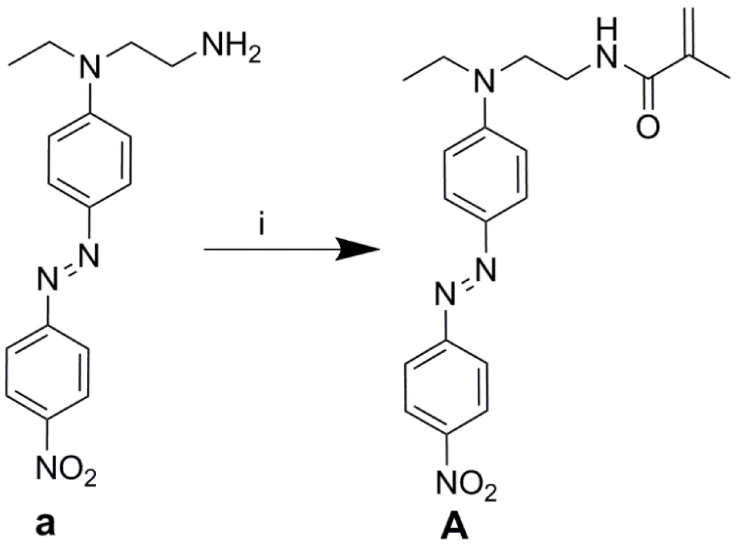

Scheme 4.1. Synthesis of monomer **A.** Reagents and conditions. i) 1.2 equiv. of methacrylic acid, 1.5 equiv. of HOBt and EDC in DMF at RT for 24 h.

Further, methacrylic acid (MA) was reacted with compound **a** by standard acid/amine coupling reaction.

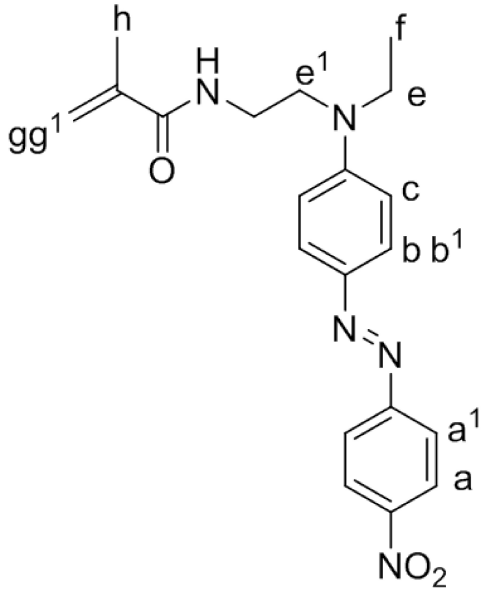

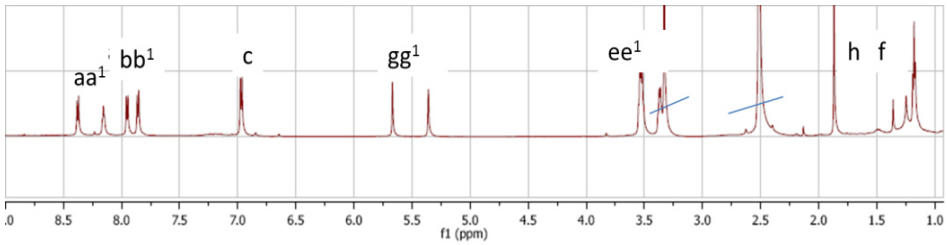

Figure 4.1. ^{1}H NMR of monomer **A** in DMSO-d6 (600 MHz) and assigned chemical shifts.

Azopolymer brushes were synthesized by reversible addition fragmentation chain transfer radical polymerization (RAFT) technique by "grafting from" method as shown in Scheme 4.2.

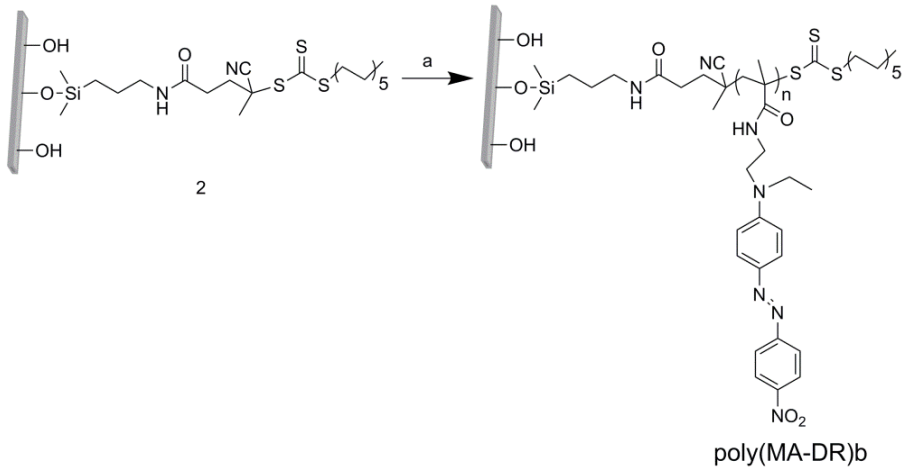

Scheme 4.2. Synthesis of poly(MA-DR)b brushes via RAFT polymerization "grafting from" method. Reagents and conditions. (a) 600 mg of monomer **A** and 1 mg initiator in MeOH/1,4-dioxane (1/1, v/v) at 70 °C for 48h. The DP of MA-DR was around 70 units (n), as calculated by ellipsometry and NMR.

RAFT polymerization technique is one of the finest synthetic approaches to have a narrow polydispersity index (PDI) and high graft density. Moreover, by using this technique, it is possible to modify both ends of the polymer chain (head and tail), as well as control the molecular weight of the polymer.

In this work the azopolymer brush was grown from one end linked to glass surface and its thickness was 150 nm with a refractive index of 1.51 as measured by ellipsometry. The topography of azopolymer brushes was measured by atomic force microscopy (AFM) and the brushes were uniformly grown on the glass surface (Figure 4.2).

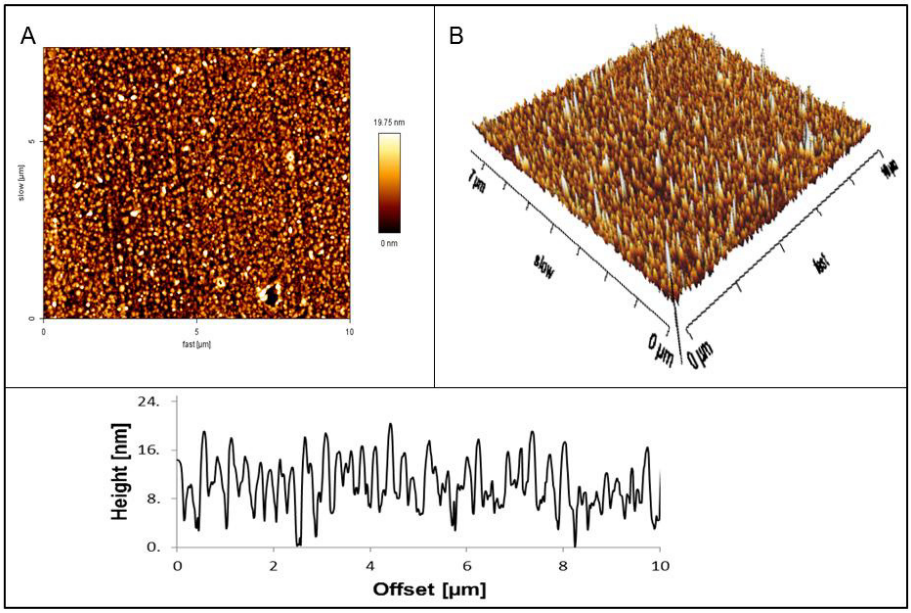

Figure 4.2. AFM images of azopolymer brushes (A) 2D image and (B) 3D view of poly(MA-DR)b. Cross section of azopolymer brushes topography is shown in the bottom image.

The X-ray photoelectron spectroscopy (XPS) analysis was done on poly(MA-DR) brushes with high resolution scan and composition of carbon, nitrogen and oxygen binding energy was in good agreement with XPS. The XPS was performed with high-resolution scan of the C_{1s} signal. The survey spectrum of the elemental composition of the brush showed carbon, oxygen and nitrogen signals. In the C_{1s} high-resolution scan, the carbon atom of the carboxyl group was clearly distinguished at 288.5 eV relative to the aliphatic carbon atoms. The binding energy at

286 eV confirmed C-CO-/C-N bonds and 285 eV confirmed the C-C/CH bonds relative to the aromatic carbon atoms. The N_{1s} peak showed a main component at 400.0 eV attributed to the amide linkage.

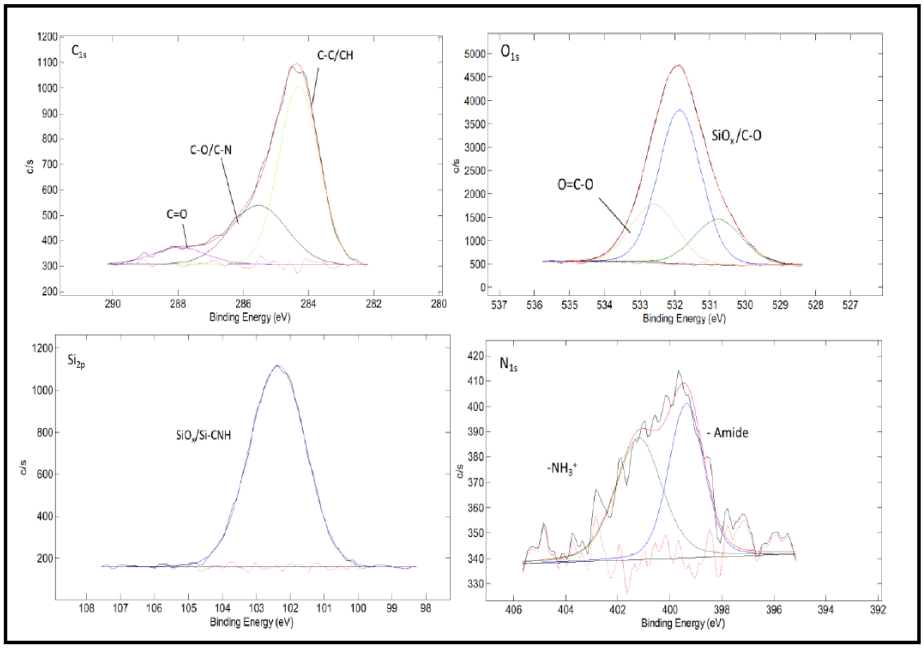

Figure 4.3. Binding energy of C_{1s}, O_{1s}, Si_{2p} and N_{1s} of the azopolymer brushes.

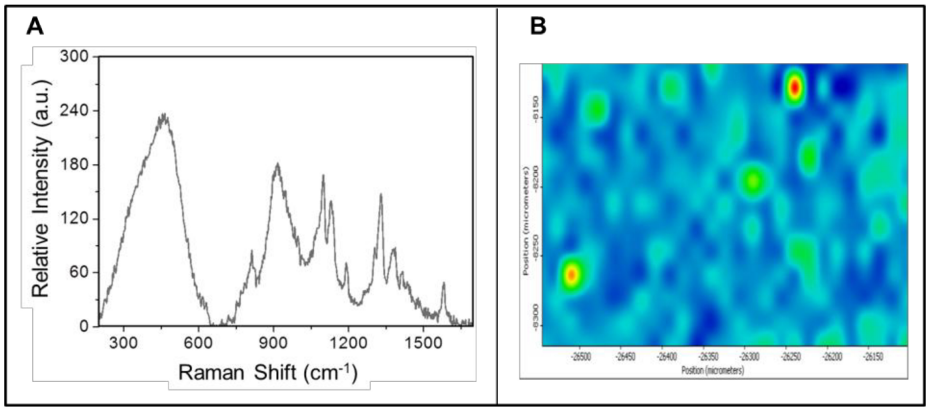

Figure 4.4. (A) Raman Spectrum of azopolymer brushes and (B) Raman mapping on azopolymer brushes.

Raman spectra were investigated in the wavenumber range of 700-1700 cm^{-1} to confirm the structure of azopolymer brushes. Characteristic Raman wavenumbers confirmed the presence of aromatic rings of DR (CH) at 1000 and 1196 cm^{-1}, NO_2 stretching at 1336 cm^{-1}, N=N at 1392 cm^{-1} and amide at 1572 cm^{-1}. This mapping corresponds to the intensity of the peak at 1392 cm^{-1} that assigned to the N=N vibrational mode as presented in Figure 4.4 B.

4.3.2 Creation of SRGs by Using Lloyd's Mirror Method

Azopolymer brushes were used to make SRGs by Lloyd's mirror setup using three different orientations of the incident linear polarized light,[22] in order to find the best orientation of the LPL to excite majority of azobenzene molecules. In fact, it is reported that S-type of LPL is more favorable in SRG formation in azopolymer brushes.[21] Irradiation of azopolymer brushes with an interference pattern at λ = 442 nm (He-Cd laser, 58 mW of power) for 1 hour with horizontal polarization of the incident laser light led to the formation of a topography pattern corresponding to the light intensity distribution (SRG) as one can see in Figure 4.5. The height of the pattern was 30 nm with 2.5 μm periodicity. The periodicity of the pattern is given as $d=\lambda/2 \sin(\theta)$. Where λ is the wavelength of the incident light and θ is the angle between the incoming laser beam and the mirror surface (5°). To increase the pattern height, we illuminated the sample using a different polarization of the incident laser light (vertical polarization), however, pattern height was almost identical, even though irradiation time was also increased in both situations. Finally, we tuned linear incident light to 45° and increased duration of irradiation from 1 to 2 hours so that a 60 nm pattern height

was obtained (Figure 4.5C). However, when we further increased the irradiation time the pattern height did not change. In general, the depth of the inscribed SRG is controlled by the exposure time and/or the polarization configurations as well as thickness of the layer.[29] Thus, we believe that we might achieve higher pattern height by increasing the brush thickness.

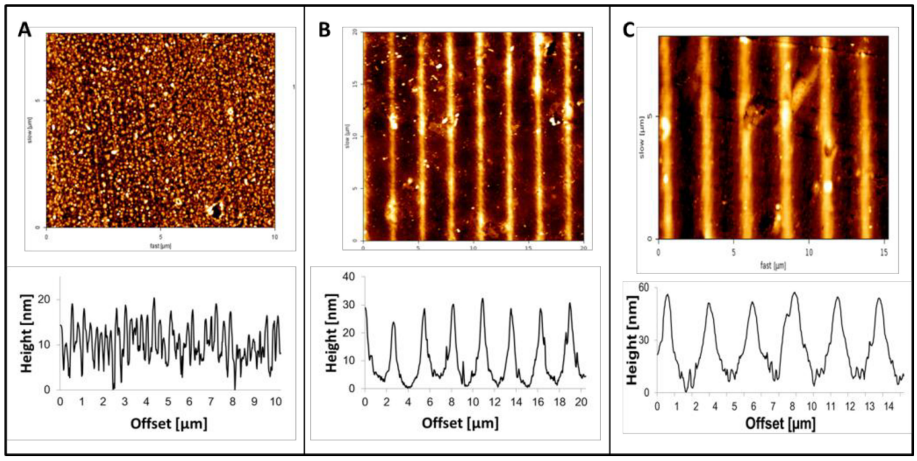

Figure 4.5. AFM images of azopolymer brushes (a) Azopolymer brushes before illumination (b) 1 hour illumination by Lloyd's mirror, 20-30 nm pattern height (45°) and (c) 2 hours illumination by Lloyd's mirror, 60 nm pattern height (45°).

To check orientation of azo-chromaphores in spin-casted film contrary to azopolymer brushes, we have synthesized azopolymers in solution as well using the same condition (Scheme 4.3). In this case, by irradiating the films horizontally to the incoming light just for 1 hour it was possible to generate more than 100 nm pattern height as shown in Figure 4.6. Spin casted film orient contrary to azopolymer brushes. Seki and co-workers[21] stated that in polymer brushes, azobenzene orients parallel to the surface, thus, in-plain with S-type LPL.[30,31]

In fact, the grafted film exhibited highly ordered in-plane optical isomerization by irradiation with linearly polarized light, whereas azopolymer brushes needed a different orientation of LPL to achieve a well-defined and relatively high pattern.

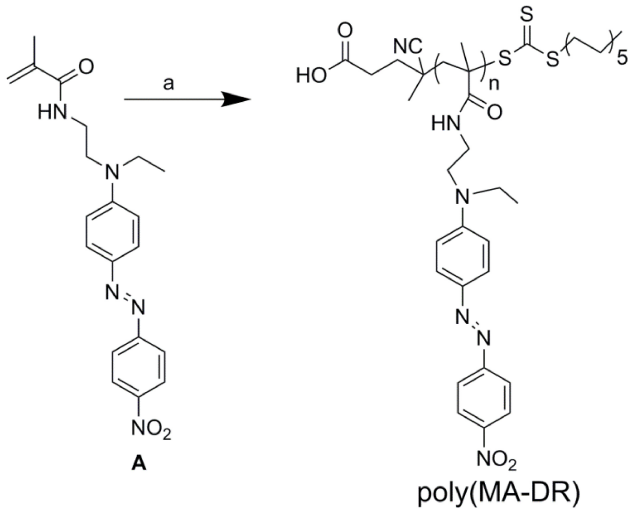

Scheme 4.3. Synthesis of poly(MA-DR) via RAFT polymerization method in solution. Reagents and conditions. a) 1.2 equiv., of RAFT agent, 600 mg of monomer **A** and 1 mg of initiator in MeOH/1,4-dioxane (1/1, v/v) at 70 °C for 48 h.

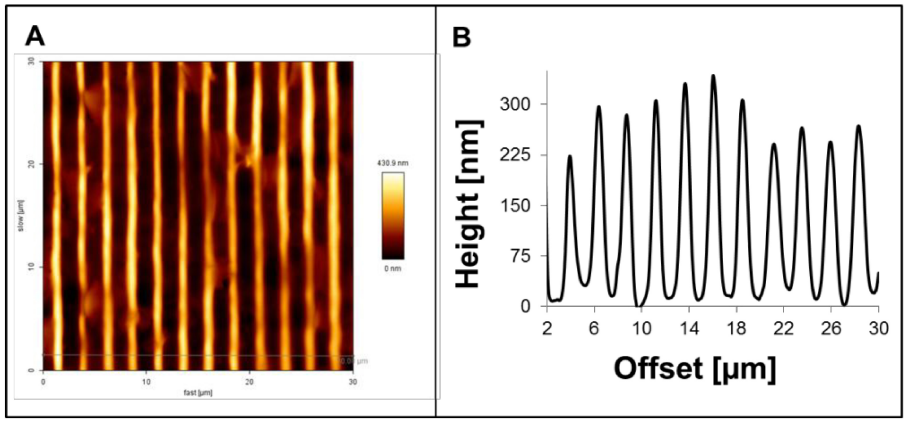

Figure 4.6. AFM images of spin casted azopolymer (a) poly(MA-DR) 1 hour illumination by Lloyd's mirror (horizontal orientation), 200-300 nm pattern height. (B) Cross section of poly(MA-DR).

As a further observation, difference in absorption band before and after illumination by Lloyd's mirror, when comparing polymer brushes to spin-casted film, were found by UV spectroscopy. For polymer brushes, the UV absorption band of the azopolymer brushes before illumination was 483 nm, and after irradiation for 2 hours by Lloyd's mirror no change in the absorption maximum was observed (Figure 4.7A). But in the case of spin casted azopolymer, the maximum absorption was at 486 nm before irradiation, while after irradiation it shifted to 496 nm, due to the aggregation of the polymer.

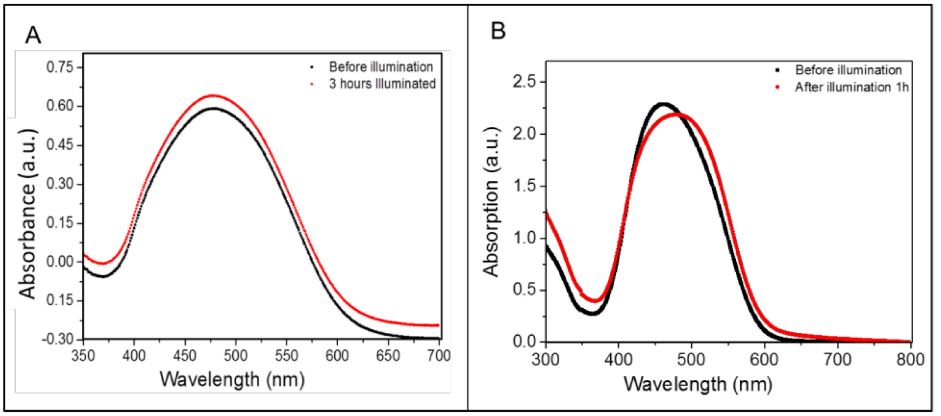

Figure 4.7. (A) UV absorption of azopolymer brushes before excitation (black line) and after illumination for 3 hours by Lloyd's mirror. (B) UV absorption of spin casted azopolymer before excitation 486 nm (black line) and after illumination for 1 hour by Lloyd's mirror 496 nm (red line).

Our interest was to use this SRG azopolymer brushes to study the NIH-3T3 and HUVEC cells behavior on patterned azopolymer brushes for biocompatibility and cells behavior on patterns. Even though spin casted polymer gave more evident results in SRG formation (200 nm pattern height) over polymer brushes, the spin casted polymer was not found to be biocompatible due to preparation of film in solvent (e.g. DMF). On

the other side azopolymer brushes were found biocompatible (as discussed later in section 4.4).

4.3.3 Erasing SRG Pattern by Ultrasonication Method

So far SRG patterns have been erased either thermally or using circular polarized light. In this work we found that sonication (59 KHz) with water at room temperature was significant to erase the pattern (Figure 4.8C).

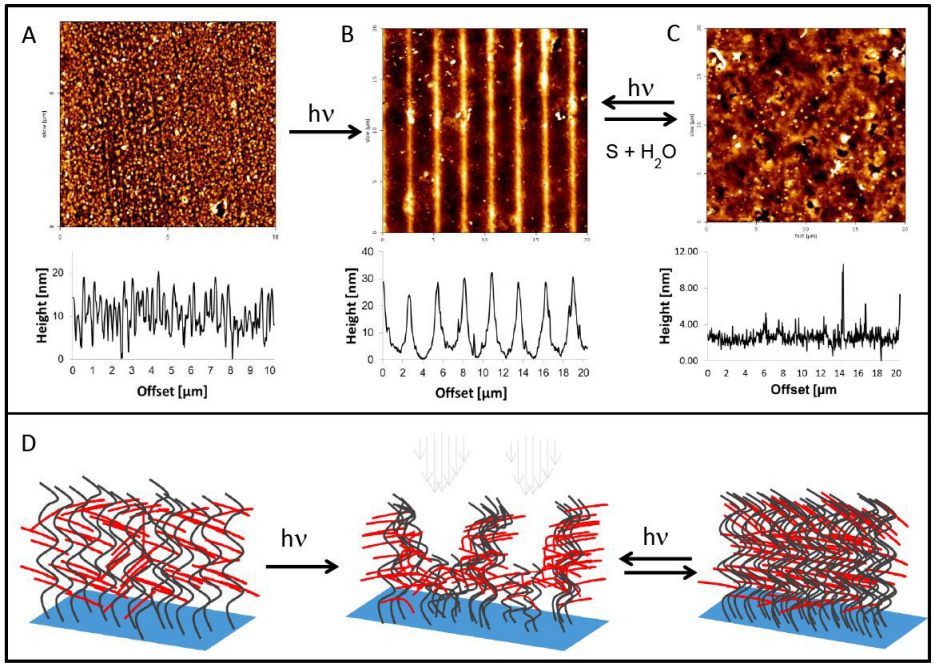

Figure 4.8. AFM images of (A) before and (B) after Lloyd's mirror illumination of azopolymer brushes. (C) AFM image of erased pattern by sonication with water at room temperature. (D) Graphical representation of azopolymer brushes after illumination by interferometry and deleted pattern by sonication (S means Sonication).

Probably, sonication itself, can distort the aggregation of polymer brushes.[32] In addition, we believe that water as medium may help to

distract the aggregation during sonication by braking possible hydrogen bond that formed in the SRG structures. This mild condition method permitted to study the reversibility of SRG azopolymer brushes without heating the materials. The summary of pre and post erasing pattern is present as graphical representation in Figure 4.8D. Although we could erase the pattern, the topography of sonicated polymer brushes looked more flat as compared to the original topography (Figure 4.8C and 4.8A). This could be due to the fact that, the original polymer brushes were washed with organic solvents, thus allowing the free stretched form of the polymer backbone. When only water was used, the brushes were more as coiled-like structure and topography became flatten.[33] Again, azopolymer brushes were illuminated by Lloyd's mirror setup and 50 nm of pattern height was rewritten. This reversibility cycle was performed 3 times and the results were consistent envisioning the possibility to use such polymer brushes as dynamic interfaces to control cell fate.

4.3.4 Movement of Azopolymer Brush Studies by Fluorescence Correlation Spectroscopy (FCS)

After understanding the formation of SRG by Lloyd's mirror method and reversing the topography of the polymer brushes by sonication, our interest was to study the behavior of patterned azopolymer brushes with a single molecule technique like fluorescence correlation spectroscopy (FCS). In our earlier work (Chapter 3) we reported on the movement as well as isomerization process of azobenzene in similar polymer brush by using FCS excitation. In the case of these new azopolymer brushes, due to FCS excitation in bright region of the confocal images, azopolymer brushes appeared to move towards darker region as shown

in Figure 4.9 but as polymers are fixed on the surface, they aggregated around the laser volume, as presented in the Figure 4.9B. This phenomenon is well established by Kumar and co-workers.[11] They explain that, the movement of polymer chains depends on combination of the forces related to the change in the susceptibility due to the light and the field gradient wave vector k.[34]

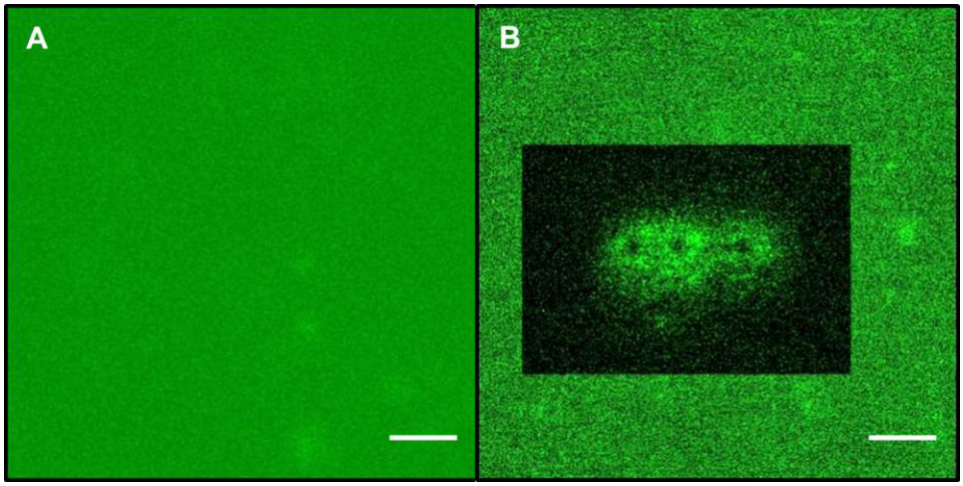

Figure 4.9. Confocal images of (A) before exciting by FCS and (B) after excited by FCS. Aggregation around the laser volume, 3 points which excited with region of interest. Scale bar 10 μm.

In this part of the work, we further studied the movement of azopolymer brushes, which were previously illuminated by the Lloyd's mirror method (Figure 4.10C), exciting them a second time at 488 nm with the FCS setup. First we studied the movement while exciting in the brighter region of the pattern. The topography of azopolymer brushes (Figure 4.10D) was locally disturbed probably because the material tended to move homogeneously to the darker neighboring regions as shown in Figure 4.10D.

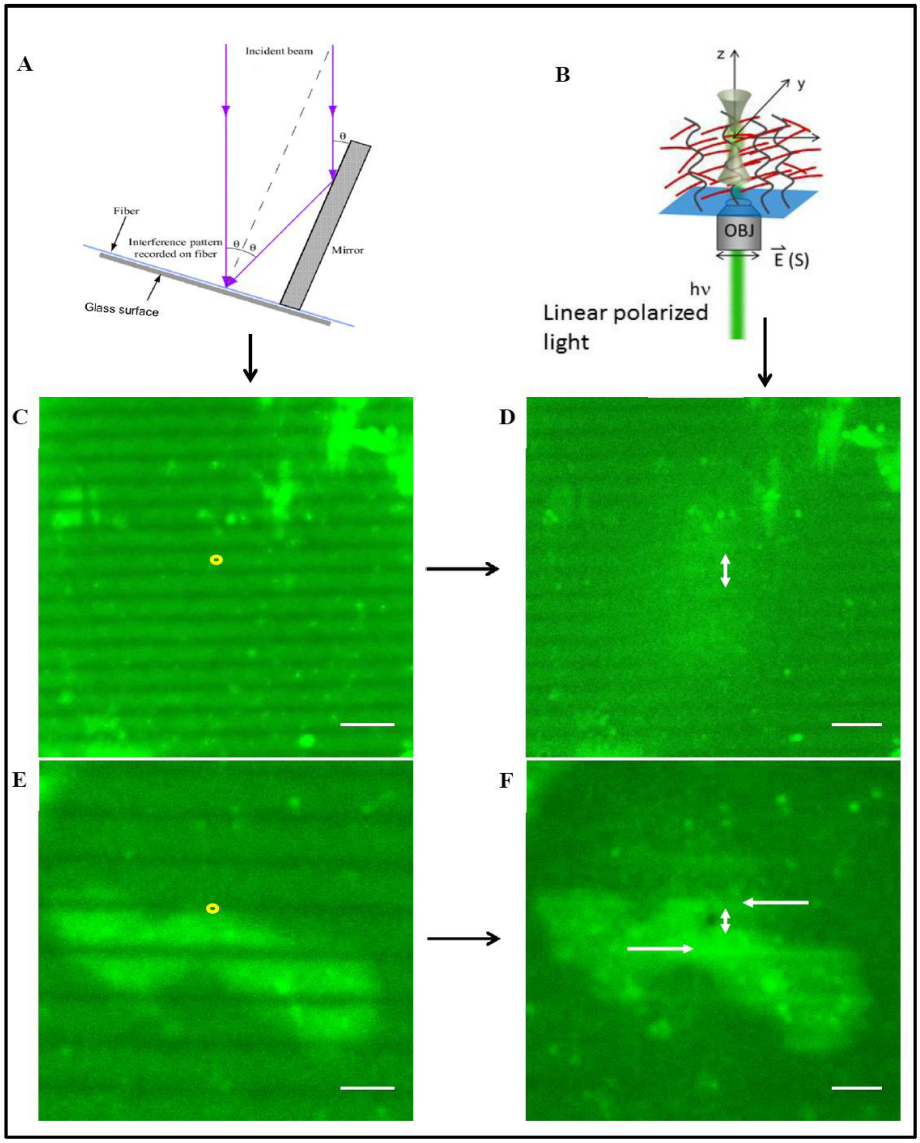

Figure 4.10. A and B represented schematic views of the Lloyd's mirror and FCS setup, respectively. (C and E) confocal image of 30 nm SRG pattern height obtained by Lloyd's mirror setup, pattern modification obtained by excitation at 488 nm by FCS for 20 seconds. Yellow circle represents the spots of FCS excitation. (D) Confocal images after excitation in brighter region (patterned), material moved to neighboring regions. (F) Confocal images after FCS excitation in a dark region of the pattern. White arrows show the movement of materials homogeneously to neighboring regions. Scale bar 10 μm.

While exciting in the darker region of the pattern, we noticed a sort of "negative replica" of the starting confocal image (Figures 4.10E and 4.10F that represent the situation before and after excitation, respectively).

To better understand this phenomenon a schematic representation of SRG structure is given in Figure 4.11. Crest regions that correspond to high region of the pattern in which material aggregate, most likely correspond to brighter regions of the FCS confocal image as well, due to the fluorescence of azomolecules. On the contrary, troughs of the SRG structures appear darker in the confocal images.

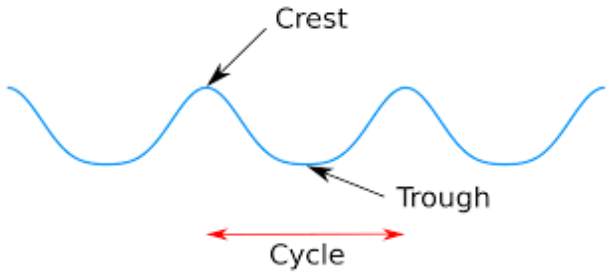

Figure 4.11. Schematic representation of the surface relief grating formation, crest (height patterned region) and trough (valley region).

It has been already reported that azopolymers travel from brighter to darker regions due to *trans-cis-trans* isomerization elicited by LPL excitation.[19,36,37] In the brighter region, when we illuminated by FCS, chromophores moved to "rest" area thus, filling up neighboring darker regions and distributing homogenously, therefore disrupting the pattern (Figure 4.10D). Furthermore, when we applied the same condition and illuminated in a darker region (trough) of the image a sort of negative replica was observed. We believe that, in this case material moves from

less bright areas, which are probably related to lower concentration of azobenzene, to neighboring brighter regions (that is where more amount azobenzene is presenting consequently to aggregation), increasing even more their brightness (white arrows in Figure 4.10F). Next, material is once more pushed away to neighboring dark area (see arrows in Figure 4.10F) to fill up empty space in a "domino"-like effect.[40,41] Azopolymer brushes are a typical organic material that shows cooperative motion. If a change in the alignment of a small number of mesogens in a patterned assembly is induced by an external stimulus such as light, then it is transferred to the whole system, like dominoes, and a change in the whole system is induced.[37]

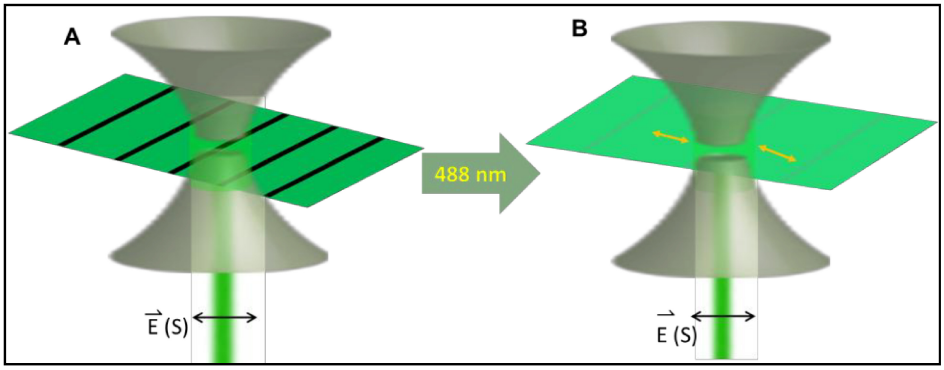

Figure 4.12. (A) General representation of "Domino"-like effect in patterned azopolymer brushes illuminated in a darker region by FCS and (B) effect of excitation by FCS polymer brushes that moved as domino blocks (yellow arrows shown the movement of patterned materials in domino-like way).

4.4 Biocompatibility Assay

Regulating cellular responses to the nanoscale patterns has been proven to be an important modality in controlling cell behaviour.[3] The interesting and promising application of the azopolymer is in the fabrication of SRG topographies for cell engineering provides useful

substrates with surface topography for controlling cellular orientation and migration. In current ongoing research most of the groups use spin coated/casted azopolymers to study cell behavior. As example primary human astrocytes have been reported to exhibit a preferred direction along the grooves.[3] About azopolymer brushes SRG elicit a strong alignment of cells along the grooves. In our work, NIH-3T3 cells were cultured on 60 nm patterned azopolymer brushes and 200 nm patterned spin casted polymers.

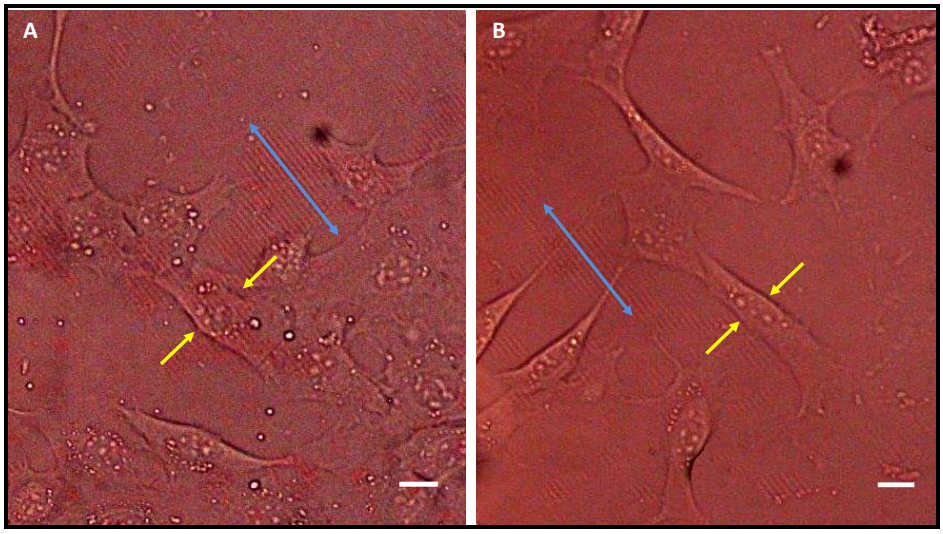

Figure 4.13. (A) and (B) represent the transmission images of NIH-3T3 cells on patterned azopolymer brushes after 24 hours. Light blue arrows represent pattern direction and yellow arrows identify cells at the nuclear regions. Interestingly, some of the cells tended to align along the underlying pattern. Bars are 10 μm.

Cells seeded on both type of polymeric material were observed in the first day after incubation, in spin casted polymer films we found that cells were dead due to trace of toxic DMF used as solvent during the preparation of the film (data not shown), whereas in azopolymer

brushes cells were alive even after 24 hours (Figure 4.13 A and B), thus showing that azopolymer brushes were biocompatible to NIH-3T3. Furthermore, few cells appeared to align along 60 nm grooves (Figure 4.13B). However, not all cells aligned probably because the height of the pattern was not deep enough to elicit a strong cellular response.

Furthermore, to check the orientation of cells on patterned azopolymer brushes, we selected HUVEC, which are known to be quite sensitive to surface geometry. Indeed, in this case, much more cells were aligned along the grooves as can be seen in Figure 4.14.

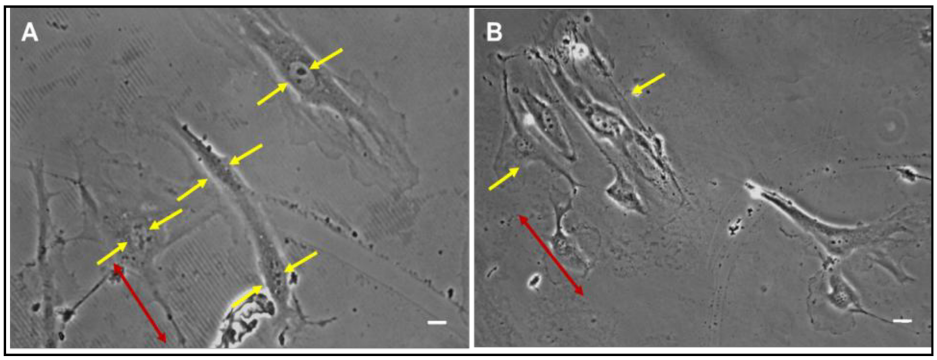

Figure 4.14. A and B represents the transmission image of HUVEC cells on patterned azopolymer brushes after 24 hours. Red arrows represent pattern direction and yellow arrows identify aligned cells. Scale bar 5 μm.

Furthermore, we applied ultrasonic cavitation method to test erasure method (Section 4.3.3) in presence of adherent HUVECs on azopolymer brushes. In this case, the cell culture medium supplemented with HEPES buffer was used and the bath temperature was set at 37 °C, in order to mimic physiological conditions. At the end of the process, cells were detached from the substrate, but, after a couple of hours of incubation, the cells were adhered again. This proves their viability and the feasibility of the erasure method in the presence of cells. In fact, the

use of ultrasonication is sometimes related to the disruption of unhealthy cell membranes and used as a selective method in the treatment of many diseases.[42] Further experiments in this direction are ongoing.

From these preliminary results, we foreseen that to achieve more performing polymeric matrixes as promising cell-guiding novel biomaterials, similar azopolymer brushes with a thicker layer and a more uniform coverage of the surface should be prepared. Such type of optimizations would allow us to synthesize new polymer brushes, which will be able to produce deeper and more uniform SRG grooves that could be more suitable to study material topography influence on the behavior of several different cell lines.

4.5 Conclusion

Here, we presented an effective synthesis of a new kind of azopolymer brushes based on in-house synthesized acrylamide derivative of a well-known azobenzene used as monomer. The thickness of the polymer brushes was 150 nm and the refractive index was 1.51. The formation of 60 nm high SRG on this material was achieved by Lloyd's mirror method, while reversibility of azopolymer brushes was obtained by sonication using water at room temperature. Furthermore, FCS proved to be a key instrument in visualizing SRG structures, thanks to the high sensitivity of this confocal instrument that was found to be able to detect the low florescent signal coming from the azobenzenes. Interferometric pattern obtained on the polymer brushes were re-excited by FCS either in the crest (brighter regions) and trough (darker regions) of the grooves. In the former case the material moved from brighter to darker regions upon FCS excitation, while in the latter case due to a "domino"-

like effect a sort of negative replica image was observed. In both case pattern was disrupted, due to cooperative mass transport elicited by linear polarized light irradiation. Further, NIH-3T3 and HUVEC cells were used to check biocompatibility of these materials. Indeed, polymer brushes were found to be biocompatible, contrarily to spin-casted azopolymers (prepared as comparison). However, pattern height was not deep enough to elicit strong alignment of NIH-3T3 cells along the grooves. Whereas, HUVECs were evidently oriented along the groove direction. Furthermore, we applied ultrasonic cavitation method to test erasure of the SRG pattern in presence of adherent HUVECs. Preliminary results proved the feasibility of sonication as pattern erasure method in the presence of cells. Future work will be focused on maximizing the pattern height by increasing thickness and homogeneity of the polymer brush layer. Such type of optimizations would allow us to synthesize new polymer brushes to study the influence of a dynamic change of material topography on the behavior of adhering cells.

References

(1) Baaca, H.; Leea, J.-H.; Seoa, J.-M.; Parka, T. H.; Chunga, H.; Leed, S.-D.; Kim, S. J.; Submicron-scale topographical control of cell growth using holographic surface relief grating. *Mater. Sci. Eng.* **2004**, *24,* 209-212.

(2) Priimagi, A.; Shevchenko, A.; Azopolymer-Based Micro- and Nanopatterning for Photonic Applications. *J. Polym. Sci. Pol. Phys.* **2013**, *52,* 163–182.

(3) Barille, R.; Janik, R.; Kucharski, S.; Eyer, J.; Letournel, F.; Photo-responsive polymer with erasable and reconfigurable micro- and nano-patterns: An in vitro study for neuron guidance. *Colloid. Surface. B.* **2011**, *88,* 63-71.

(4) Lee, J. K.; Baac, H.; Song, S.-H.; Lee, S.-D.; Park, D.; The Topographical Guidance of Neurons cultured on Holographic Photo-Responsive Polymer. *Conf. Proc. IEEE Eng. Med. Biol. Soc.* **2004**, 4970-4973.

(5) Rocha, L.; Paius, C.-M.; Luca-Raicub, A.; Resmeritaa, E.; Rusua, A.; Moleavin, I.-A.; Hamel, M.; Branza-Nichitada, N.; Hurduc, N.; Azobenzene based polymers as photoactive supports and micellarstructures for applications in biology. *J. Photoch. Phtobio. A* **2014**, *291,* 16-25.

(6) Ahmadi-Kandjani, S., University of Angers, **2007**.

(7) Georgiou, M. A. W. a. T. K.; Thermoresponsive Polymers for Biomedical Applications. *Polymers.* **2011**, *3,* 1215-1242.

(8) Beharry, A. A.; Woolley, G. A.; Small molecules in biology themed issue. *Chem. Soc. Rev.* **2011**, *40*.

(9) Yager, K. G.; Barrett, C. J.; All-optical patterning of azo polymer films. *Curr. Opin. Solid. St. M.* **2001**, *5,* 487-494.

(10) Ubukata, T.; Seki, T.; Ichimura, K.; Surface Relief Gratings in Host-GuestSupramolecular Materials. *Adv. Mater.* **2000**, *12,* 1675-1678.

(11) Kumar, J.; Li, L.; Jiang, X. L.; Gradient force: The mechanism for surface relief grating formation in azobenzene functionalized polymers. *Appl. Phys. Lett.* **1998**, *72*. 2096-2098

(12) Lefin, P.; Fiorini, C.; Nunzi, J.-M.; Anisotropy of the photo-induced translation diffusion of azobenzene dyes in polymer matrices. *Pure. Appl. Opt.* **1998**, *7*. 71-82

(13) Pedersen, T. G.; Johansen, P. M.; Holme, N. C. R.; Ramanujam, P. S.; Mean-Field Theory of Photoinduced Formation of Surface Reliefs in Side-Chain Azobenzene Polymers. *Phys. Rev. Lett.* **1998**, *80,* 89-92.

(14) Bian, S.; Williams, J. M.; Kim, D. Y.; Li, L.; Balasubramanian, S.; Kumar, J.; Tripathy, S.; Photoinduced surface deformations on azobenzene polymer films. *J. Appl. Phys.* **1999**, *86,* 4498-4508.

(15) Naydenova, I.; Nikolova, L.; Todorov, T.; Diffraction from polarization holographic gratings with surface relief in side-chain azobenzene polyesters. *J. Opt. Soc. Am. B.* **1998**, *15*.345-351
(16) Vishwanathan, N. K.; Balasubramanian, S.; Li, L.; Triphaty, S. K.; Kumar, J.; A Detailed Investigation of the Polarization-Dependent Surface-Relief-Grating Formation Process on Azo Polymer Films. *Jpn. J. Apl. Phys.* **1999**, *38,* 5928–5937.
(17) Ambrosio, A.; Maddalena, P.; Marrucci, L.; Molecular Model for Light-Driven Spiral Mass Transport in Azopolymer Films. *Ph. Rev. Lett.* **2013**; Vol. 110. 146102-146105
(18) Ambrosio, A.; Marrucci, L.; Borbone, F.; Roviello, A.; Maddalena, P.; Light-induced spiral mass transport in azo-polymer films under vortex-beam illumination. *Nat. Comm.* **2012**, *3,* 1-9.
(19) Viswanathan, N. K.; Kim, D. Y.; Bian, S.; Williams, J.; Liu, W.; Li, L.; Samuelson, L.; Kumar, J.; Tripathy, S. K.; *J. Mater. Chem.* **1999**, *9,* 1941.
(20) Bian, S.; Liu, W.; Williams, J.; Samuelson, L.; Kumar, J.; Tripathy, S.; Photoinduced Surface Relief Grating on Amorphous Poly(4-phenylazophenol) Films. *Chem. Mater.* **2000**, *12,* 1585-1590.
(21) Uekusa, T.; Nagano, S.; Seki, T.; Highly Ordered In-Plane Photoalignment Attained by the Brush Architecture of Liquid Crystalline Azobenzene Polymer. *Macromolecules.* **2008**, *42,* 312-318.
(22) Schuh, C.; Lomadze, N.; Ruhe, J.; Kopyshev, A.; Santer, S.; Photomechanical degrafting of azo functionalized poly(methacrylic acid) (PMMA) Brushes. *J. Phys. Chem. B.* **2011**, *115,* 10431–10438.
(23) Lomadze, N.; Kopyshev, A.; Rühe, J. r.; Santer, S.; Light-Induced Chain Scission in Photosensitive Polymer Brushes. *Macromolecules.* **2011**, *44,* 7372-7377.
(24) Seki, T.; Photoresponsive self-assembly motions in polymer thin films. *Curr. Opin. Solid. St. M.* **2006**, *10,* 241–248.
(25) Lomadze, N.; Kopyshev, A.; Ruhe, J.; Santer, S.; Light-Induced Chain Scission in Photosensitive Polymer Brushes. *Macromolecules.* **2011**, *44,* 7372–7377.
(26) Schuh, C.; Lomadze, N.; Rühe, J. r.; Kopyshev, A.; Santer, S.; Photomechanical Degrafting of Azo-Functionalized Poly(methacrylic acid) (PMAA) Brushes. *J. Phys .Chem B.* **2011**, *115,* 10431-10438.
(27) Weisshart, K.; Fluorescence Correlation Spectroscopy: A Powerful Tool to Study Dynamic Processes on a Single-Molecule Level. *Rev. Las. Eng.* **2002**, *6,* 388-391.
(28) Buschmann, V.; Krämer, B.; Koberling, F.; Macdonald, P. G. R.; Rüttinger, S.; Bundesanstalt, P. T.; Quantitative FCS:Determination of the Confocal Volume by FCS and Bead Scanning with the MicroTime 200. *Pico. Quant.* **2009**, *1.1,* 1-8.

(29) Grosjean, T.; Courjon, D.; Photopolymers as vectorial sensors of the electric field. *Opt . Express.* **2006**, *14*, 2203-2210.
(30) Ubukata, T.; Seki, T.; Ichimura, K.; Surface relief gratings in host-guest supramolecular materials. *Adv. Mater.* **2000**, *12,* 1675–1678.
(31) Seki, T.; Meso- and Microscopic Motions in Photoresponsive Liquid Crystalline Polymer Films. *Macromol. Rapid. Commun.* **2014**, *35,* 271-290.
(32) Huang, Y. Y.; Terentjev, E. M.; Dispersion of Carbon Nanotubes: Mixing, Sonication, Stabilization, and Composite Properties. *Polymers.* **2012**, *4,* 275-295.
(33) Penga, S.; Bhushan, B.; Smart polymer brushes and their emerging applications. *Roy. Soc. Ch. Advances.* **2012**, *2,* 8557–8578.
(34) Kuma, J.; Li, L.; Jiang, X. L.; Gradient force: The mechanism for surface relief grating formation in azobenzene functionalized polymers. *Appl. Phys. Lett.* **1998**, *72*. 2096-2098.
(35) Labarthet, F. L.; Buffeteau, T.; Sourisseau, C.; Molecular Orientations in Azopolymer Holographic Diffraction Gratings as Studied by Raman Confocal Microspectroscopy. *J. Phys. Chem. B.* **1998**, *102,* 5754-5765.
(36) Tuma, J.; Lyutakov, O.; Huttel, I.; Slepicka, P.; Svorcik, V.; Reversible patterning of poly(methylmethacrylate) doped with disperse Red 1 by laser scanning. *J. Appl. Phys.* **2013**, *114*. 93104-93108
(37) Ikeda, T.; Ube, T.; Photomobile polymer materials: from nano to macro. *Mater. Today.* **2011**, *14,* 480-487.
(38) Ichimura, K.; Photoalignment of Liquid-Crystal Systems. *Chem. Rev.* **2000**, *100,* 1847-1873.
(39) Garcia-Amoros, J.; Szymczyk, A.; Velasco, D.; Nematic-to-isotropic photo-induced phase transition in azobenzene-doped low-molar liquid crystals. *Phys. Chem. Chem. Phys.* **2009**, *11,* 4244–4250.
(40) Yua, Y.; Ikeda, T.; Alignment modulation of azobenzene-containing liquid crystal systems by photochemical reactions. *J. Photochem. Photobio. C.* **2004**, *5,* 247–265.
(41) Hagen, R.; Bieringer, T.; Photoaddressable Polymers for Optical Data Storage. *Adv. Mater.* **2001**, *23,* 1805-1810.
(42) Yu, T.; Wang, Z.; Mason, T. J.; A review of research into the uses of low level ultrasound in cancer therapy. *Ultrason. Sonochem.* **2004**, *11,* 95–103.

Chapter 5

5.1 Conclusions and Future Prospects

Polymer brushes with stimuli-responsive properties have attracted substantial research interest in the past few years. They offer a wealth of opportunities to design responsive materials triggered by external stimuli and have a number of applications in particular we are interested in their application as new biomaterials. Smart polymer brushes (SPBs) with azo-chromophores have a photo-responsive nature and act as superior materials that can alter their properties by light. The work reported in this thesis described the design and synthesis of new azopolymer brushes for the formation and erasure of micro-scale surface relief gratings (SRGs). An interesting and promising application of azopolymer is in the fabrication and modification of topographical feature using mild conditions for cell engineering in order to provide useful substrates for controlling cellular orientation and migration. In **Chapter 1** a general overview about current and future challenges of SPBs was given, focusing mainly on the synthesis of a light-responsive type of SPBs (e.g. azopolymer brushes) and discussing their photochemistry and their possibility to form SRGs. In **Chapter 2**, the synthesis of azopolymer brushes via RAFT technique by "grafting from" approach was presented and thickness (150 to 200 nm) of the polymer brushes was controlled by tuning concentration of the RAFT agent immobilized on the glass surface as well as polymerization time. Furthermore, a full characterization of such polymer brushes was described using several techniques as ellipsometry, XPS, AFM, contact

angel, NMR, SEM and GPC. In **Chapter 3** the influence of the azobenzene molecules on polymer brush dynamics was investigated for the first time by fluorescence correlation spectroscopy (FCS). For this purpose three types of polymer brushes were studied: the first one containing an azobenzene (an amine-derivative of Disperse Red 1, here in short DR) on the side chains and a cyanine 5 dye (Cy5) on top of the polymer brush and two other polymer brushes, one having only DR on the side chains and the last one with just Cy5 on top of the chains. In the first case two dynamics were observed, a short one coming from the fluctuations of DR and a long one related to the main chain of the polymer brush, where Cy5 was linked. The reversibility of brush dynamics was investigated upon excitation at 488 nm with 15 minutes of interval time at room temperature in wet conditions. Furthermore, by using the 488 nm channel as excitation as well as measuring wavelength, we were able to study the short dynamics of azobenzene isomerization mechanism of *trans-cis-trans* cycle with increasing the laser power. While, long diffusion time was measured through Cy5 illumination in both brushes were no DR excitation was caused, thus to be addressed to the main chain of the polymer brushes. In our proposed mechanism when illuminating at 17.5 mW laser power, azopolymer brushes aggregated in the confocal volume (increase number of emitting particles moving within the confocal volume), this was attributed to a cooperative self-assembling and mass movement provoked by the fast isomerisation of azobenzenes, which were oriented parallel to the substrate and therefore favourable excited by the in-plane linear polarized light used in the FCS setup. We believe that azobenzenes got excited until they aligned inside the confocal volume in a direction

perpendicular to $\vec{E}$(S) that is where they were no longer excitable and consequently aggregated. Finally, when DR concentration was increased (up to 20% of DR functionalization), a pattern, resembling to SRG was observed. In **Chapter 4** we report on the synthesis of new azopolymer brushes based on DR-methacryl amide (monomer **A**). The formation of SRG on this material was achieved by Lloyd's mirror method, while reversibility of azopolymer brushes was obtained by sonication using water at room temperature. Furthermore, FCS proved to be a key instrument in visualizing SRG structures. Interferometric obtained pattern on the polymer brushes were re-excited by FCS either in the crest (bright area in the confocal image) or in the trough (darker regions) of the grooves. In the former case the material moved from lighter to darker regions upon FCS excitation, while in the latter case due to a "domino"-like effect a sort of negative replica image was observed. Further, NIH-3T3 and HUVEC cells were used to check the biocompatibility of these materials. We found that HUVEC cells were aligning better along the direction of pattern compared to NIH-3T3 cells. Furthermore, we applied ultrasonic cavitation method to test erasure of the SRG pattern in presence of adherent HUVECs. Preliminary results proved the feasibility of sonication as pattern erasure method in the presence of cells. These results foresee the possibility to use these azopolymer brushes as novel cell instructive biomaterials. Materials that are capable of conformational and chemical changes caused by the external stimuli, accompanied by variations in their physical properties, can modulate cell adhesion and migration at the liquid-solid interface and can be tremendously useful in diverse biological and medical applications in the field of tissue engineering.

For instance, dynamic synthetic substrates can control the presentation of regulatory signals to a cell providing unprecedented opportunities in the study of cell behaviour by mimicking the dynamic properties of biological systems. In this respect, the results presented in this thesis envision the possibility to develop new biomaterials, based on our synthesized light-responsive polymer brushes, which may respond dynamically to applied stimuli and performed as new cell-instructive materials.

Acknowledgements

At the end of my thesis, it is a pleasant task to express my thanks to all those who contributed in many ways to the success of my Ph.D. and made it an unforgettable experience for me.

First of all I would like to thank my advisor, ***Prof. Paolo Antonio Netti***, who has given me an opportunity to pursue my Ph.D. He has been actively interested in my work and has always been available to advise me. I am very grateful for his motivation and immense knowledge in the subject that, taken together, make him a great mentor.

My deepest gratitude to my tutor, ***Dr. Silvia Cavalli***. With her enthusiasm, inspiration, and her great efforts to explain things clearly and simply, helped me lot during my Ph.D. Throughout my thesis-writing period, she provided encouragement, sound advice, good teaching, good company and lots of good ideas. I would have been lost without her support.

I take this opportunity to sincerely acknowledge the ***Istituto Italiano di Tecnologia (IIT), Center for Advanced Biomaterials for Healthcare,*** for providing me financial support.

I would like to thank Ph.D. coordinator ***Prof. Giuseppe Mensitieri*** and committee members at the ***University of Federico II*** for giving me an opportunity to pursue my Ph.D. degree.

I am also indebted to my collaborator, ***Dr. Ilaria De Santo*** for helping me by doing the FCS measurements and getting out the good results.

I would like to acknowledge my lab mates for providing a stimulating and fun filled environment. My thanks go to ***Miss. Chiara Fedele***, who

helped me for doing biological experiments. I am ever indebted to ***Miss. Carmen Rianna*** with whom I started this work and many rounds of discussion with her helped a lot. I wish to thank ***Miss. Elisa Vaselli*** for teaching ellipsometry. Once again thanks to my magic team for creating a good atmosphere in the lab and also teaching me some Italian words (Grazie Mille).

My sincere thanks to ***Dr. Luca Raiola*** for analyzing NMR data, ***Dr. Anastasios C Manikas*** for helping and providing useful information about RAMAN analysis, ***Dr. Massimiliano Porzio*** helping in GPC analysis and ***Dr. Fabio Formiggini*** for collaborating to do FRAP and confocal analysis.

Most of the results described in the thesis would not have been obtained without a close collaboration with few laboratories. I owe a great deal of appreciation and altitude to ***Prof. Pietro Ferraro***. CNR-Istituto di Cibernetica "E. Caianiello" in Pozzuoli (Naples, Italy), for Lloyd's mirror setup and helping us to create SRGs on our azopolymer brushes, ***Prof. Fabrizio Pirri*** (IIT, Torino. Italy) and ***Dr. Micaela Castellino*** for XPS experiments and my heartfelt thanks to the JEOL Company (France) for analyzing the morphology of polymer brushes by using special SEM techniques.

I would like to pay high regards to my IIT Human Resource department especially to ***Ms. Arianna Pezzuolo*** for helping to get all the documents without any delay.

I also thank to all my colleagues and seniors at ***CRIB*** for supporting me throughout my Ph.D. degree.

I would like to acknowledge my Indian friends ***Dr. Pankaj Thakur*** and ***Dr. Narayana Reddy*** for giving moral support. Thanks to my neighbor

and my friend ***Dr. Hojath Madadi*** for giving me a positive vibe every day.

Finally, but by no means least, thanks to my family, in-laws for the support they provided me throughout my entire life and in particular, I must acknowledge my mom, my wife and best friend, ***Soorya***, without whose love, encouragement and motivation, I would not have finished my Ph.D.

Appendix

Study the Mobility of Polymer Brush by Confocal Microscopy

Abstract. Studies on the mobility of azopolymer brushes with fluorescence correlation spectroscopy (FCS) were discussed in details in Chapter 3. In this appendix additional important information about the mobility of polymer brushes without azobenzene on side chain of the polymer are reported as supplementary relevant data. Thus, mobility of Cy5-pMAb was investigated before and after treatment with calcium chloride by both fluorescence recovery after photo-bleaching (FRAP) and FCS technique.

Firstly, we have studied the mobility of Cy5-pMAb by Fluorescence recovery after photo-bleaching (FRAP) technique. By FRAP we could measure the ability of the polymer brushes to recover fluorescence signal after photobleaching in a particular time. Using a confocal microscope, (650-750 nm wavelength bands and 2 photon modes using LAC-AF software and FRAP wizard) it was possible to visualize the fluorescently tagged molecule by using a low intensity light. In details, we bleached Cy5-pMAb at 633 nm with regions of interest 20×20 μm for 200 seconds to ensure that the entire area was completely bleached and a recovery time for observation of 8-10 minutes was given. Interestingly, a recovering of 30 % of fluorescent for Cy5-pMAb maximum was observed. To confirm the recovery of the polymer brushes we have further analyzed the control sample by diffusing Cy5 maleimide solution in Cy5-pMAb. In this case fluoresce intensity was completely recovered (Figure 1).

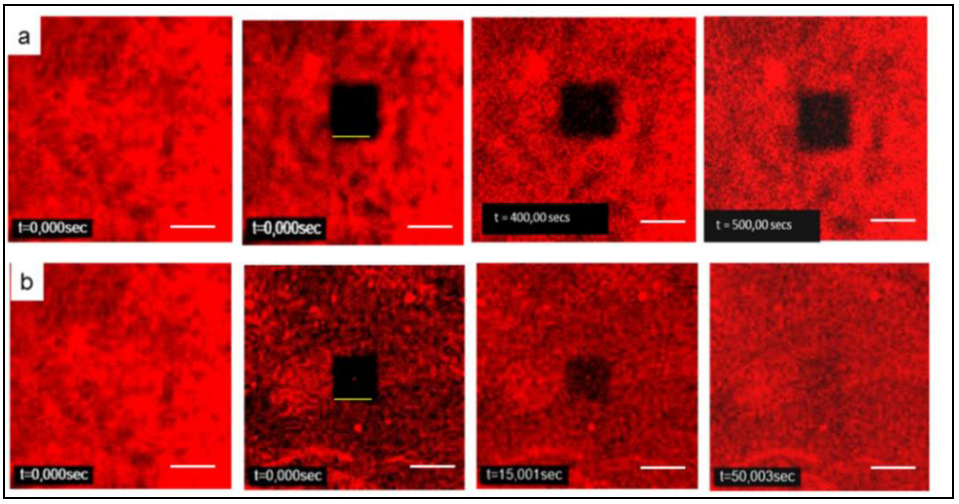

Figure 1. (a) Cy5-pMAb. Bleached for 20 seconds and recovered after 500 seconds (30% recovery) and (b) Cy5-pMAb brushes diffused with Cy5 solution, bleached for 20 seconds and completely recovered after 50 seconds. Scale bar 20 μm.

When polymer brushes get bleached due to fluidity in the backbone some percentage of Cy5-pMAb were folded down and recovers after bleaching. To recheck the mobility of the polymer brushes we have changed the morphology of the polymer backbone by treating with calcium chloride. $CaCl_2$ is well known in making bi and trivalent bond with carboxylic acid groups (Scheme 1).

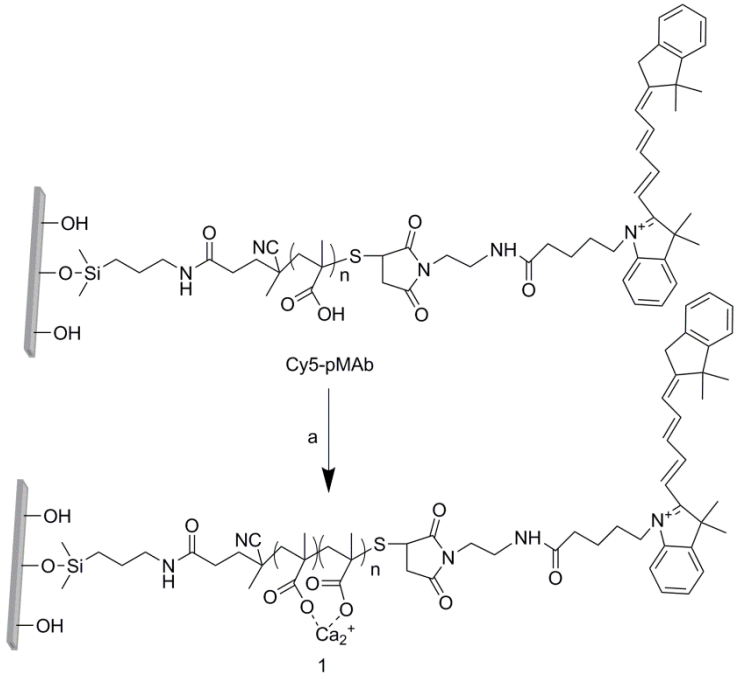

Scheme 1. Preparation of calcium treated surface 1. (a) 20 mM solution of calcium chloride at RT for 12h.

When we treated with $CaCl_2$ the polymer backbone became rigid and the mobility got "frozen" (Figure 2). However, the information from FRAP did not give complete information regarding the mobility. To confirm the real dynamics we decided to use Fluorescent Correlation Spectroscopy.

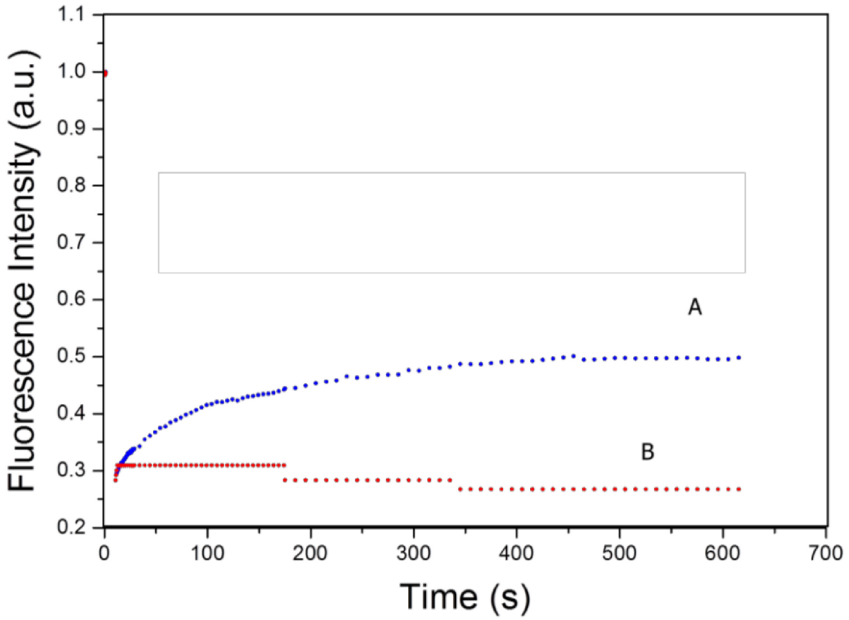

Figure 2. Cy5-pMAb after photo bleaching, (A) 30 % recovery for the was "fluid"-like polymer structure and (B) No recovery of calcium treated sample 1 due to the "frozen crystalline"-like polymer structure.

Fluorescence Correlation Spectroscopy (FCS)

FCS is a powerful tool to study the single molecule movement by selecting a fluorophore. In this case we have used FCS to study fluctuations of Cy5-pMAb at 633 nm channel (Cy5 channel). Cy5-pMAb brushes bleached at 633 nm for 100 seconds and measured the fluctuations in the same channel. Count rates of brush at 100 seconds showed that more fluctuations were observed. In fact, at 158 seconds, we noticed that the brushes were more fluctuating and the movement become restricted as shown Figure 3. On the contrary, when we have analyzed calcium treated surface 1, there was no dynamics observed because the brushes were "frozen" and turned into a "crystalline"-like structure.

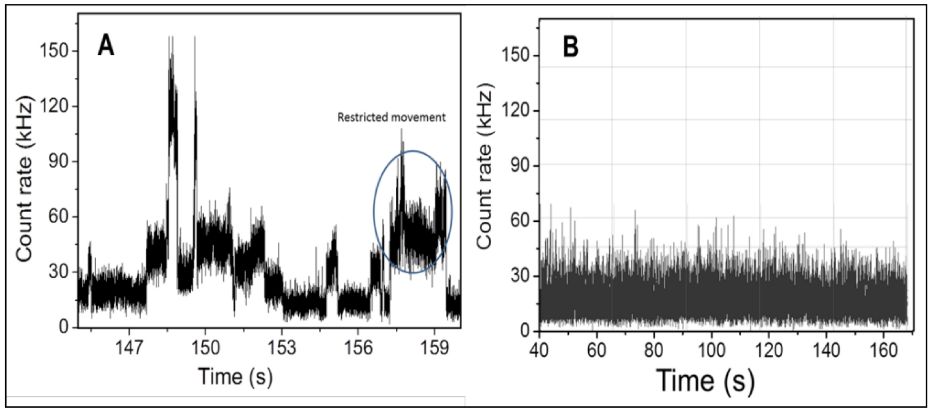

Figure 3. Counts rates of (A) Cy5-pMAb at 140-160 seconds, at 158 seconds. The movement of the brushes became restricted and dynamics got slow down. (B) Calcium treated sample 1, no dynamics was observed till 160 seconds.

In summary, FRAP and FCS results reveal that the Cy5-pMAb showed slow dynamics due to a "fluid" backbone of the polymer brushes. At 158 seconds more than two polymer brushes were sticking on glass surface and aggregated in the confocal volume, thus the dynamics got slow down but when methacrylic acid polymer brushes were treated with a $CaCl_2$ solution the brushes became "frozen" and no dynamics was observed.